Interaction between Vascular Endothelial Cells and Surface Textured Biomaterials

By

Lin Qiu

Supervisors: Professor Wen Wang

Professor Ton Peijs

Professor Cees W.M. Bastiaansen

A THESIS SUBMITTED TO THE UNIVERSITY OF LONDON

FOR THE DEGREE OF DOCTOR OF PHILOSOPHY

School of Engineering and Materials Science

Queen Mary University of London

2014

Declaration

I declare that the work presented in this thesis was performed entirely by myself during the course of my PhD studies at Queen Mary University of London and has not been previously submitted for a degree at this or any other university.

Acknowledgement

I would like to thank the Queen Mary University of London and the China Scholarship Council (CSC) for funding my PhD study in the past 4 years. I would also like to thank my supervisors, Professors Wen Wang, Ton Peijs and Cees W.M. Bastiaansen for their support and encouragement throughout my PhD.

I am grateful to my supervisors for the opportunity to do a PhD and the invaluable experience I have acquired at Queen Mary University of London. I appreciate their helpful suggestions and strong support.

Particularly, I would like to convey my gratitude to Dr. Julien Gautrot, who has provided training and advice during my research. I thank Dr. Nanayaa Freda Hughes-Brittain for the training on photoembossing and help throughout my research. Many thanks to Mr. Weiqi Li for his help on confocal imaging and advice on my cell work. I thank Dr. Urszula Stachewicz for her help on focused ion beam – scanning electron microscope (FIB-SEM) imaging.

My research was also supported by staffs and technicians in SEMS. I thank Mr. Chris Straw, Mr. Chris Mole and Mr. Shafir Iqbal who were always there to provide help when needed. Many thanks to Dr. Zofia Luklinska and Dr. Russell Bailey for their help on SEM imaging.

Many thanks also, to all the current and former group members for the happy team spirit they created: Dr Yiling Lu, Dr. Shangjun Ye, Dr. Chanyuan Chai, Dr. Yankai Liu, Dr. Ke Bai, Dr. Hong Chang, Mr. Xiaotian Yu, Mr. Devendra Inder Deo, Mr. Zhengjun Lv, Ms. Miao Lin, Mr. Xia Chen, Ms. Junyao Yang and Ms. Baoqi Yu.

Finally, I would like to thank my family for their support and understanding throughout my PhD. My parents Zhigang Qiu and Mingxiu Yu, you have always been my rock and I could not have done this without your moral support. My loving husband Hao Liu, you are always around to provide me with support and encouragement. I really could not have asked for more.

Abstract

A promising approach to overcome thrombus and neointima formation on vascular grafts is to create a functional, quiescent monolayer of endothelial cells on the surface of implants. Surface topography of these implants is proven to enhance cell attachment and to reduce the inflammation associated with a smooth surface.

Photoembossing is a relatively new, simple, environment-friendly and cost-effective technique to create surface topographies, since there is no etching step or mould needed. In this study, photopolymer films are photoembossed through contact mask photoembossing, while fibres are photoembossed through holographic lithography. Surface relief textures of ridges and grooves with various pitch sizes and heights are successfully obtained through both methods. Furthermore, we introduce this technique to fabricate, for the first time, reproducible surface textures on electrospun fibres.

Human umbilical vein endothelial cells (HUVECs) are used in the study. Three different systems are investigated: non-degradable PMMA-TPETA, semi-degradable PLGA-TPETA and fully degradable PLGA-PEGDA-DTT, for different applications and therapeutic requirements. Both non-degradable PMMA-TPETA photopolymer and semi-degradable PLGA-TPETA photopolymer are shown to improve biocompatibility compared to PMMA and PLGA, respectively. Photoembossed films made from these two photopolymers show significantly improved cell attachment and proliferation,

with a water contact angle around 70 º. It is shown that the pitch size of surface topographies affects cell adhesion and migration in the wound healing assay study.

Interaction between HUVECs and fibres shows that cells grow from their initial locations at fibre crossings. Focal adhesions are seen to be more aggregated on the surface textured fibres, while those on the glass cover slips are more dispersed near the edge of the cell membrane. The appearance of F-actin in the cytoplasm is also seen to be influenced by the surface topography, where changes in the diameter of the fibre and its surface texture result in F-actin rearrangement.

Our study shows that a surface textured, fully degradable, gel-like photopolymer PLGA-PEGDA-DTT has great potential to be further developed for tissue engineering applications.

List of publications

Journal Publication

Hughes-Brittain, N. F., **Qiu, L.**, Wang, W., Peijs, T. & Bastiaansen, C. W. 2014. Photoembossing of Surface Relief Structures in Polymer Films for Biomedical Applications. Journal of Biomedical Materials Research. Part B, Applied Biomaterials, 102, 214-20.

Hughes-Brittain, N. F., Picot, O. T., **Qiu**, **L.**, Sanchez, C., Peijs T., and Bastiaansen, C. W. Photoembossing for Surface Texturing of Films and Fibres for Biomedical Applications. MRS Proceedings, 2012. Cambridge Univ Press.

Conference

Qiu L., Hughes-Brittain N. F., Peijs T., Wang W. Responses of Vascular Endothelial Cells to Photo-embossed Topography on Polymer Films and Fibers. Society For Biomaterials 2013 Annual Meeting and Exposition, Boston, USA, April 2013

Contents

Abbreviations

2D	Two-dimensional
3D	Three-dimensional
AFM	Atomic force microscopy
Anti-mouse	Alexa Fluor® 594 Donkey Anti-Mouse IgG (H+L) Antibody
Anti-vinculin	Monoclonal Anti-Vinculin antibody produced in mouse
BSE	Back-scattered electrons
C_6H_5Cl	Chlorobenzene
$CHCl_3$	Chloroform
CL	Cathodoluminescence
DAPI	4′, 6-diamidino-2-phenylindole
DI-water	Deionized water
DMF	Dimethylformamide
DMSO	Dimethyl sulfoxide
DPBS	Dulbecco's Phosphate-Buffered Saline

DPPHA	Dipentaerythritolpenta-/hexa-acrylate
DSC	Differential scanning calorimetry
DTT	DL-Dithiothreitol
ECM	Extracellular matrix
ECs	Endothelial cells
ESEM	Environmental SEM
F-actin	Actin filaments
FAs	Focal adhesions
FBS	Foetal bovine serum
FDA	Food and Drug Administration
Fn	Fibronectin
GA	Glycolic acid
HUVECs	Human umbilical vein endothelial cells
Irgacure 369	2-Benzyl-2-(dimethylamino)-4′-morpholinobutyrophenone
LA	Lactic acid

MTS	3-(4,5-dimethylthiazol-2-yl)-5-(3-carboxymethoxyphenyl)-2-(4-sulfophenyl)-2H-tetrazolium, inner salt
PDMS	Polydimethylsiloxane
PEG	Poly(ethylene glycol)
PEGDA	Poly(ethylene glycol) diacrylate
PEO	Polyethylene oxide
PFA	Paraformaldehyde
PGA	Polyglutamic acid
PGMEA	Propylene glycol monomethyl ether acetate
PLA	Polylactic acid
PLGA	Poly(lactic-co-glycolic acid)
PMMA	Poly(methyl methacrylate)
POE	Polyoxyethylene
PSD	Position sensitive detector
RT	Room temperature
SE	Secondary electrons

SEM	Scanning electron microscope
T_g	Glass-transition temperature
TPETA	Trimethylolpropane ethoxylate triacrylate
UV	Ultraviolet
WCA	Water Contact Angle

List of tables

List of figures

Chapter 1 Introduction

1.1 Background information

Cell-biomaterial interaction is used to describe the cellular responses to biomaterials in vitro and in vivo. This is of particular interest because it enables a better understanding of the regulation of cell behaviour during wound healing and tissue regeneration. Cell-biomaterial interaction involves a complex interplay of various activities such as cell adhesion, spreading, migration and proliferation.

A biomaterial is normally defined as ‘a nonviable material used in a medical device, intended to interact with biological systems’ (Williams, 1987) which contains various forms of matter, surfaces or constructs(Wang et al., 2013). It can be derived from two main sources, natural and synthesized. Silk and catgut sutures are classic natural biomaterials while synthesized biomaterials can be produced from ceramics, metallic components, polymers and composite materials.

Humans have a long history of using implants in the body. The use of iron dental implants can be traced back to 2nd Century Europe, and the Mayans used sea shells to make nacre teeth around 600 AD (Ratner et al., 2004).

The field of modern biomaterials has grown at an intense pace since its beginnings more than 60 years ago and new ideas and productive branches (Ratner and Bryant, 2004, Harrison et al., 2014) are constantly evolving. In the beginning, researchers concentrated on developing implants with sufficient mechanical support and minimal inflammation. Later on, in the 1980s, biomaterials with controlled biological activity were intensively studied. Smart biomaterials which could interact with cells began to develop since then. Moreover, the use of biomaterials promises to have an even greater effects on patient care in the near future (Dusastre, 2009). A biomaterial can be as simple as an intraocular lens which can help to restore sight in a great number of cataract patients. It can also be extremely complex, interacting with and even directing the body's response while providing proper mechanical properties (Dusastre, 2009). Artificial scaffolds have already become integral part to be used in skin (Supp and Boyce, 2005), bone (Thesleff et al., 2011), bladder (Oberpenning et al., 1999) and cartilage (Freed et al., 1997) treatment. The ultimate goal of tissue engineering is to regenerate lost or damaged tissue by recreating the progress of tissue generation that occurs during human embryonic development (Place et al., 2009). Great achievement have been made by each generation of researchers who have begun to realize the potential of biomaterials in the treatment of a much broader range of conditions such as osteoarthritis, retinopathy, myocardial infarction, liver cirrhosis etc. According to one report, a tissue-engineered skin equivalents was first introduced into clinical use in 1997 (Viola et al., 2003). Since then, studies and applications of replacement devices have increased rapidly. Table 1.1 shows the various stages

of development of commercial tissue-engineered products and biomaterials for skin and bone. Moreover, exciting new results were announced in two high-profile studies recently. According to the report, seven patients, aged 4-19 years, with myelomeningocele benefitted from tissue-engineered bladders (Atala et al., 2006). In another case, a 30-year-old woman was the first person to receive a tissue-engineered tracheal segment which saved her left lung by an innovative large airway replacement (Macchiarini et al., 2008).

Table 1.1 Commercial tissue-engineered products and biomaterials for skin and bone at various stages of development (Place et al., 2009)

Tissue	Product name	Regulatory status	Description	Use	Form
Skin	Integra Dermal Regeneration Template, Integra Lifesciences	1996	Porous bovine collagen cross-linked with chondroitin-6-sulphate with upper layer of silicon	Burns	Sheet
	TransCyte, Advanced Biohealing	1997	Nylon mesh coated with porcine collagen, containing non-viable human fibroblasts, with upper layer of silicon	Burns	Sheet
	Apligraf, Organogenesis	1998	Lower layer of human fibroblasts and bovine collagen, upper layer of keratinocytes	Leg ulcers	Sheet
	Dermagraft, Advanced BioHealing	2001	Cryopreserved human fibroblasts on a polyglactin 910 (2-hydroxy-propanoic acid polymer with	Diabetic foot ulcers	Sheet

			polymerized hydroxyacetic acid) mesh		
	Xelma, Molnlycke	2005	ECM protein (amelogenins) in propylene glycol alginate carrier	Leg ulcers	Gel
	Oasis Wound Matrix, Healthpoint	2006	Decellularized porcine small intestinal submucosa	Burns, ulcers, other wounds	Sheet
	Integra Flowable Wound Matrix, Integra Lifesciences	2007	Granulated bovine collagen crosslinked with chondroitin-6-sulphate	Ulcers	Gel
	PriMatrix, TEI Biosciences	2008	Decellularized fetal bovine skin	Wounds	Sheet
Bone	OP-1, Stryker	2001	Bovine type I collagen with rhBMP-7	Bone injury	Paste
	INFUSE Bone Graft, Medtronic	2002	Bovine type I collagen sponges soaked in rhBMP-2 in LT-CAGE Lumbar Tapered Fusion Device	Spinal fusion	Solid
	Vitoss Scaffold FOAM, Orthovita	2004	Porous foam comprising β-TCP and bovine type I collagen	Bone injury	Foam
	Regenafil, Regeneration Technologies/ Exatech	2005	Human mineralized bone matrix in porcine gelatin carrier	Bone injury	Paste
	GEM 21S, BioMimetic Therapeutics	2005	β-TCP particles and recombinant human platelet-derived growth factor-BB (PDGF-BB)	Dental bone/ gum defects	Paste
	Bioset IC, Pioneer surgical	2008	Human demineralized bone matrix with bovine bone chips in type I collagen	Bone injury	Paste

			carrier		
	FortrOss, Pioneer Surgical	2008	Nanocrystalline hydroxyapatite and E‑matrix (porcine collagen co‑polymerized with dextran)	Bone injury	Paste

Despite the current benefits of biomaterials and their much greater future potential to improve the quality of life of human beings, this field still faces many ethical questions, such as the sources of the samples and how advances should be deployed into clinical care. As a result, researches in this area are regularly being scrutinized and influenced by external factors. The well-known main ethical debate is about the sourcing of stem cells. Stem cells are commonly used in bioengineering studies because of their ability to grow into different types of cells depending on demand. Their harvesting from embryos has been going on for some years. Moreover, the use of stem cells is not limited to biomaterials research.

1.2 Endothelial cells (ECs)

With relevance to possible future cardiovascular applications, the behaviour of ECs on different biomedical polymer scaffolds was studied in this thesis. ECs are cells forming the endothelium which is a thin layer of cells lining the interior surface of lymphatic vessels and blood vessels(Furchgott and

Zawadzki, 1980). When cultured in vitro after confluence, ECs normally densely packed in a monolayer with polygonal shape at 35-50 μm in wide (Gimbrone et al., 1974).

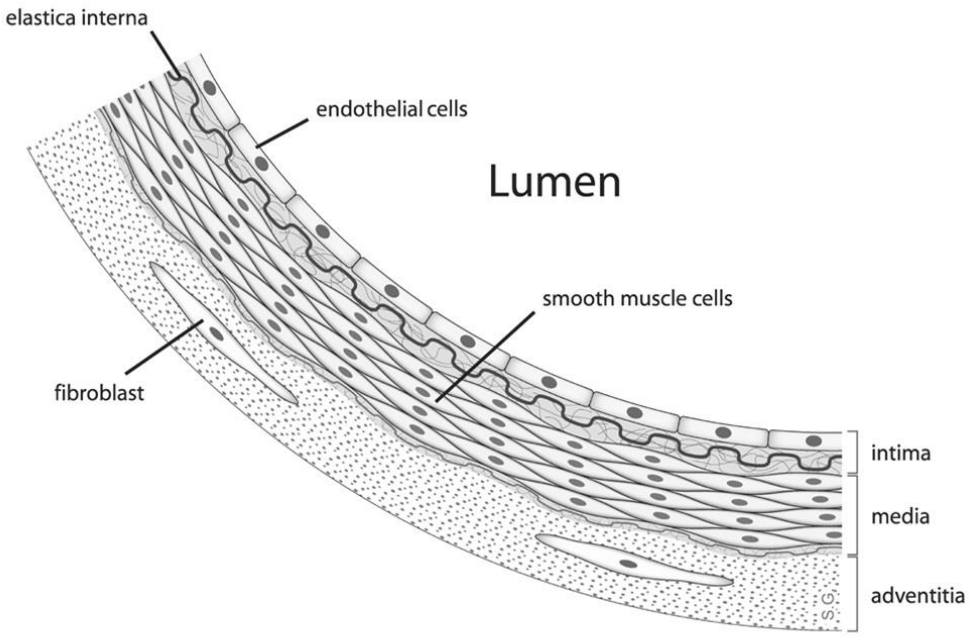

Figure 1.1 The location of endothelial cells (Portal)

In native vessels, ECs play a pivotal role in vascular biology, such as in the regulation of coagulation and vasomotor tone, white cell trafficking, hemostatic balance (Aird, 2007), the growth of vascular smooth muscle cells, ischemic and reperfusion injuries, control of the nutrient transportation across the vessel wall (Shireman and Pearce, 1996) and the development of arteriosclerosis (Cines et al., 1998).

Failure of vascular grafts are normally caused by the lack of a durable and adherent endothelium covering the graft which leads to thrombus (L'Heureux et al., 2007, Seifalian et al., 2002, Williamson et al., 2006). A promising approach to overcome this issue is to create a functional, quiescent monolayer of endothelial cells on the surface of implants. The vascular endothelium also controls the transport of substances from the blood into the vessel wall (Dejana, 2004, Dejana et al., 2009, Franco et al., 2012). The destruction of this control can cause cardiovascular disease (Komatsu et al., 1998). Therefore, to understand and accelerate the healing of the endothelium after wounding is important to avoid the beginning of focal disease (Franco et al., 2012).

1.3 Surface texturing techniques

The smooth surfaces of biomaterials are known to promote inflammation whereas textured surfaces have been proven to lessen this problem (Recum et al., 1996). Topography can be defined as the morphology of a surface. A variety of techniques are used to create surface topographies used in cell scaffolding. These fall into two main categories, those techniques that create ordered topographies and those that create unordered topographies (Norman and Desai, 2006).

Unordered topographies are generally spontaneously formed during processing. Polymer demixing, chemical etching and colloidal lithography are typical

methods to create unordered topographies (Norman and Desai, 2006). Polymer demixing can create nanoscale pits, islands, and ribbons. The shape and size of these features can be controlled to an extent by adjusting the polymer ratio and concentration although there is little control in the horizontal direction. Chemical etching can only increase the roughness of the surfaces without any specific geometry or organization. Colloidal lithography can create large patterned surfaces with heights and diameters controlled by varying the colloid size and the area covered by colloids. However, the area covered by the colloids is modified by changing the ionic strength of the colloid solution.

The techniques used to create unordered topographies are normally more time and cost effective than those to create ordered topographies. However, the organization and orientation of the patterns obtained are randomly distributed, the geometry of which cannot be controlled with any precision (Norman and Desai, 2006). Furthermore, early researchers have already demonstrated that cells not only respond to the surface roughness in general but also selectively discriminate between surface roughness details. However, the biocompatibility literature demonstrates a lack of knowledge on which cells respond to which specific surface roughness cues as well as an adequate qualification and quantitation of 'roughness'. In this case therefore, it becomes more important to have controlled topographies. Luckily, with the modern techniques, it is possible to create ordered topographies which can be refabricated and characterized precisely.

Ordered topographies can be fabricated in several ways: photolithography, microcontact printing, cast moulding and electron beam lithography are commonly used techniques. Photolithography is the most commercially advanced method and is used to pattern parts of a thin film or a substrate in microfabrication. A wet-etching step is required after the Ultraviolet (UV) exposure. The feature sizes can be extended to below 50 nm(Tseng et al., 2005). Microcontact printing is nowadays widely used in cell biology, surface chemistry and microelectronics. The technical problems with this technique are that the direct contact method causes stamp deformation, substrate contamination, swelling of the stamp and ink mobility(Miller et al., 2009, Byrne et al., 2002). All these problems make this technique very costly. Cast moulding has similar problems. In this process, a polymer precursor is poured into a mould and allowed to cure to form an inverse replica of the mould (Zhao et al., 1997). Electron beam lithography is a commercially well-established technique. It is capable of obtaining much greater patterning resolution as well as very small features down to nanoscale. It is maskless and the final pattern achieved directly from a digital representation on a computer. But it is time-consuming compared with photolithography(Tseng et al., 2003, Quake and Scherer, 2000).

The above mentioned techniques to fabricate ordered topographies are either time consuming or costly or both. In this thesis, we introduced photoembossing which is both time saving and cost effective.

Photoembossing is a relatively new, simple and environment-friendly technique to create surface topographies, where a mixture of a multifunctional monomer, a polymer binder and a photo-initiator are used. The photoembossing procedure through photomask involves creating a thin film from the mixture by UV light irradiation through a patterned contact photomask followed by heating and flood UV exposure (Hughes-Brittain et al., 2012). There is no etching step as in the photolithography process.

Photoembossing through holographic lithography is used to texture the surface of electrospun fibres. This is more effective than photoembossing through a contact photomask on fibres, because it doesn't require a contact mask to create the texture as the fibres used are randomly oriented and not in the same plane. In this technique, an interference pattern between two or more coherent light waves which are split from one laser beam is set up and recorded in a recording layer (photoresist)(Toader et al., 2004). However, it also limited to patterning arrayed features only.

Both of these methods of photoembossing were used in this research to fabricate very precise surface topographies.

1.4 The influence of biomaterial surface characteristics on cells

Because of its chemical component, surface topographies, mechanical properties etc., biomaterials influence the cells in various ways, such as in cell viability, cell adhesion, cell proliferation, cell migration, cell morphology and even endothelialisation. In this thesis, we focus on the influence of surface characteristics. It should be noted that there are no biomaterials with truly smooth surfaces on a molecular level except certain mica surfaces which are rare in any case.

Harrison (Harrison, 1912) first reported the migration of cultured cells that were guided by spider webs. This discovery was later supported by other researchers (Loeb and Fleisher, 1917, Weiss, 1929). The term ‘contact guidance’ was introduced by Weiss (Weiss, 1945) to describe cell orientation and cell migration in response to topographic underlying substrata. Contact guidance of different cell types on a variety of topographic textures was later observed but very little quantitative examinations of cell reactions to the topographies was made (Curtis and Wilkinson, 1998). Actually, the fact that cells are influenced by the surface topography did not receive much attention until the early 1970s (Rovensky et al., 1971). Dunn and Brown (Dunn and Brown, 1986) demonstrated that, on grooved surfaces, 90% of fibroblasts (which are less than 20 μm diameter) elongation is determined by the ridge width while the groove width has little influence, and the alignment is

inversely proportional to ridge width on grooved surfaces. Samples with groove width from 1.65 μm to 8.96 μm, repeat spacing from 3 μm to 32 μm and the same depth at 0.69 μm were used in their study. Clark *et al.* (Clark et al., 1990) also found that cell alignment is inversely proportional to spacing, and that the depth of groove plays the dominant role in cell alignment. Samples with pitches from 4 μm to 24 μm and depth from 0.2 μm to 1.9 μm were used in their study. Oakley and Brunette (Oakley and Brunette, 1993) exhibited a sequence of the alignment of microtubules, focal contacts and microfilament bundles when the fibroblasts spread on a grooved substrate. Korman *et al.* (Korman et al., 1984) suggested that agents such as fibronectin that stimulate cell attachment and cell spreading were produced by cells when they attach to the textured surfaces. Schmidt and von Recum (Schmidt and von Recum, 1992) showed that, in macrophages, cell metabolic rates were modified by the surface texture. Green *et al.* (Green et al., 1994) demonstrated that on a pillared surface, cells have a higher growth rate on the pillars compared with the wells. Meyle *et al.* (Meyle et al., 1993) proved that dependent on the groove width, focal adhesions prefer to form on top of ridges rather than in grooves. For grooved patterns which contain ridges and channels, strong alignment in the direction of the channel was observed by either varying the width of ridge (Den Braber et al., 1996, Britland et al., 1996a) or depth of channel (Britland et al., 1996a, Clark et al., 1990). According to the literature, most cell types are distinctly aligned to the ridge at 4 μm (Den Braber et al., 1996) and channel at 6 μm (Clark et al., 1990) widths which are both narrower than the diameter (10-20 μm) of the cells in suspension (Singhvi et al., 1994). Contact guidance

has also been reported to stimulate growth (Singhvi et al., 1994, Uttayarat et al., 2005b, Laco et al., 2013), protein synthesis (Chesmel et al., 1995, Teixeira et al., 2003, Mukhatyar et al., 2011), proteinase secretion (Hong and Brunette, 1987, Williams et al., 2011, Ludwig et al., 2002), and phagocytosis activities (Wójciak-Stothard et al., 1996, Brandhonneur et al., 2009, Arora et al., 2013) in different cell types.

A frequently asked question in this area is whether it is the chemical cue or topography or both that is the reason for cell reaction to the surfaces of the substrates. Britland *et al.* (Britland et al., 1992) introduced photolithographed patterned protein substrates to investigate the effect of topography, the resultant guidance of the cell movement confirming the influence of surface topography. This was also supported by other research using the same method (Clark et al., 1992, Britland et al., 1996b). However, this did not prove whether the cells were reacting to the height of individual molecules or just the discontinuities from the molecular ordering (Curtis and Wilkinson, 1997). In order to investigate this question, Pritchard *et al.* (Pritchard et al., 1995) designed another system with the height of adjacent steps less than the size of a molecule by filling the spaces with proteins or silicones. The results, which showed successful cell attachment, could be explained by the cells attaching to the junctions where there might be molecular discontinuity. From the above studies, it appears that cells show greater attachment at the junctions or at areas of molecular discontinuity. Further work by Britland *et al.* (Britland et al., 1996b) suggested that when the height of grooves was less than 500 nm, chemical cues would be the leading influence whereas topographic cues

become the dominant influence when groove height is higher than 500 nm up to a height of 5 μm. This conclusion is supported by other research (Curtis et al., 1996, Den Braber et al., 1995). Table 1.2 shows the most commonly studied topographies.

Table 1.2 Types of commonly studied topographies

Type of topography	Typical references
Single cliffs	(Clark et al., 1987, Nuzzo, 1996, Berry et al., 2004, Lee et al., 2014)
Grooves and ridges ❖ V-section ❖ Rectangular section ❖ Multiple grooves ❖ Branching ❖ Spiral grooves	(Curtis and Varde, 1964, Riehle et al., 1998, Meng and Hou, 2011) (Clark et al., 1991, Seemann et al., 2005, Guvendiren and Burdick, 2013) (Clark et al., 1990, Brunette et al., 1983, Lim and Donahue, 2007, Carpenter et al., 2012) (Ternaux et al., 1992, Frey et al., 2006, Ding et al., 2013) (Dow et al., 1987a, Li and Shi, 2007, Anene-Nzelu et al., 2013)
Dots and pits ❖ Spikes ❖ Hill	(Rovensky Yu and Samoilov, 1994, Craighead et al., 2001, Koufaki et al., 2011) (Olson, 1993, Barbucci et al., 2003, Wang et al., 2011)
Tunnels and tubes	(Aebischer et al., 1990, Sanford et al., 1948, Parker and Kinnersley, 2004, Kristl et al., 2013)
Fibres	(Weiss, 1934, Weiss, 1945, Nair et al., 2004, Cardwell et al., 2012)
Cylinders	(Rovensky Yu and Samoilov, 1994, Rosa et al., 2003, Le et al., 2011)
Mesh	(Curtis and Seehar, 1978, Chua et al., 2006, Nandakumar et al., 2013)
Random roughness	(Lydon and Clay, 1985, Dalby et al., 2007, Rosales-Leal et al., 2010)

The effects of topography depth have not been studied extensively until recent years. This is perhaps partly because of the lack of development in methods of measuring such small scale textures. Moreover, researchers have suggested that the situation is complicated by the fact that different cell types may react differently to the same substrates (Wójciak-Stothard et al., 1996, Clark et al., 1990, Clark et al., 1991). Clark *et al.* (Clark et al., 1987) demonstrated that the reaction of cells to a single cliff increases as the height increases from 1 μm to 20 μm. He also demonstrated that cells react to the groove width and the number of adjacent grooves on the groove and ridge substrates (Clark et al., 1990, Clark et al., 1991). Wójciak-Stothard *et al.* (Wójciak-Stothard et al., 1996, Wojciak et al., 1995) reported that macrophage-like cells can react with surface topographies as shallow as 44 nm. Other studied cell types, such as epitena, endothelia, epithelia and fibroblasts, are not as reactive but can still respond to topographies as shallow as 70 nm. On grooved and ridged surfaces, most types of cells grow along the groove length, but Nagata *et al.* (Nagata et al., 1993) exhibited neurites that grow perpendicular to the length of grooves. It is widely known that cell orientation increases as the relief structure grows from 1 μm to 25 μm in height (Rajnicek et al., 1997, Rajnicek and McCaig, 1997). Additionally, according to Den Braber *et al.* (Den Braber et al., 1995, Den Braber et al., 1996), when the grooves are deeper and narrower, cells might bridge across the ridges. Moreover, when the grooves are wider and shallower, cells show good conformation to the surfaces (Curtis and Wilkinson, 1998).

On a groove and ridge substrate, when the pitch is larger than the cell, there is no noticeable influence on cell orientation (Clark et al., 1987), such an influence only becoming apparent when the pitch is reduced to the cell size or less. Clark *et al.* (Clark et al., 1992) demonstrated that BHK cells can react to a pitch as small as 260 nm with a height of 500 nm. Rajnicek *et al.* (Rajnicek et al., 1997) compared grooves sizes at 1, 2, 4 μm width and 14 nm–1.1 μm depth with different cells, Xenopus cell and hippocampal cell. The former one presents alignment along the grooves of all sizes while the later one only align the wide and deep grooves. Lu *et al.* (Lu and Leng, 2003) presented that when the feature sizes are close to the cell size, human osteoblasts show improved alignment when the features are 4–38 μm in width and 2, 4, 10 μm in depth. They also exhibited that myoblasts show better alignment compared to osteoblasts when the feature sizes are 8, 24 μm in width and 2–10 μm depth (Lu and Leng, 2009). Transfected human corneal epithelial cells elongate on the grooves with 0.2–2 μm width and 0.4 μm depth (Karuri et al., 2008). Uttayarat *et al.* (Uttayarat et al., 2005a) demonstrated that the alignment of endothelial cells are enhanced by increasing the depth when the feature sizes are 3.5 μm in width and 0.2–5 μm in depth. Further more, Biela *et al.* (Biela et al., 2009) presented that the alignment of endothelial cells increase as the groove width decrease and the depth increase when the feature sizes are 2–10 μm in width and 0.05–0.2 μm in depth.However, with some cell types, there will be greater alignment when the cells are not in contact with each other but are isolated from each other (Clark et al., 1991).

Cells move randomly on flat surfaces (Gail and Boone, 1972), whereas cell movement is normally oriented to grooves and ridges surfaces. Biela *et al.* (Biela et al., 2009) exhibited that smooth muscle cells migrate along the grooves.Curtis *et al.* (Curtis et al., 1995) reported that cells on a grooved substrate tend to move in one direction for a considerable time before reversing or changing direction. But there are exceptions. According to Dow *et al.* (Dow et al., 1987b), cells move centrifugally instead of along the grooves and no cells move centripetally. The phenomenon of contact inhibition also affects cell movement. Curtis and Varde (Curtis and Varde, 1964) demonstrated that chick-heart fibroblasts on grooved substrates with pitches between 12.5 μm and 25 μm showed stronger contact inhibition than on flat surfaces. Moreover, contact inhibition increases as pitch size decreases while decreasing with fibre size.

There are very few studies of cell movement on surface topographies. Curtis *et al.* (Curtis et al., 1995) examined accelerated cell movement on grooves but did not present quantitative data. Li *et al.* (Li et al., 2001) claimed that endothelial cells exhibit a higher migration speeds on 15 μm pitch grooves when compared with 30 μm and 60 μm pitches. Only recently, Franco *et al.* (Franco et al., 2012) elucidated more details about cell movement on textured surfaces.

Fibres are also commonly used in tissue repair nowadays. Jenkins *et al.* (Jenkins et al., 1977) were the first to successfully repair tendinous-ligament using commercial carbon fibres. Recent research used randomly packed fibres in cartilage tissue repair and dermal replacements (van Wachem et al., 1994).

Curtis and Varde (Curtis and Varde, 1964) suggested that cells accumulated along the concave side of curved fibres. Curtis and Seehar (Curtis and Seehar, 1978) found that fibroblasts and endothelia grow from the intersections of fibres and form a monolayer by filling in the mesh holes. Wojciak-Stothard *et al.* (Wojciak-Stothard et al., 1997) demonstrated cell alignment and enhanced movement along the very fine fibronectin fibres.

The way the actin cytoskeleton organizes when reacting to topography is generally accepted to be related to cell movement. Moreover, the sensitivity of movement is similar on grooved and flat surfaces (Wójciak-Stothard et al., 1996). Furthermore, focal adhesions are believed to be aligned over or close to the contact with grooves and ridges (Wójciak-Stothard et al., 1996, Meyle et al., 1994, Meyle et al., 1995, Den Braber et al., 1998, Uttayarat et al., 2005a).

Van Wachem *et al.* (van Wachem et al., 1987b) demonstrated that initial cell adhesion of HUVECs is promoted by the pre-adsorption of fibronectin (Fn) from a serum contained culture medium. Dickinson *et al.* (Dickinson et al., 2012) presented that endothelial cells show enhanced elongation and alignment on the soft polydimethylsiloxane (PDMS) substrate compared with the stiff SiO_2 substrate with the similar surface topographies. Additionally, there is only one surface of endothelial cells attach to the basement membrane (Watt and Huck, 2013). Other researchers also indicated that the full adhesion response involved both cross-linking of integrins and mechanical input through these transmembrane receptors (Craig and Johnson, 1996, Wang et al., 1993, Ingber, 1993, Burridge and Chrzanowska-Wodnicka, 1996, Choquet et al., 1997).

Pelham and Wang (Pelham and Wang, 1997) demonstrated that not only were focal adhesions more regular and stable on rigid substrates compared to those on flexible ones, but also the phosphorylation was greatly reduced on flexible substrates.

Yim *et al.* (Yim et al., 2010) expressed the view that the actin cytoskeleton was aligned with patterned substrates while it was random and denser on unpatterned ones. He also indicated that both nanotopography and substrate stiffness were important to the mechanical properties of the cells, while nanotopography was more dominant in organizing the cytoskeleton and focal adhesions.

A crucial problem of artificial vascular implants, especially those with diameters less than 4 mm, is thrombus and neointima formation. One approach to prevent thrombosis and to improve the biocompatibility of artificial implants is to create a functional, quiescent monolayer of endothelial cells on the lumenal surface of implants (Lin et al., 1994, Uttayarat et al., 2005b). Vascular endothelium controls the transport of substances from the blood into the vessel wall (Dejana, 2004, Dejana et al., 2009, Franco et al., 2012), so the destruction of this control can cause cardiovascular disease (Komatsu et al., 1998). It is important therefore, to understand and accelerate the healing of the endothelium after wounding in order to avoid the beginning of focal disease (Franco et al., 2012). On a polymer scaffold, adhesion and proliferation of endothelial cells are both affected by chemical constitution and roughness of the surface. But according to the literature, when the depth of the groove

texture is higher than 500 nm, the topography will have a much stronger effect on the cells (Curtis and Wilkinson, 1998). In addition, surface topography has been proven to incite changes in the morphology and orientation of adherent endothelial cells (Uttayarat et al., 2005b, Kooten and Recum, 1999, Jiang et al., 2002).

Surface topography also affects the surface wettability which is also an important factor in cell attachment and proliferation. According to van Wachem (van Wachem et al., 1987a), a substrate which is too hydrophilic or too hydrophobic is not ideal for the attachment and proliferation of HUVECs. Tzoneva *et al.* (Tzoneva et al., 2007) demonstrated that cell adhesion and the organization of the cytoskeleton of endothelial cells are controlled by the surface wettability of the substrate. Similar results are also shown in other cell types and materials (Grinnell, 1977, Baier et al., 1968, Coleman et al., 1982, Horbett et al., 1985, Lydon et al., 1985, Hattori et al., 1985). Den Braber *et al.* (Den Braber et al., 1995) suggested that wettability influences cell viability but does not affect cell shape and orientation on microtextured surfaces. Moreover, the most suitable water contact angle of the substrates for culturing cells could be different from cell to cell as well as on various kinds of material substrates. For instance, Tamada and Ikada (Tamada and Ikada, 1993) pointed out that a polymer surface with a water contact angle of 70 º is most suitable for fibroblastsadhesion. However, Lee *et al.* (Lee et al., 1998) demonstrated that 55 º is the most suitable water contact angle for culturing Chinese hamster ovary, fibroblast, and endothelial cells when comparing polyethylene substrates with different water contact angles from 43 º to 96 º. Arima and Iwata (Arima

and Iwata, 2007) showed that HUVECs reached the highest attachment when the water contact angle is 60-70 °while HeLa cells is 50 °when using CH_3/OH mixed SAMs substrates with contact angles from 30 °to 110 °. Shen *et al.* (Shen et al., 2013) exhibited that the cell migration is enhanced with the increase of hydrophobicity of the substrate with water contact angles from 26 °to 98 °.

In vivo research has also taken place and has shown great advances. Powell and Gibbons (Powell and Gibbons, 1982) demonstrated that there were huge differences between breast capsules containing smooth or textured implant material. The sac containing textures with 75 μm square pillars and 150 μm heights showed greater cellularity and lower collagen density compared with the smooth implants. However, their results also showed that these textured implants with those dimensions still stimulated chronic inflammation. Pollock (Pollock, 1993) published a retrospective study of nearly 200 patients, the results of which showed that less capsular contraction happened with the silicone implants with textured surfaces than the ones with smooth surfaces. Additionally, Smahel *et al.* (Smahel et al., 1993) demonstrated in rats that compacted capsule development was prevented by textured polymeric surfaces compared with smooth ones. However, neither Pollock nor Smahel gave details of the textures they used, such as shape, size and distribution. When reviewing the published histologic response literatures, Schmidt and Von Recum (Schmidt and Von Recum, 1993) found significant differences in cell response between higher and lower parts of the surface profile of National Institutes of Health (NIH) reference material, polydimethylsiloxane (PDMS). In those

literatures, the sides were not identified but the histological variance could only be because of the surface topography.

Even though how the surface topographies influence the tissue response has not been fully elucidated, a great number of studies show that the capsule thickness and tissue interfacial motion have a direct correlation. Kupp *et al.* (Kupp et al., 1982) demonstrated that the surface roughness of intramuscular implants was related to capsule thickness and speculated that the causative factor was the degree of interfacial motion. Picha and Drake (Picha and Drake, 1990) reported a reduction of interfacial motion on fixing the capsule to sutures thereby reducing capsular thickness which resulted in significantly improved tissue response. It seems clear that the micro motion between the tissue and implant must be taken into consideration as a cause of contraction, chronic inflammation and capsule thickening.

Porous implants were introduced to avoid the consequences of the dead space between tissue and implants in 1950s (Edwards and Tapp, 1955), and have been extensively studied since then. According to the bulk of results published, porous implants allow the ingrowth of soft and hard tissue when the pore sizes are larger than 10 μm and 75 μm, respectively. However, they do not promote the attachment of the ingrowing tissue to the implant (Gangjee et al., 1985), so it seems that these porous implants do not completely eliminate the dead space but achieve a mechanical interlocking between the tissue and implants.

Micropores and groove surface topographies were introduced to promote tissue attachment and a significant influence on cell migration and cell proliferation were reported (Vonrecum, 1990). Recum *et al.* (Recum et al., 1996) investigated a nylon fibre mesh coated with polyvinylchloride/polyacrylonitrile with pore sizes varying between 0.5 μm to 10 μm and found pore sizes between 1 μm to 3 μm showed excellent tissue attachment without any inflammation.

Jenkins *et al.* (Jenkins et al., 1977) successfully used the first commercial carbon fibre to reconnect a ruptured ligament, but it was not as successful with other sites in the body. During the following twenty years, rough surfaces and woven and non-woven fibre meshes were used without quantitative assessment. It is only recently that quantitative experiments with cells have taken place before the use of topographies in implants. However, it is obvious that in order to design the best implants, quantitative analysis with cells in vitro is a prerequisite for in vivo utilization.

It is crucially important to be able to characterize the surface topographies of the substrates for both in vitro and in vivo researches and subsequent applications, which requires the substrates to be accurately produced to controlled specifications. Moreover, precision and quantification are both needed in examining cells for bioengineering. It is well known that surface topographies ranging from 1 μm to 100 μm can affect individual cells (Desai, 2000) and that alignment is inversely proportional to ridge width on grooved

surfaces (Dunn and Brown, 1986). Additionally, sharp edges of about 90 degrees can promote cell attachment (Recum et al., 1996).

1.5 Biodegradable materials

In therapeutic applications, both permanent and temporary aids are needed to meet various functional requirements. Non-degradable biomaterials can provide mechanical support required for a permanent aid. However, biodegradable materials are necessary for temporary aids which are only required to stay in the body for a limited time until the tissue or organs recover and rebuild. For the design and development of biodegradable materials, it is necessary to understand the fundamentals of the biodegradation phenomena and the response of cells and tissue to these materials.

There are two main sources of biodegradable materials: naturally derived and synthetically fabricated (Minal and John, 2008). Degradation may also proceed along two main routes: hydrolytic and enzymatic (Nair and Laurencin, 2007). Collagen, elastin, chitosan, gelatin and hyaluronic acid are commonly used as natural biomaterials. Enzymatically degradable natural polymers such as albumin, fibrin, collagen, chitin and hyaluronic acid (Domb et al., 1997) were already in use in biomedical applications since thousands of years ago, but the use of synthetic degradable biomaterials only began in the late 1960s (Barbucci, 2002). Due to the difficulty in controlling the physical and chemical properties

and the limitation in applications of natural biomaterials, the majority of researchers now focus on studying synthetically fabricated biomaterials. These can be modified according to the physical and chemical properties required and most importantly, can be repeatedly produced.

Biodegradable materials used in medical engineering are normally organic materials that can eventually degrade into CO_2 and H_2O. The majority of biodegradable materials contain in their molecular backbones, labile linkages such as amides, anhydrides, carbonates, esters, orthoesters, ureas and urethanes (Li, 1999). The most commonly used hydrolytically degradable biomaterials are derivatives of glycolic acid (GA), lactic acid (LA), and polyester (Minal and John, 2008). The most promising biodegradable polymer is believed to be the copolymer constituted from LA and GA which has great biocompatibility and a variable degradation rate that can be controlled by changing the ratio between LA and GA (Kronenthal, 1975, Holland et al., 1986, Vert et al., 1992, Li and Vert, 2002). The commercial products made from these copolymers, such as sutures, drug delivery devices, clips and staples, plates and screws, are already widely used in therapeutic applications.

The copolymer of Polylactic acid (PLA) and Polyglutamic acid (PGA) is obtained from cyclic diesters through ring-opening polymerization (Gilding and Reed, 1979, Zhang et al., 1994, Löfgren et al., 1995, Schwach et al., 1996). The chirality of the LA units enables the adjustment of degradation rates and mechanical properties of the poly(lactic-co-glycolic acid) (PLGA) copolymers (Miller et al., 1977, Vert, 2004, Nakamura et al., 1989). The higher the

proportion of LA the copolymer has, the more slowly it degrades. However, when the LA and GA is at 1:1 ratio, the shortest degradation period of two months is reached. The degradations of PLGA polymers have been broadly studied both in vivo and in vitro, and researchers are agreed that amorphous regions degrade preferentially during the degradation process due to the carboxyl end groups which are obtained from chain cleavage (Holland et al., 1986, Vert et al., 1992, Li and Vert, 2002). However, there are still controversies in the literature concerning the degradation location, degradation rates and the role of enzymes in vitro (Holland et al., 1986, Vert et al., 1992, Li and Vert, 2002).

Poly(ethylene glycol) (PEG) is another biocompatible and degradable material which has been extensively studied in medical engineering since the 1970s (Davis, 2002), because it does not generally cause immune responses (Zalipsky and Harris, 1997). PEG can be formed into a hydrogel, which can be chemically well-defined, through cross-linking (Macromers). The molecular weight of PEG may vary, and hence, is also known as polyethylene oxide (PEO) or polyoxyethylene (POE)(Alcantar et al., 2000). PEG is widely used in pharmaceutical products as the basis of laxatives and excipient (Smolinske, 1992). When attached to different protein medications, PEG slows down the clearance of the carried protein from the blood resulting in an extended medicinal effect and reduced toxicity (Bowman, 2004).

An eligible biodegradable material must meet the following requirements. Firstly, it should not be toxic or cause any sustained inflammation in the body.

Secondly, the degradation time and mechanical properties should be sufficient for the healing or regeneration process. Thirdly, the degradation products also should not be toxic and should eventually be metabolized and cleared. Additionally, it should have an adequate shelf life and ideally, be capable of modification for other intended applications. (Lloyd, 2002)

Due to the complicated nature of biodegradable biomaterials in which the physical, chemical and biological properties have to be considered for clinical use and which also may vary over the degradation period, the development of the biodegradable material has been quite slow compared with other kinds of materials (Nair and Laurencin, 2007).

1.6 Aim

Our aim is to investigate how HUVECs reacts with the newly developed photopolymers formed into various substrates with specific surface topographies by observing their attachment, proliferation, morphology and migration.The precisely fabricated surface topographies enable us to quantify the influences on cells, so that ideal substrates to meet different requirements can be designed.

1.7 Objectives

With the premise that surface topography influences cell behaviour and that increased surface roughness could enhance cell adhesion, growth (Chung et al., 2003) and migration of endothelial cells, we patterned photopolymer films by photoembossing with a variety of depth and pitches to investigate their influence on cell proliferation, shape and migration of HUVECs through MTS assay, SEM and fluorescence observations, and wound healing assay. Additionally, we textured electrospun fibers by photoembossing through holographic lithography to investigate the effects on cell adhesion and cell shape with regard to both the physical characteristics of fibres (such as sizes and directions) and the surface textures by examine the FAs and F-actin under confocal microscope. Lastly, the degradation and biocompatibility of fully degradable photopolymer is discussed.

Chapter 2 Materials and methods

2.1 Cell culture

HUVECs (Lonza Group Ltd. UK) were cultured in T25 flasks (Sigma-Aldrich Co. LLC) using M199 (Life Technologies Ltd.) supplemented with 10 % foetal bovine serum (FBS), 3 μg/ml Endothelial cell growth supplement from bovine neural tissue, 1 ng/ml β-endothelial cell growth factor, 10 μg/ml Heparin,1.25 μg/ml Thymidine, 10 units/ml Penicillin, 0.2 mMol/ml L-glutamine, and 10 mg/ml Streptomycin (all supplements were purchased from Life Technologies Ltd.) at 37 ℃ in 95% air/5% CO_2. Cells were sub-cultured every 7 days, and the culture medium was changed every 2 days. Cells only at passages 3-7 were used in all reported experiments. It has been previously shown that cells between passages 3-7 behaved in a similar manner in response to surface topography (Uttayarat et al., 2005a).

Before seeding HUVECs on to any substrates in the following experiments, they were washed 3 times with Dulbecco's Phosphate-Buffered Saline (DPBS) (Life Technologies Corporation) and then trypsinised with Trypsin-EDTA Solution (Sigma-Aldrich Co. LLC) for 1 min in an incubator at 37 ℃. 1 ml FBS and 3 ml culture medium were added to the flask. With a pipette, as many cells as possible were gently flushed off the culture surface. The cell suspension was transferred into a Corning® 15 ml centrifuge tube (Sigma-

Aldrich Co. LLC) and centrifuged for 5 min at 2000 r/min. The supernatant was discarded, 3 ml fresh culture medium was added and this cell suspension was again centrifuged for 5 min at 2000 r/min. The supernatant was again discarded and 1 ml fresh culture medium added to suspend cells again. The cells were counted with a Haemocytometer and then seeded onto the substrates at the required density. The remaining cells were subcultured or frozen, the medium being changed every 2 days until required further.

2.2 Photopolymer mixture

Various mixtures of polymers, monomers and photo initiator, which we called the photopolymer mixture, were used in the production of substrates by photoembossing. We set up three systems meeting different real-life requirements to produce non-degradable-, semi-degradable- and fully-degradable substrates. In the photopolymer mixtures presented in our work, there is a polymer binder, one or two multifunctional monomer(s) and a photo initiator dissolved in solvent(s).

Polymer binders are required to have a high glass-transition temperature (T_g) so that the mixtures can be solid at room temperature (RT) and weak interactions with the monomers can lead to a good monomer mobility (Hughes-Brittain, 2013). Poly(methyl methacrylate) (PMMA) and PLGA are used as polymer binders. Due to its excellent biocompatibility and low cost, PMMA is

already extensively used in medical technologies such as in hard contact lenses (MacRae et al., 1985), bone cement in orthopaedic surgery (Rho et al., 1993), dentures (Vallittu, 1996), intraocular lenses (Apple, 2006) and has also been injected under the skin to reduce wrinkles or scars permanently in cosmetic surgery (Lemperle et al., 1998). PMMA was first used in bone cement in 1943, is still in wide clinical use today. PLGA is mainly used for therapeutic devices which are readily approved by the Food and Drug Administration (FDA) because of its biocompatibility and biodegradability. It is a copolymer of PLA and PGA, the ratio between them deciding the properties of the copolymer, such as solubility and biodegradability (Chung et al., 2006). In the body, PLGA degrades by hydrolysis into lactic and glycolic acid (Zolnik and Burgess, 2007). Additionally, these two monomers are also by-products of various metabolic processes in the body under normal physiological conditions. PLGA is commonly used in implants (Bhardwaj and Blanchard, 1998), grafts (Lee et al., 2003), drug delivery (Bala et al., 2004), prosthetic devices (Kim and Martin, 2006), sutures (Lim et al., 2009) and surgical sealant films (Zhang et al., 2012).

The monomers we used were required to be miscible with the polymer binders, and this was confirmed by differential scanning calorimetry (DSC) with the assistance of a co-worker, Dr. Hughes-Brittain and data presented in her thesis (Hughes-Brittain, 2013). The monomer used in both the non-degradable and semi-degradable systems is trimethylolpropane ethoxylate triacrylate (TPETA). We compared TPETA and dipentaerythritolpenta-/hexa-acrylate (DPPHA) and chose TPETA for the following experiments due to its better biocompatibility demonstrated in cell viability results. Details can also be found in the thesis of

my partner, Dr. Hughes-Brittain (Hughes-Brittain, 2013). For the degradable system, poly(ethylene glycol) diacrylate (PEGDA) and DL-Dithiothreitol (DTT) are used as the multifunctional monomers.

2-Benzyl-2-(dimethylamino)-4′-morpholinobutyrophenone (Irgacure 369) is used as photo initiator which is an UV curing agent and was confirmed to be biocompatible in our experiments.

The solvent used consisted of propylene glycol monomethyl ether acetate (PGMEA), chlorobenzene (C_6H_5Cl), dimethyl sulfoxide (DMSO), chloroform ($CHCl_3$) and dimethylformamide (DMF) and used as required.

2.3 Film preparation and photoembossing

In the film preparation process, each of the polymer binders PMMA and PLGA, TPETA monomer and biocompatible photo initiator Irgacure 369 were dissolved in the organic solvent PGMEA. The films were prepared using a wire bar coater (Figure 2.1) which can create, on a flat surface, thin films of a smooth and uniform thickness ranging from 4 μm to 80 μm depending on the size of the trough produced between the adjacent coils of the wire wound round the bar coater. The photopolymer mixture was coated onto 13 mm glass cover slips, and the solvent was evaporated in an oven at 80 ℃ resulting in dry films with a thickness of 60±5 μm. To produce smooth surface films, the dry films were exposed to the UV light (OmniCure® S1500 spot UV curing lamp)

directly at full power for 1000 seconds (sec) causing the photopolymer to fully polymerize. For grooved films, the dry films (Figure 2.2 A) were overlaid with a photomask designed to produce repeated grooves of the desired pitch and then exposed to UV light (Figure 2.2 B) of the required dosage, followed by a heating stage (Figure 2.2 C). In this stage, the unreacted monomer diffuses into the reacted areas and the relief structure is created. Finally, the prepared films are again exposed to UV light at full power for 1000 sec allowing the monomer to fully polymerize. All the samples were further dried under vacuum at room temperature for 24 hours to evaporate any possible remaining solvent.

Figure 2.1 Wire bar coaters

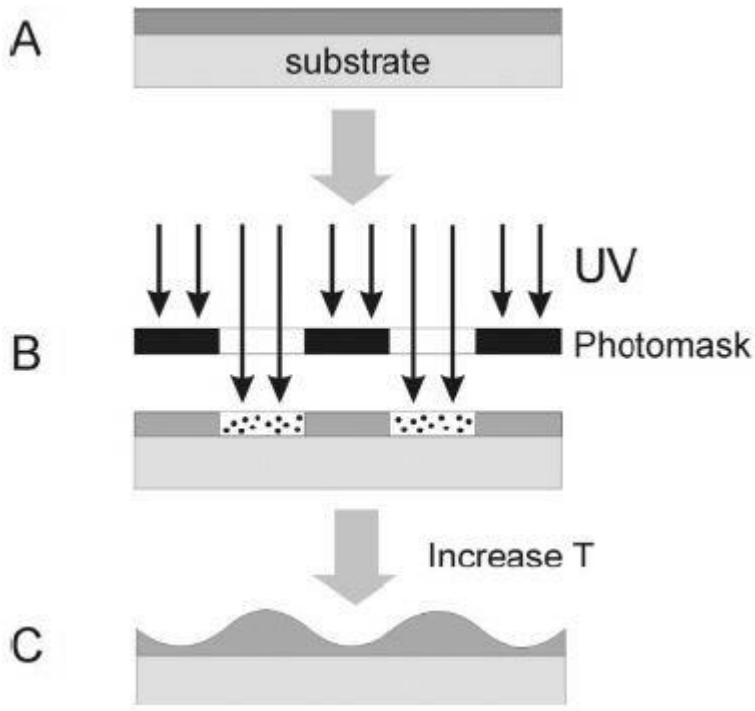

Figure 2.2 Schematic of photoembossing process (Adams et al., 2006) (A) a film on a substrate (B) the film is exposed to UV through a photomask (C) a relief structure is created by the diffusion of the unreacted monomers with a certain heating temperature.

The glass cover slips on which the various substrates were fabricated and investigated were first specially treated to remove any static electricity which may cause the polymer films to detach from the glass cover slips in the culture medium. Before coating with pure PMMA and PLGA, any static charge was removed from the glass cover slips using a static eliminator bar. The cover slips to be coated with photopolymers were acrylate functionalized by immersing overnight in a solution containing 30 ml toluene, 30 µl acrylate silane and 50 µl triethylamine and drying in a fume cupboard.

Figure 2.3 Photomask

Different sizes of photomasks (Figure 2.3) were used to obtain grooved films with different pitches. Our previous work confirmed that relief heights can be controlled by changing temperature during the heating stage and the UV dosage used in the first exposure with the photomask (Hughes-Brittain et al., 2014b).

Our choice of texture heights employed in this research was based on the agreed concept that vertical walls beyond a maximum height prevented adequate cell contact (Curtis and Wilkinson, 1998), and on our previous and other available research that confirmed the effectiveness of cell response

within a certain range of heights. This thesis focussed on the reaction of HUVECs to photoembossed substrates within these height parameters.

2.4 Electrospinning fibre

Electrospinning is a fabrication technique widely used in producing ultrafine non-woven nanofibres from polymer solutions or melts in a relatively simple way (Formhals, 1934, Miqin, 2007, De Vrieze et al., 2007, Frenot et al., 2007, De Vrieze and De Clerck, 2009). This method combines the features of electrospraying and conventional solution dry spinning of fibres (Ziabicki, 1976). It can produce solid threads from solution without using either high temperature or coagulation chemistry which is especially suitable for making fibres with large and complex molecules. The molten precursors guarantee there is no solvent left in the obtained product.

Electrospraying was first reported in the early 17^{th} century by Gilbert and Lochman (Gilbert and Lochman, 1628) in an early investigation of magnetic and electrostatic phenomena. According to their report, when a piece of amber was electrostatically charged within a certain range, a cone shape would form from a droplet of water which is near the amber and small droplets would be ejected from the tip of the cone. The similar process of electrospinning was initially patented by J.F. Cooley (Cooley, 1902) and W.J. Morton (Morton, 1902). John Zeleny (Zeleny, 1914) published the behaviour of fluid droplets at

the end of metal capillaries during the electrospinning, attempting to model the electrostatic forces mathematically.

In the early 20th century, natural silk was much in demand but extremely expensive, stimulating a search for a cheap substitute. Formhals (Formhals, 1934) reported a device which could be used to produce silk-like fibres and was soon followed by Norton (Norton, 1936) who formed fibres from a melt by air-blast assisted electrospinning. In the early 1990s, organic polymers were used to fabricate nanofibres by electrospinning (Doshi and Reneker, 1995, Li and Xia, 2004). Electrospun nanofibres ranging from 50 nm to 1000 nm were later produced by drawing polymer solution or melt from a capillary to a collector in an electric field (Reneker and Chun, 1996, Huang et al., 2003, Inai et al., 2005).

Taylor (Taylor, 1964, Taylor, 1966, Taylor, 1969) began a systematic investigation of electrospinning in the1960's. He mathematically modeled the shape of the fluid droplets formed under an electric field during electrospinning. This characteristic droplet shape is now known as the Taylor cone. Later, he worked with Melcher (Melcher and Taylor, 1969) and developed the 'leaky dielectric model', which illustrated theoretically the behavior of the conducting fluids.

Reznik *et al.* (Reznik et al., 2004) reported extensive work on the shape of the Taylor cone and the subsequent ejection of a fluid jet. Hohman *et al.* (Hohman et al., 2001) investigated the relative growth rates of the numerous proposed

instabilities in an electrically forced jet and endeavored to describe the most important instability in the electrospinning process, namely, the bending (whipping) instability.

The physical principle of electrospinning is based on forces acting on a droplet of a solution at a tip of a needle. The droplet at the needle tip has a surface tension which causes the droplet to be more rounded to minimize surface area. When a high electrical potential difference is applied between the needle and the earthed charged collector, electrostatic forces are then generated by electrostatic repulsion between the surface charges and Coulombic forces exerted by the applied electric field. When the electric potential increases, the droplet at the tip of needle elongates till the Taylor cone is formed. When the electric field gets higher, the electrostatic forces overcome the surface tension causing further elongation of the droplet to form a jet (Figure 2.4) (Yang et al., 2002, Enayati et al., 2011). The solution properties, flow rate, needle diameter, distance between needle and collector and the potential difference can all affect the resulted fibres (Pareta et al., 2005, Xie et al., 2008, Ahmad et al., 2008, Yao et al., 2008).

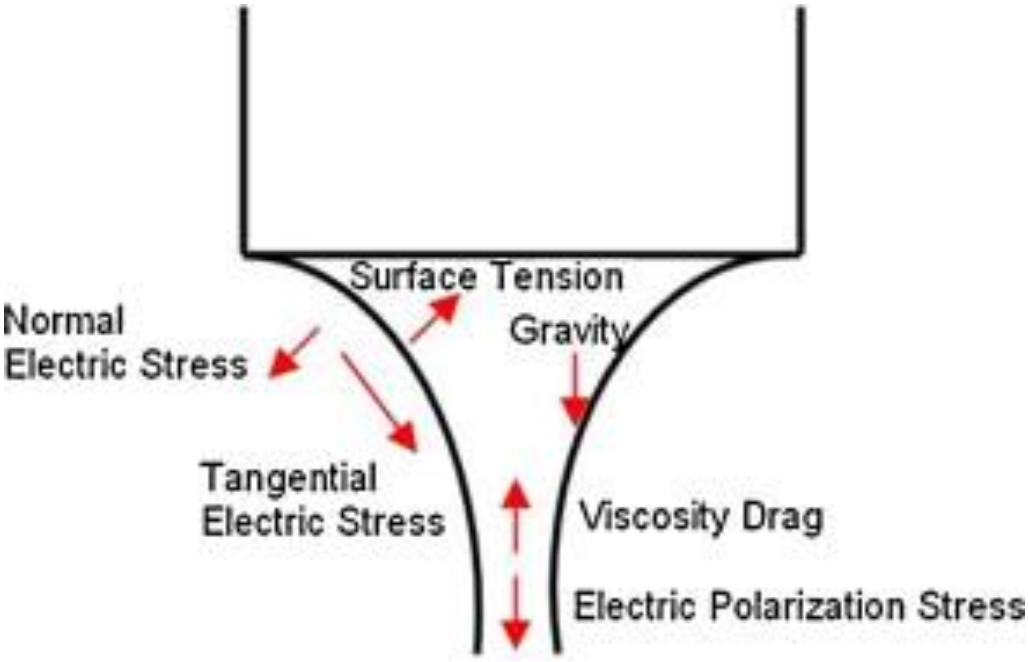

Figure 2.4 Schematic of the jet formation in the electrospinning process (Enayati et al., 2011)

Different systems of electrospinning can produce a variety of nanofibrous structures with two-dimensional (2D) or three-dimensional (3D) shapes, such as aligned nanofibres (Yang et al., 2005, Xu et al., 2004), nanofibrous yarn (Teo et al., 2007, Wang et al., 2008), tubular structures (He et al., 2009) and core-shell nanofibres (Zhang et al., 2006) (Figure 2.5). As a result of this flexibility and versatility in the electrospinning process, it has become the most popular method for the fabrication of microfibres and nanofibres (Dong et al., 2009).

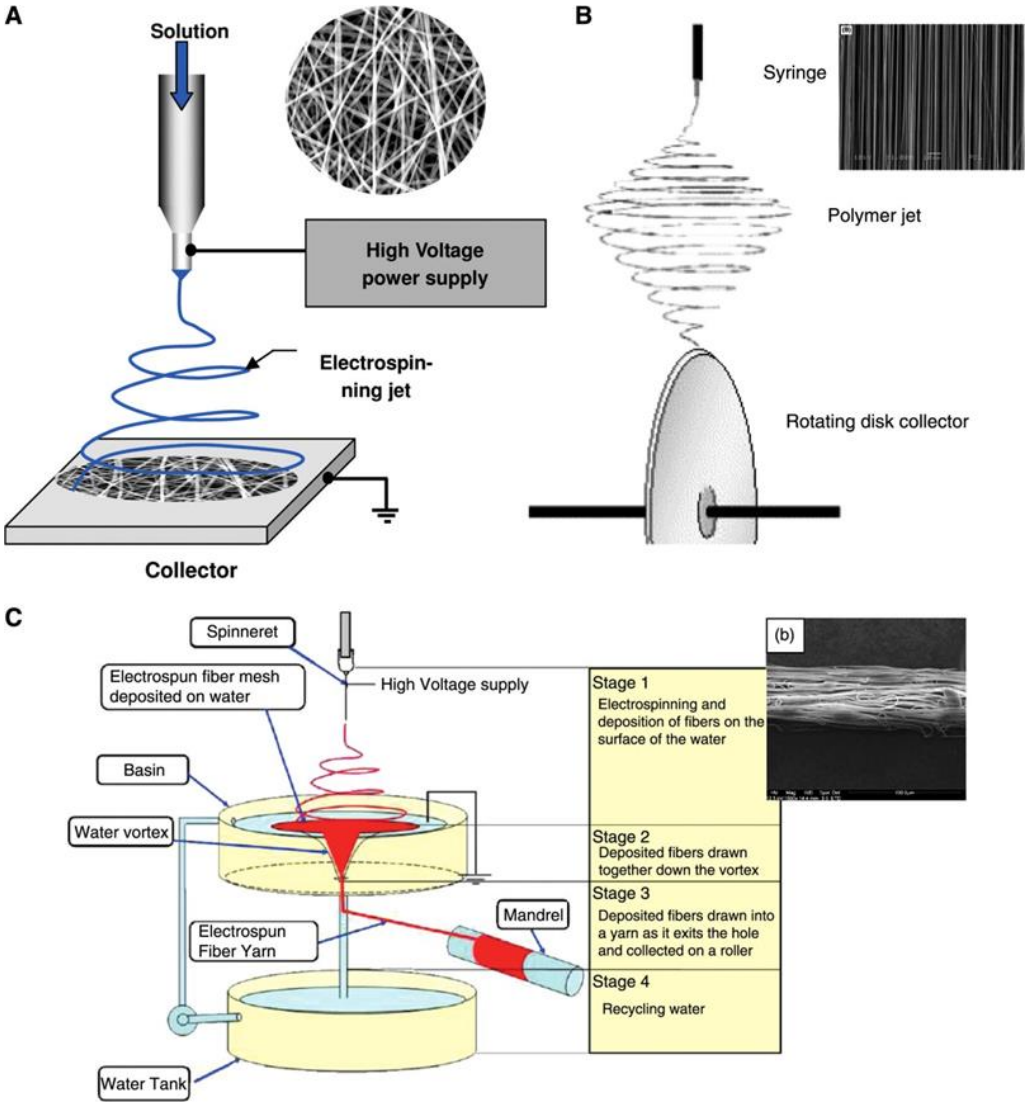
A
Solution
High Voltage
power supply
Electrospin-
ning jet
Collector
B
Syringe
Polymer jet
Rotating disk collector
C
Spinneret
Electrospun fiber mesh
deposited on water
High Voltage supply
Basin
Water vortex
Electrospun
Fiber Yarn
Mandrel
Water Tank
Stage 1
Electrospinning and
deposition of fibers on the
surface of the water
Stage 2
Deposited fibers drawn
together down the vortex
Stage 3
Deposited fibers drawn into
a yarn as it exits the hole
and collected on a roller
Stage 4
Recycling water
(b)

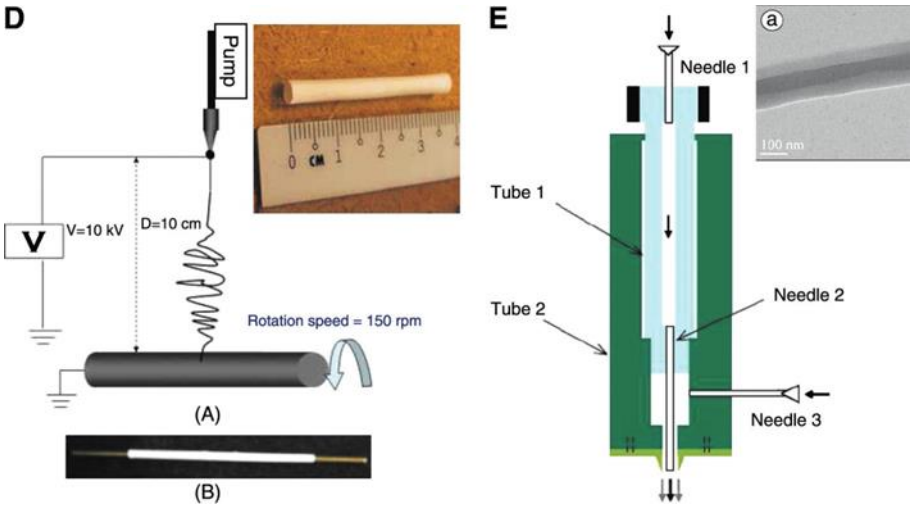

Figure 2.5 Schematic diagrams of different electrospinning setups with resultant structures in the upper right corner. (A) Standard electrospinning setup (Dong et al., 2009). (B) Aligned electrospinning, with the fibre collected on the edge of a fast rotating disk (Xu et al., 2004). (C) Nanofibrous yarn collected from fluidic system (Teo et al., 2007). (D) Tubular structure collected from a rotating wire (He et al., 2009). (E) Core-shell nanofibre fabricated using a coaxial electrospinning setup (Zhang et al., 2006).

2.5 Holographic photoembossing

Holography is a 3D imaging technique. Holographic photoembossing is based on the concept of interference and diffraction of light. In our experiments (Figure 2.6), a pulsed Nd:Yag laser is coupled to second and third harmonic modules emitting 4 ns pulses of 355 nm linearly polarized light with vertical polarization (repetition rate 10 Hz). The laser is used as the sole light source in this process because it has a fixed wavelength and can be precisely controlled. The laser beam was split into two laser beams with the same wave length by the beam splitter, so that interference is caused when they are superimposed. The photopolymers samples are placed at the point where diffraction occurs

and the photoembossed texture result from the interference patterns produced by the laser. The exposure was made in air at room temperature.

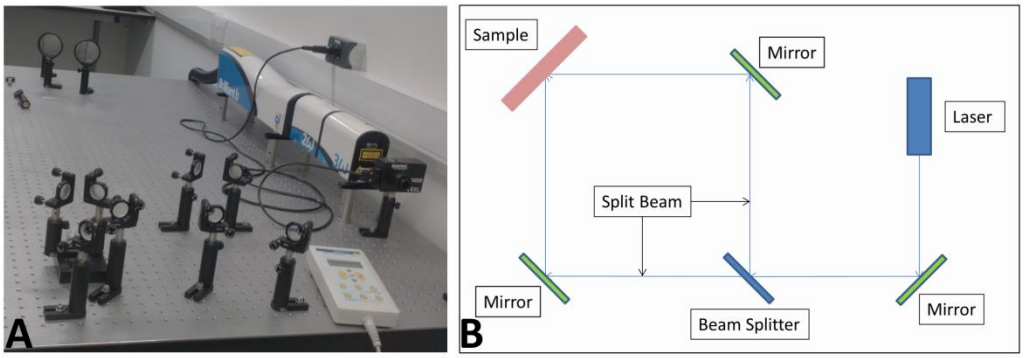

Figure 2.6 (A) Holographic photoembossing set up and (B) schematic of holographic photoembossing

This is followed by heating and UV exposure stages as in the procedure used in photoembossing with a photomask. However, this method does not require the samples to be in contact with anything which makes it extremely suitable for embossing fibres which are randomly orientated and not in the same horizontal plane.

2.6 Cell proliferation

Cell proliferation was measured with CellTiter 96® AQueous One Solution Cell Proliferation Assay (Promega Corporation) containing 3-(4,5-dimethylthiazol-2-yl)-5-(3-carboxymethoxyphenyl)-2-(4-sulfophenyl)-2H-

tetrazolium, inner salt (MTS). The live cells react with the tetrazolium salt in the MTS reagent to produce a formazan dye which can be observed at 490nm with a 96-well plate reader. The extent of cell proliferation on the surface of both smooth and grooved photopolymers films was determined at time points of 1, 2, 3, 5 and 7 days. 13 mm glass cover slips, pure PMMA and PLGA films were used as control respectively for the different systems. At each time point, samples were washed 2 times with a serum free culture medium to remove non-adherent cells and then transferred to a new 24-well plate. These samples were incubated for 3 hours with 50 µl MTS reagent in 250 µl of serum free culture medium. The recommended incubation time is between 1 and 4 hours, but based on our experiments (Figure 2.7), 3 hours was selected in all MTS assays. Aliquots of the samples were put into a 96-well plate and their absorbance was read on a FLUOstar Galaxy Multi-functional Microplate Reader at 450nm (According to the instructions, data can be recorded at wavelengths of 450-540 nm). The absorbance of five known cell numbers 5,000, 10,000, 25,000, 50,000 and 75,000 were used to produce a standard curve to convert absorbance readings to cell numbers (Kumbar et al., 2008).

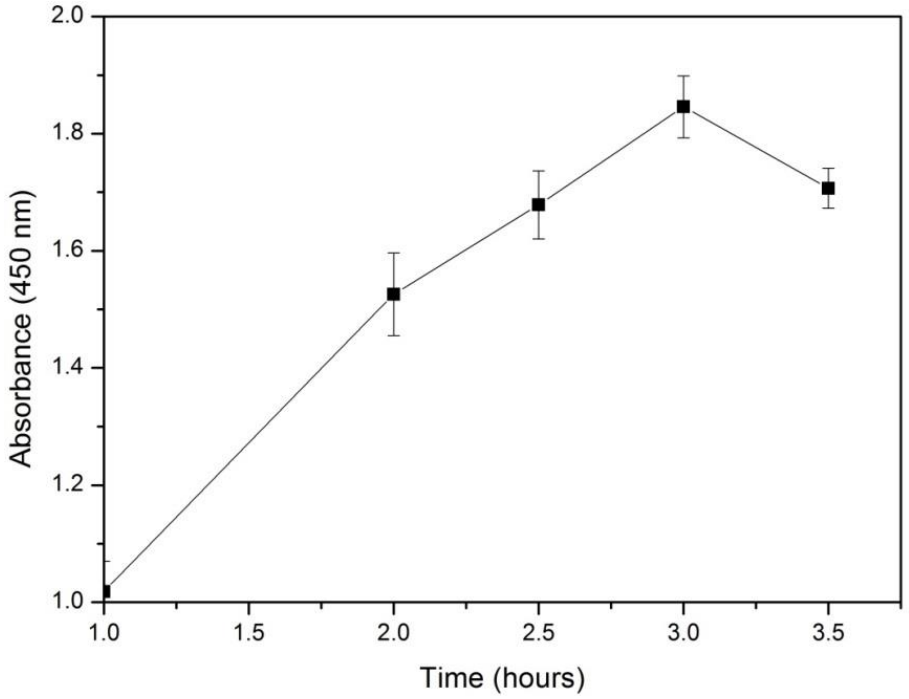

Figure 2.7 Time points results of MTS assay with 2.5×10^4 cells

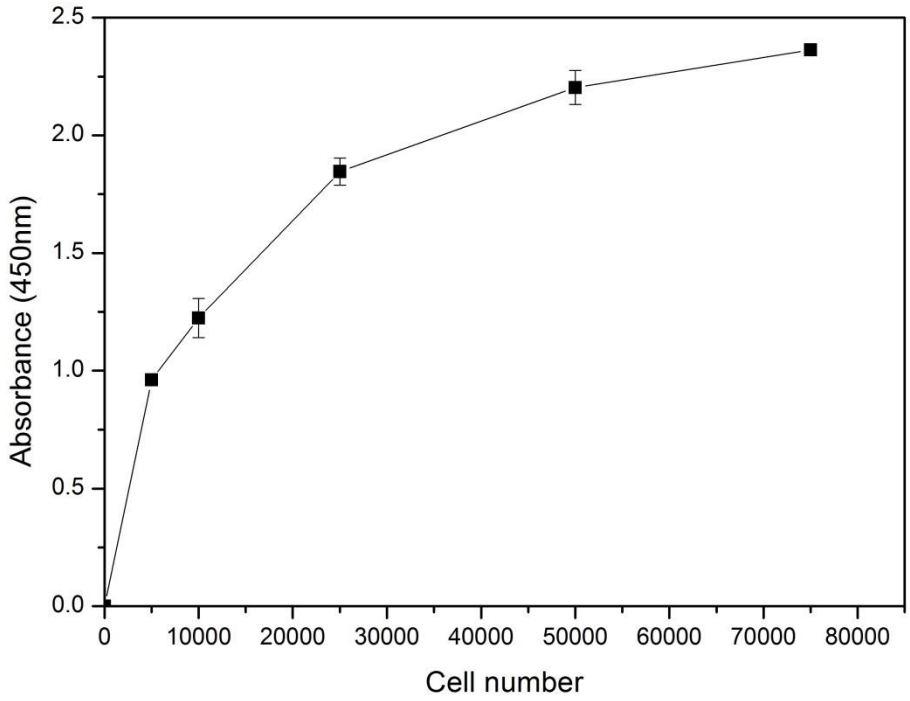

Figure 2.8 The absorbance readings of standard cell numbers

2.7 Epifluorescence microscope

An epifluorescence microscope (Figure 2.9) is a simple version of the fluorescence microscope, a kind of optical microscope that uses fluorescence and phosphorescence to study properties of substances (Webb and Brown, 2013).

The fluorescence microscope is based on the phenomenon that certain materials emit energy detectable as visible light when irradiated with the light of a specific wavelength(Lichtman and Conchello, 2005). As shown in Figure 2.9, the excitation filter only allows radiation of a desired wavelength to pass through and collide with the atoms in the sample, exciting the electrons to a higher level. As they revert to a lower energy level, the electrons emit visible light. An emission filter between the detector and the objective is used to eliminate the remaining excitation light from fluorescent light leaving a background of high contrast(Lichtman and Conchello, 2005, Sarder and Nehorai, 2006).

However, there are limitations to the fluorescence microscope, which also apply to both the epifluorescence microscope and the confocal microscope which will be introduced in the next section. First of all, photobleaching limits the time available for examining samples due to the chemical damage caused during the electron excitation process. Secondly, short wavelength light is toxic to live cells. Additionally, it can only detect the specific structures which are

labelled for fluorescence; however, this could also be an advantage when only these specific structures are needed to be examined.

Samples were prepared in a sterile environment. They were washed 3 times with DPBS and fixed with 4% paraformaldehyde (PFA) for 8 minutes (min). They were again washed 3 times with DPBS after each stage in the fluorescence staining procedure which followed. Finally, when all the staining steps were completed, a 3 times wash with DPBS and 2 wash with deionized water (DI-water) completed the procedure.

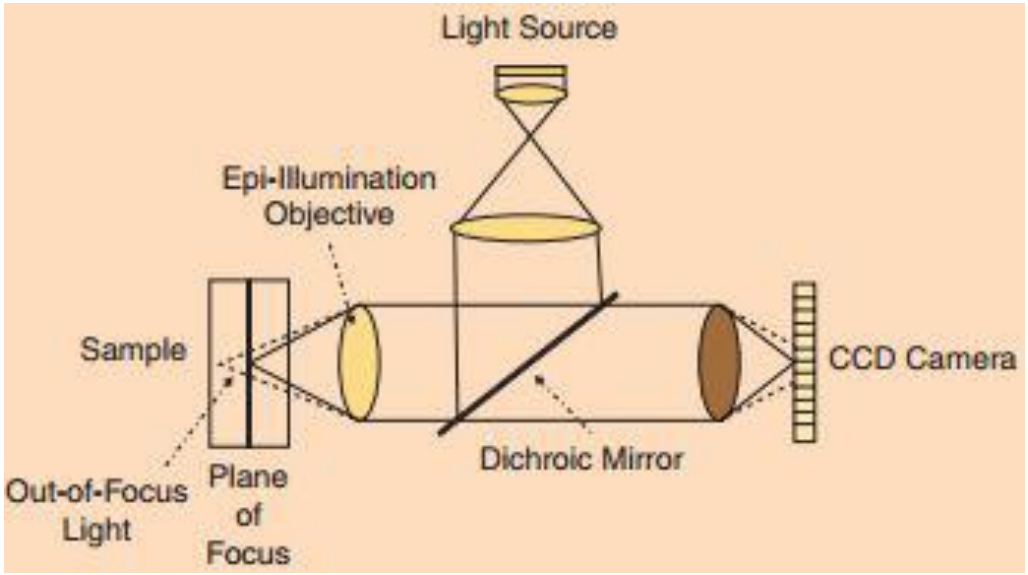

Figure 2.9 Schematic of epifluorescence microscope (Sarder and Nehorai, 2006)

2.8 Confocal microscope

A confocal microscope is both a scanning microscope and a more complicated design of fluorescence microscope to increase optical resolution and

micrograph contrast (Pawley, 2006). Marvin Minsky (Minsky, 1961), a young postdoctoral fellow, first patented the principle of confocal microscopy in 1957. Compared with the conventional epifluorescence microscopy, by using point illumination and a pinhole before the signal detector, confocal microscopy can eliminate out-of-focus signals and leaving only those in focus. Additionally, only one point at a time will be illuminated which prevents photobleaching of the whole sample.

As the only light source, a laser provides monochromaticity, coherence, polarisation and intensity. Moreover, the image resolution, especially in the depth direction is improved because the stage scanning technology allows it scan the specimen accurately along each focal plane(Gu, 1996).

As shown in Figure 2.10, the laser beam passes through a beam splitter and is focused by an objective lens into a small focal volume within the sample. The signals emitted by the sample come back through the objective, dichromatic mirror and pinhole after which the intensity of the signal is detected, converted into a digital signal and recorded by the computer. Then the scanner directs the laser beam onto the next focal volume and the procedure is repeated until the whole sample is scanned. Each focal volume is represented by a pixel in the resulting image.

Samples are prepared in the same way as those for the epifluorescence microscope.

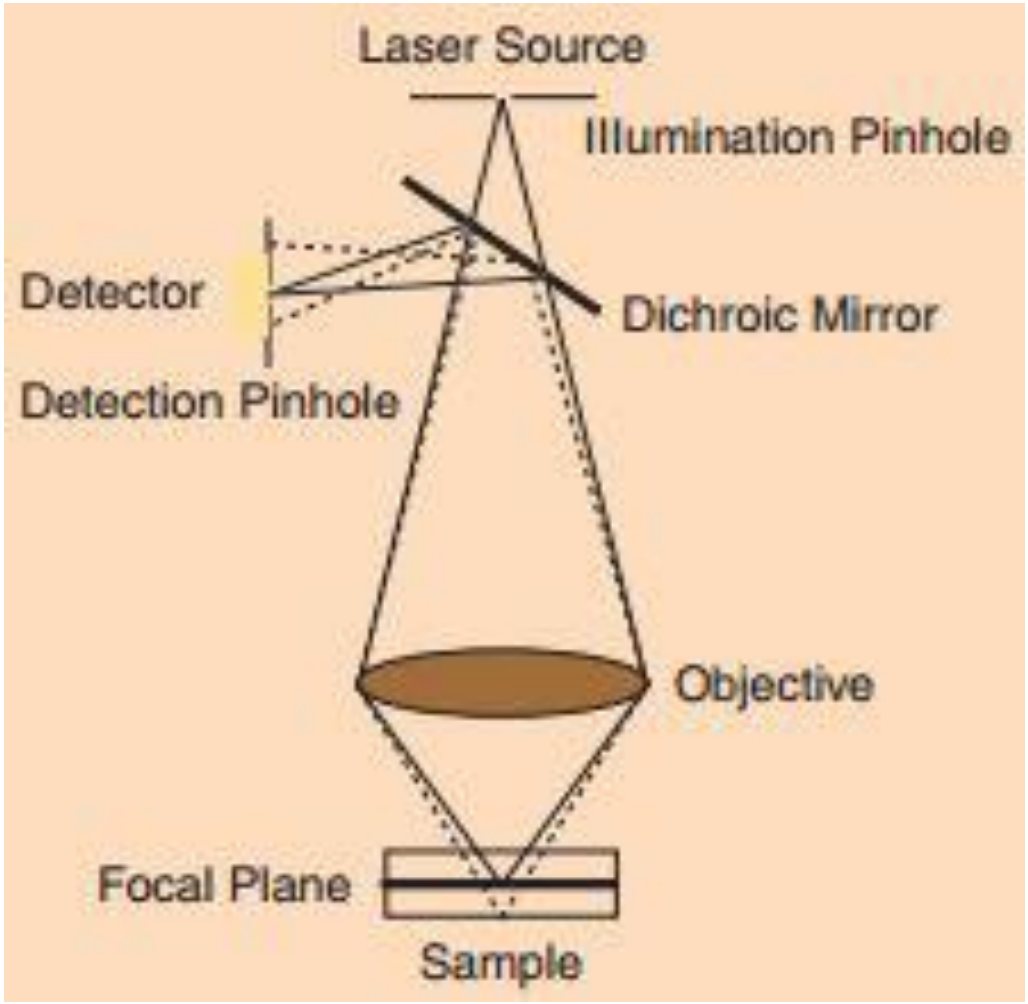

Figure 2.10 The principle of the confocal microscope (Sarder and Nehorai, 2006)

2.9 Scanning electron microscope (SEM)

An SEM is a type of electron microscope that uses electrons instead of light to form an image of a sample. In comparison to traditional microscopes, an SEM has many advantages including higher resolution, large depth of field, and more control in the degree of magnification (Smith and Hashemi, 2010), which allows it to be used in microstructure studies, fracture characterization, surface

contamination examination, thin film evaluation, and failure analysis of materials. During characterization, a high energy electron beam, produced from an electron gun in an evacuated column above the sample surface, focuses onto the target surface. The low-angle backscattered electrons interact with the surface atoms generating a variety of electronic signals as shown in Figure 2.11. The types of signals include secondary electrons (SE), back-scattered electrons (BSE), characteristic X-rays, light cathodoluminescence (CL), specimen current and transmitted electrons (Joshi et al., 2008).

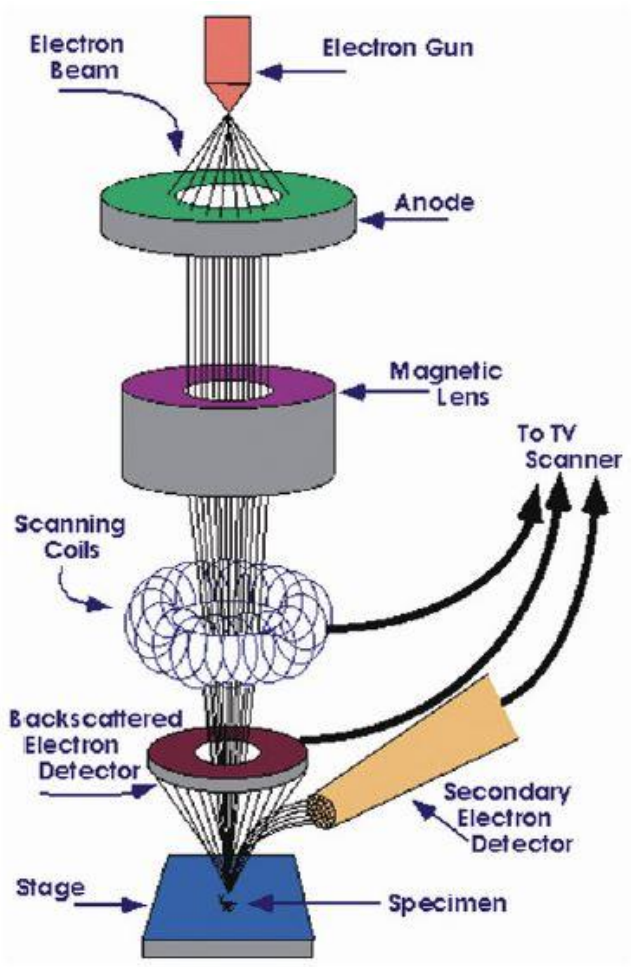

Figure 2.11 Schematic diagram of SEM (Joshi et al., 2008).

The surface of the specimen must be electrically conductive in a traditional SEM examination. However, the Environmental SEM (ESEM) can be used to image uncoated non-conductive samples by placing them in a high-pressure chamber with a short working distance between the electron gun and the specimens (Donald, 2003).

Samples seeded with cells for SEM were dehydrated with ethanol of different concentrations at 10%, 30%, 50%, 70%, 90%, 95% and 100% for 15 min each after fixation with 4% PFA. The samples were then dried overnight in a vacuum. The dried samples as well as samples without cells were attached to aluminum stubs using sticky carbon tabs and coated with gold. In this study, a secondary electron detector was used. The prepared samples were placed in the vacuum chamber of the SEM which was operated with a working energy of 10 kV, a beam size at a value of 3 and a working distance of 10 mm. Images at a variety of magnifications were collected.

2.10 Atomic force microscopy (AFM)

AFM was used to quantitatively characterize the morphology of photoembossed surfaces. Figure 2.12 shows the basic principles of AFM (Microscopy, 2005). The tip precisely situated on a flexible silicone cantilever is mounted to a piezoelectric driver. During the scanning, the tip is brought to a

chosen point over the sample surface where the resultant force can repel or attract atoms from the tip leading to a deflection of the cantilever. The degree of cantilever deflection, which is changed relatively by the surface topography, can be measured by a laser light reflected from the cantilever into a position sensitive detector (PSD). In this way, the roughness of the material surface can be mapped out point by point without any direct contact. AFM enables scanning in the x/y or x/y/z directions and the construction of a surface image from different viewpoints without extra surface treatment such as metal or carbon coating (Giessibl, 2003).

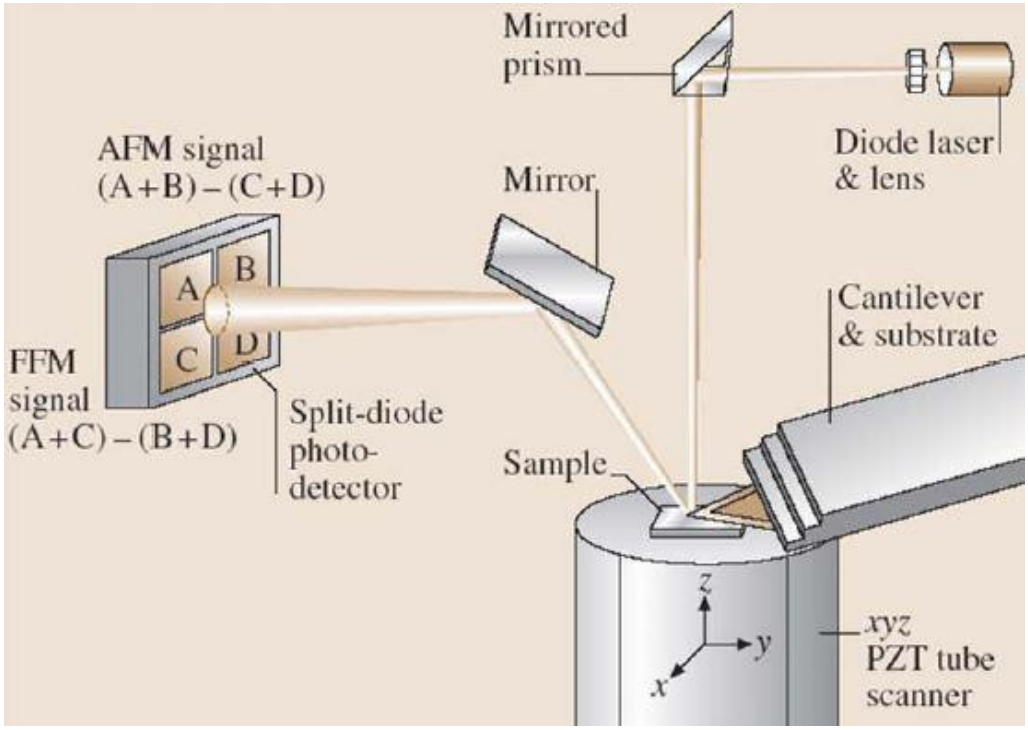

Figure 2.12 The basic principles of atomic force microscopy (AFM) (Microscopy, 2005)

The surface morphology of photoembossed samples was characterized using an AFM (AFM, NT-MDT®) in contact mode at a 512 x 512 scanning resolution. Scan areas ranged from 600 nm x 600 nm to 10 μm x 10 μm. In the contact mode, the tip makes a soft physical contact with the sample surface and scans at a constant small height above the surface where the overall force is repulsive. The force between the tip and the sample is fixed during scanning by maintaining a constant deflection.

2.11 Contact angle

The wettability of biomaterial surfaces is an important factor in their use and is expressed by the Water Contact Angle (WCA). This is a measure taken at the interface between liquid/vapor and a solid surface. The characteristics of a WCA are a result of the surface free energies between the liquid, solid and surrounding vapor when a small liquid droplet rests on a flat horizontal solid surface. In order to mathematically express the WCA, the shape of the dropped liquid is measured to calculate the slope of the tangent to the droplet at the liquid-solid-vapor interface line (Kwok et al., 1997, Buschow et al., 2001). The WCA is commonly used in membrane material science to describe the relative hydrophobicity/hydrophilicity of a membrane surface.

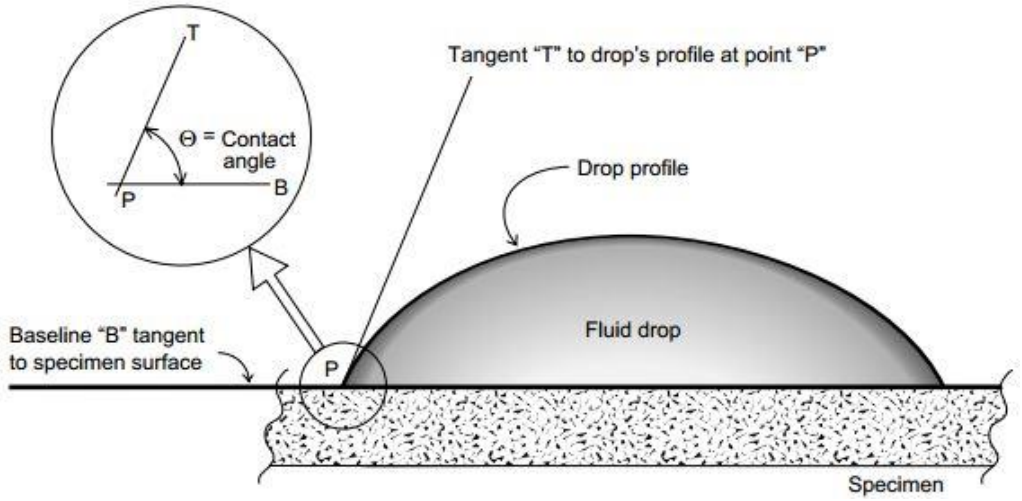

Figure 2.13 The schematic diagram of contact angle measurement (Woodward).

The WCAs of both smooth and embossed photopolymer films were measured with a dynamic contact angle system, as shown in Figure 2.13 (Woodward). The water droplet was observed spontaneously spreading along the dry surface until an equilibrium angle was established. The equipment can also be used to measure the surface tension, adhesion characteristics, and surface energy and uses drop shape analysis to measure contact angles and thereby determines surface energy. The image of the drop shape is captured by an equipped camera. The shape and size of the droplets were analyzed using FTA 32V 2.0 software. The contact angle was measured 5 times for each individual sample and at least 5 samples were measured for each kind of films, the average value then being calculated. Wettability is divided into three classes: absolute wetting when $\theta = 0°$, partial wetting for $\theta < 90°$, and non-wetting for $\theta > 90°$ (Drelich et al., 2000).

Chapter 3 Interaction between HUVECs and photoembossed non-degradable biomaterial films

The major problem in vascular grafts is thrombus. A promising approach to overcome these issues is to create a functional, quiescent monolayer of endothelial cells on the surface of implants. In this way, cell adherence to the extracellular matrix (ECM), morphogenesis, immunity and wound healing may be influenced (Burridge and Chrzanowska-Wodnicka, 1996, Geiger et al., 2001). In this study, photoembossing is introduced as a method of creating surface relief structure. PMMA is used as the polymer binder and TPETA is used as a multifunctional monomer. Biocompatibility of pure PMMA film, which is confirmed to have good biocompatibility and used widely in medical devices nowadays, is compared to that of both smooth and embossed photopolymer PMMA-TPETA films. The influence of surface texture on surface wettability and cell attachment, morphology and proliferation is then discussed. Finally, cell migration is studied through a wound-healing assay on photoembossed films with surface texture of various dimensions and orientations.

3.1 Materials and methods

3.1.1 Materials

Apolymer binder PMMA with a molecular weight of 120,000 g/mol, multifunctional monomer TPETA, photo initiator Irgacure 369 and solvent PGMEA (all obtained from Sigma Aldrich) were used in this study. The CellTiter 96® AQueous One Solution used in the MTS assay was purchased from Promega Corporation. CellTracker™ Probes for Long-Term Tracing of Living Cells were obtained from Invitrogen.

3.1.2 Smooth and grooved films

The polymer binder PMMA, TPETA monomer and biocompatible photo-initiator Irgacure 369 were dissolved in the organic solvent PGMEA. PMMA and TPETA were in the proportion of 50:50 by weight and Irgacure 369 at 5% by weight of TPETA. All components were dissolved in 60% by weight of PGMEA. All films were prepared as described in 2.3. To produce surface textured samples, films were covered with a photomask and exposed to UV light for 30 sec and then heated for 20 min at 120 ℃, which our previous studies had indicated was the optimum developing temperature (Hughes-Brittain et al., 2014b). Different specifications of photomasks and UV dosages were used to produce grooved films with different pitches of 6 μm, 10 μm, and 20 μm and at a height of 1 μm for the majority of our experiments. Films with

a groove pitch of 20 μm were also fabricated with a groove height of 2.5 μm for comparison purposes.

3.1.3 Cell culture

HUVECs from passages 3 to 7 were cultured as described in 2.1. Before cell seeding, the substrates were washed 3 times with 75% ethanol and rinsed 3 times with DPBS. When the cells reach around 80% confluency in a T25 (25 cm^2) cell culture flask, cells were seeded onto the substrate at a density of 1.5×10^4 cells/cm^2 in 24-well plates and cultured up to 7 days for a proliferation assay and 14 days for a wound-healing assay. As the normal endothelial cells are at 35-50 μm in wide and get into logarithmic phase at day 3 (Gimbrone et al., 1974), in order to avoid cell inhibition caused by too many cells on a 13 mm glass cover slip, in the meantime, cells are expected to be confluence after 7 days, so that cell seeding densities at 1×10^4 cells/cm^2, 1.5×10^4 cells/cm^2 and 2×10^4 cells/cm^2 were tested. Cell seeding density at 1×10^4 cells/cm^2 showed less confluence at day 7 and cell inhibition was observed at 2×10^4 cells/cm^2. Untreated glass cover slips were seeded with cells and used as controls.

3.1.4 Cell proliferation assay

Cell proliferation on the surfaces of both smooth and grooved PMMA-TPETA films was determined at time points of 1, 2, 3, 5 and 7 days. Untreated 13 mm glass cover slips and cover slips coated with pure PMMA films were used as

controls. Cell proliferation was measured as described in 2.6. Each experiment was repeated at least 5 times in triplicate.

3.1.5 Analysis of films and cells morphology

Groove sizes were measured by AFM (NT-MDT®) in semi-contact mode at randomly selected locations on a number of samples ($n \geq 5$). The surface wettability of each kind of film was also measured by a dynamic contact angle system.

After the cell culture stage, the surface morphology of both the smooth and grooved substrates was examined using an SEM (FEI Inspect-F®). Following 3 washes with DPBS, cells were fixed in 4% PFA for 8 min. After rinsing 3 times each with DPBS and DI-water, samples were dehydrated as described in 2.9. Dried samples were sputter coated with gold before being examined in an SEM at a voltage of 10 kV.

3.1.6 Wound-healing assay

After cells were confluenced, a scratch was made across each sample surface using a 200 μm width metal slice after which the medium was replaced with 1 ml fresh complete medium. At the start of the experiment (t=0) and at time points 2, 3 and 4 hours after beginning incubation, samples were stained and analysed under an epifluorescence microscope. Each experiment was repeated at least 5 times in triplicate.

3.1.7 Immunostaining

HUVECs seeded on 20 μm pitch photoembossed films always seem to fade into the substrates when observed under an optical microscope. To avoid this problem, the cells were stained with the CellTracker™ Red CMPTX and examined under an epifluorescence microscope. The HUVECs were washed 3 times with culture medium and then stained with the CellTracker for 15 min at room temperature, again washed 3 times with culture medium and then kept in culture medium with 10% FBS. At the beginning of the experiment (t=0), cells were stained before being scratched. At the other time points, cells were stained before analysing in order to prevent the fluorescence intensity of the samples from being quenched. Due to the bleaching of the samples during examination, different samples were used for each group at different time points. Experiments are repeated 5 times and each time samples are prepared in triplicate.

3.1.8 Data analysis and statistical methods

All quantitative measurements are reported as mean values ± standard deviation. To determine the statistical difference when comparing different groups, a student's t-test was used.

3.2 Results

3.2.1 Synthesis and characterization of photoembossed PMMA-TPETA films

The polymer binder PMMA, TPETA monomer and biocompatible photo-initiator Irgacure 369, at a ratio of 1:1:0.05, were dissolved in 60% by weight of PGMEA as we have published previously (Hughes-Brittain et al., 2012). The films were obtained by wire bar coating on 13 mm glass cover slips, resulting in a thickness of 60±5 μm, and then placed into an oven at 80 ℃ to evaporate the solvent. To produce smooth films, after drying, the pre-coated films were exposed to direct UV light for 1000 sec at full power causing all the monomers to polymerize. For grooved films, the pre-coated films were exposed through contact photomask of the desired characteristics, exposed to UV light for 30 sec and then heated at 120 ℃ for 20 min to accelerate the diffusion of unreacted monomer. It was necessary to adjust the UV output to produce different groove heights. The percentage of UV lamp output was at 30% for 6 μm and 10 μm pitch samples to obtain a height of 1 μm and 20% and 40% for 20 μm pitch samples which resulted in a 2.5 μm and 1 μm height, respectively. This was followed by a further exposure to UV light for 1000 sec at full power to cause any remaining monomers to fully polymerize. Photoembossed PMMA-TPETA films with pitches of 6 μm, 10 μm and 20 μm were successfully fabricated. All the samples were dried under vacuum at room temperature for 24 hours to evaporate any remaining solvent.

Table 3.1 Comparison table of displayed percentage of UV lamp output and the measured UV dosage

Percentage of UV lamp output (%)	Measured UV dosage for 30 sec (mJ/cm^2)
3	49.9
5	85.2
7	116.6
10	158.2
20	344
30	522
40	704
50	867
60	1027
70	1197
80	1385
90	1549
100	1701

Grooved films with a groove height of 1 μm and all three pitches previously given were fabricated for the wound-healing assay. In addition, 20 μm pitch samples but with a groove height of 2.5 μm were also prepared for comparison purposes. Figure 3.1 shows how the height of the relief structure varies with the UV energy dosage used and this relationship determined the energy dosage

chosen to fulfil the height requirements of each particular film. To be specific, 522 mJ/cm^2 was used to create a 1 μm depth for 6 μm and 10 μm pitch films, 344 mJ/cm^2 was used to create a 2.5 μm depth and 704 mJ/cm^2 was used to create a 1 μm depth for the 20 μm pitch samples.

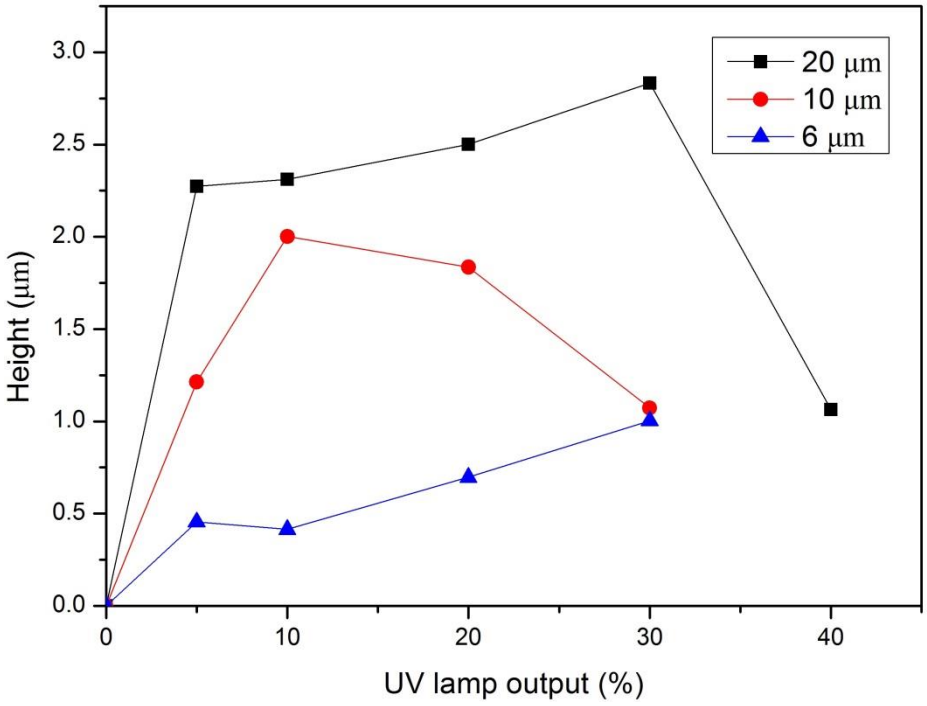

Figure 3.1 AFM measurement of photoembossed PMMA-TPETA films with pitches at 6 μm, 10 μm and 20 μm

The surface wettability of a cell culture substrate is also important in cell adhesion and proliferation. The contact angle which can express the wettability of a surface was measured with the static sessile drop method. At least 10 samples were measured for each pitch size, and 5 measure points were taken for each sample. Figure 3.2 shows the typical measurements for each kind of PMMA-TPETA films.

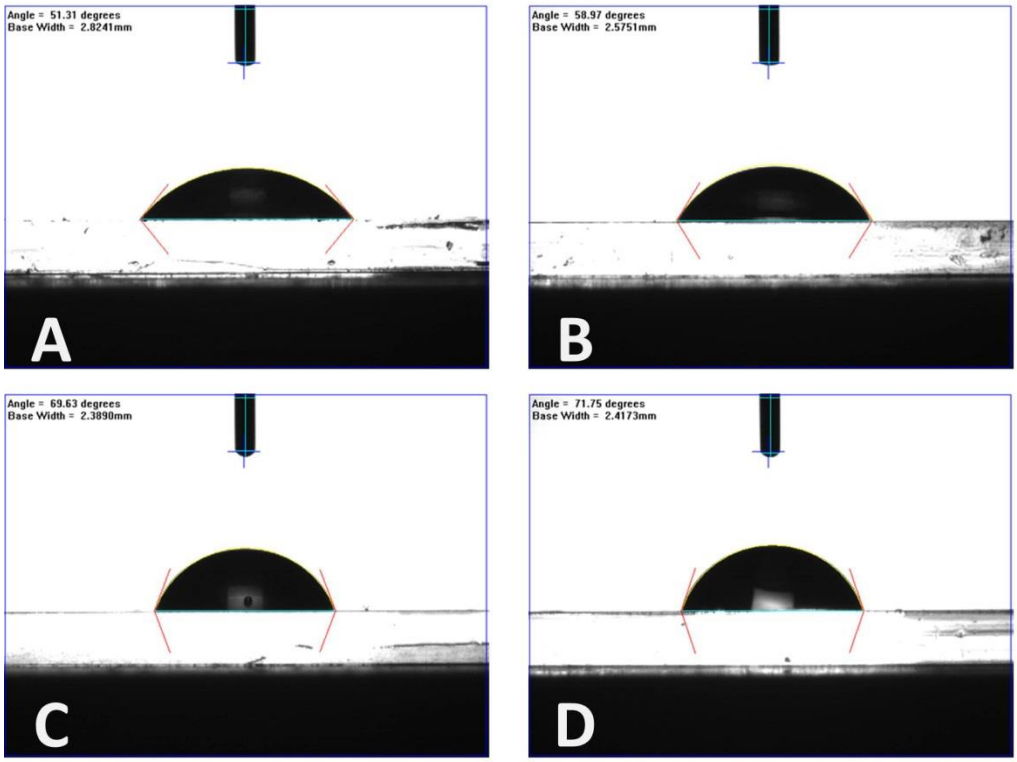

Figure 3.2 Typical contact angle measurements for each kind of PMMA-TPETA film (A) smooth surface (B) 6 μm pitch (C) 10 μm pitch (D) 20 μm pitch

We can see from the contact angle results (Table 3.2) that all PMMA-TPETA films are hydrophilic. However, as the pitch size of the relief structure increases, the contact angle also gets slightly larger. This means that the surfaces with smaller texture sizes are more hydrophilic. Nevertheless, we do not consider the differences between textures of 10 μm and 20 μm to be significant. Moreover, the approximate contact angle of 70 º for these two pitches is considered to be the most suitable for cell adhesion reported by Tamada and Ikada (Tamada and Ikada, 1993). This was confirmed by the following MTS assay.

Table 3.2 Contact angles of PMMA-TPETA films with different surfaces

PMMA-TPETA films	Contact angle (degrees)
Smooth	49.81 ± 1.56
6 μm pitch	59.15 ± 1.45
10 μm pitch	69.57 ± 0.30
20 μm pitch	70.57 ± 0.94

3.2.2 HUVECs proliferation and morphology

PMMA-TPETA non-embossed films and PMMA-TPETA embossed films with 20 μm pitch and 2.5 μm height were used for the MTS assay. Untreated glass cover slips and cover slips coated with pure PMMA films were used as controls. The MTS results (Figure 3.3) showed that cell numbers of all the samples had increased by the end of the time period studied. To be specific, cell numbers on pure PMMA films and PMMA-TPETA non-embossed films dropped on the 5^{th} and 3^{rd} day, respectively, but increased later. However, cells seeded on the embossed films grew steadily throughout the experimental period and showed significantly higher proliferation compared with the other two sample categories at the end of the experiment. Cells on embossed PMMA-TPETA films showed significantly higher proliferation compared with those on pure PMMA films and significantly higher proliferation than on non-

embossed surface for the majority of the experimental period but especially from day 3. Cells on non-embossed PMMA-TPETA films also showed significantly higher proliferation than those on pure PMMA films by the end of the experiment. These results suggest that the photopolymer improved the cell attachment on PMMA, and the grooved texture greatly enhanced cell proliferation. Additionally, confluenced cells are still in good condition when they are used for cell migration assay after up to 14 days culture. The glass cover slips used in all the MTS assays in this thesis are mainly used to check whether the examined cells are in good condition. During the culture process, agents which can help cell attachment in the medium such as Fn attach to the glass cover slips, so that cells on the glass cover slips grow steady throughout the culture period.

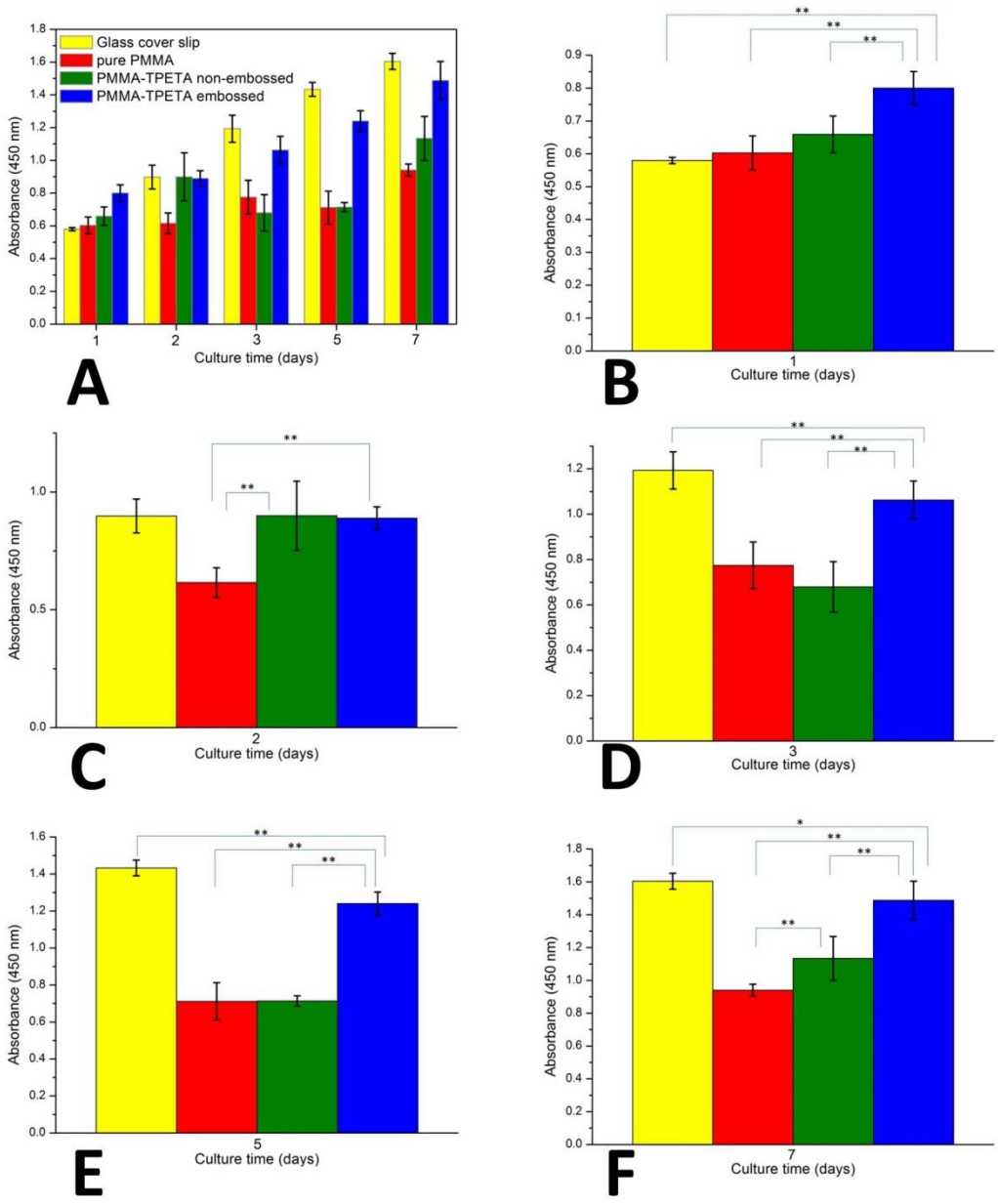

Figure 3.3 Proliferation of HUVECs (* and ** indicates statistical significance) (A) HUVEC proliferation on glass cover slips, pure PMMA films, non-embossed PMMA-TPETA films and embossed PMMA-TPETA films, (B)HUVEC proliferation on day 1, (C) HUVEC proliferation on day 2, (D) HUVEC proliferation on day 3, (E) HUVEC proliferation on day 5, (F) HUVEC proliferation on day 7.

On embossed PMMA-TPETA films, clear cell alignment along the surface relief texture is observed at day 1 (Figure 3.4 B) while cells allocated

themselves randomly on the smooth surfaces. As the culture time increased, cells became more flattened and dispersed on all samples. The SEM pictures also show a decreased cell density on non-embossed PMMA-TPETA films at day 3 (Figure 3.4 C), which is in accordance with the MTS results. Also by day 3, cells begin to show a tendency to bridge the relief structures and less alignment can be seen (Figure 3.4 D). By day 7, we can see that cells almost fully cover the surface of the substrates on both non-embossed (Figure 3.4 G) and embossed (Figure 3.4 H) samples. However, it seems that by providing a larger surface area, the grooved films allowed more cells to attach. This could be another reason why, by the end of the assay, cell proliferation on embossed films is significantly higher than on non-embossed surfaces.

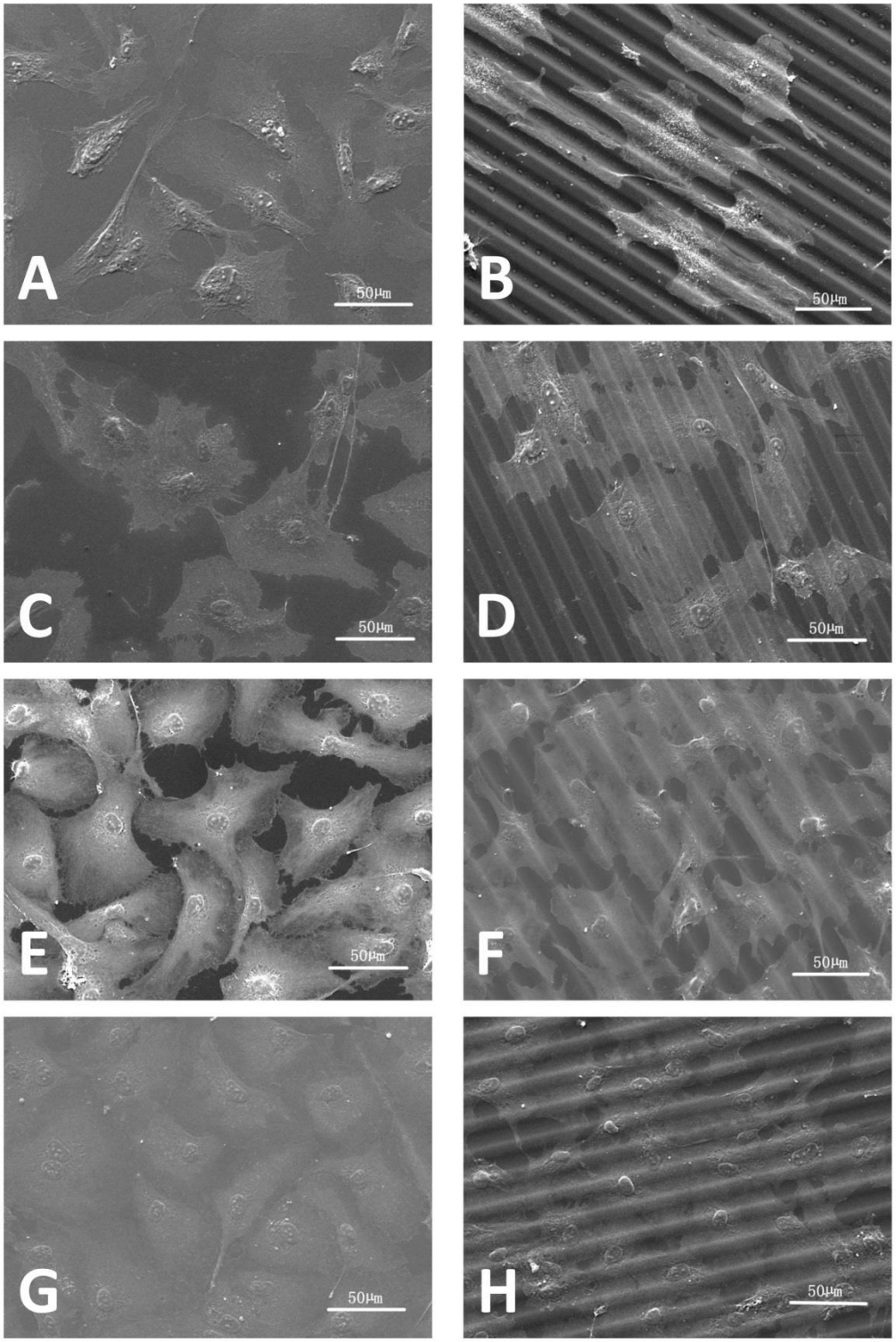

Figure 3.4 HUVECs seeded on non-embossed PMMA-TPETA films at (A) day 1 (C) day 3, cell density is decreased (E) day 5 (F) day 7, cells are almost confluence and embossed PMMA-TPETA films at (B) day 1, clear cell alignment along the surface relief texture is observed (D) day 3, cells bridge the relief structures and less alignment can be seen (F) day 5 (H) day 7, cells are almost confluence.

3.2.3 Cell migration

A wound-healing assay was used to investigate cell migration both on smooth and photoembossed films with different pitches and depths. The width of the wounds was 200±10 μm with the exception of the 6 μm pitch on which the wounds were 150±10 μm. Cells were stained with Cell Tracker and examined under an epifluorescence microscope.

The non-embossed PMMA-TPETA films were first compared with the embossed PMMA-TPETA films with 20 μm pitch and 2.5 μm height (Figure 3.5). The results show that after 2 hours, there is a noticeable difference between these two samples and after 3 hours, cells on the textured film have almost filled the wound, whereas cells on the smooth film still show a significant gap at the wound site.

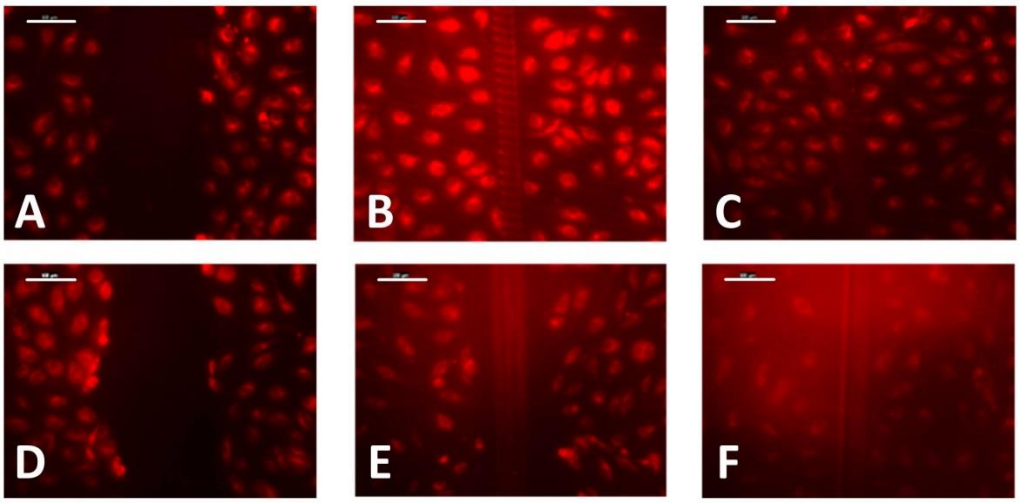

Figure 3.5 Wound-healing assay on photoembossed (top) and smooth (bottom) films at time points (A) (D) 0 hour, (B) (E) 2 hours, (C) (F) 3 hours. (Scale bars present 100 μm)

On films embossed with grooves of 20 µm pitch and 2.5 µm height, a comparison was made between wounds made perpendicular to and parallel with the grooves (Figure 3.6). With approximately the same pressure to scratch the wound, the wounds made in the parallel direction were initially significantly narrower and differences between the perpendicular and parallel samples were still apparent after 3 hours. The results showed that grooves seem to inhibit cell migration when the wounds are parallel to the grooves. On the other hand, the comparatively smaller size of wounds made parallel to grooves would indicate that, in this case, cells are less likely to detach from the substrate.

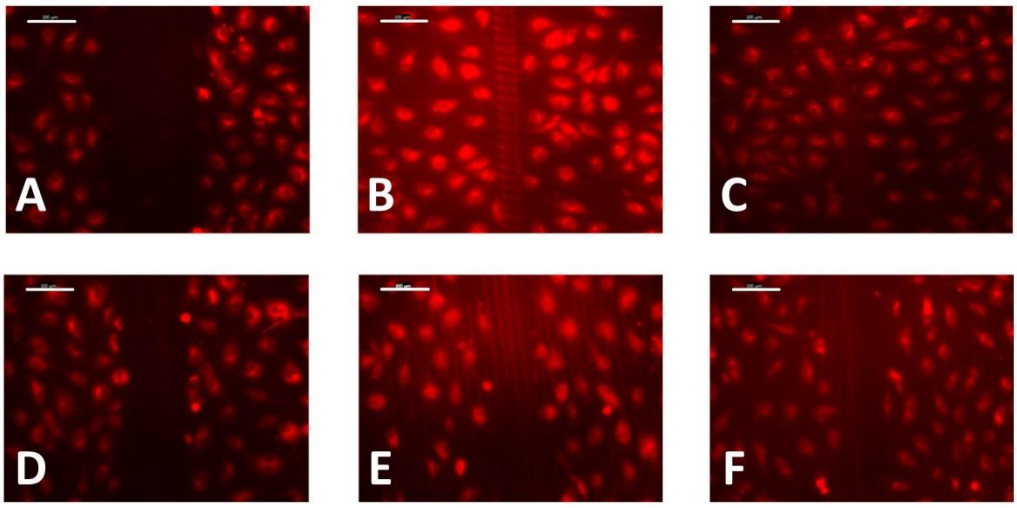

Figure 3.6 Wound-healing assay on photoembossed films with perpendicular (top) and parallel (bottom) wounds to the direction of the grooves at time points (A) (D) 0 hour, (B) (E) 2 hours, (C) (F) 3 hours. (Scale bars present 100 µm)

Photoembossed PMMA-TPETA films with 20 µm pitch and depths of 2.5 µm and 1 µm are compared as follows (Figure 3.7). The results show that no

significant differences can be seen in the initial wound sizes, cell migration speed and wound recovery time.

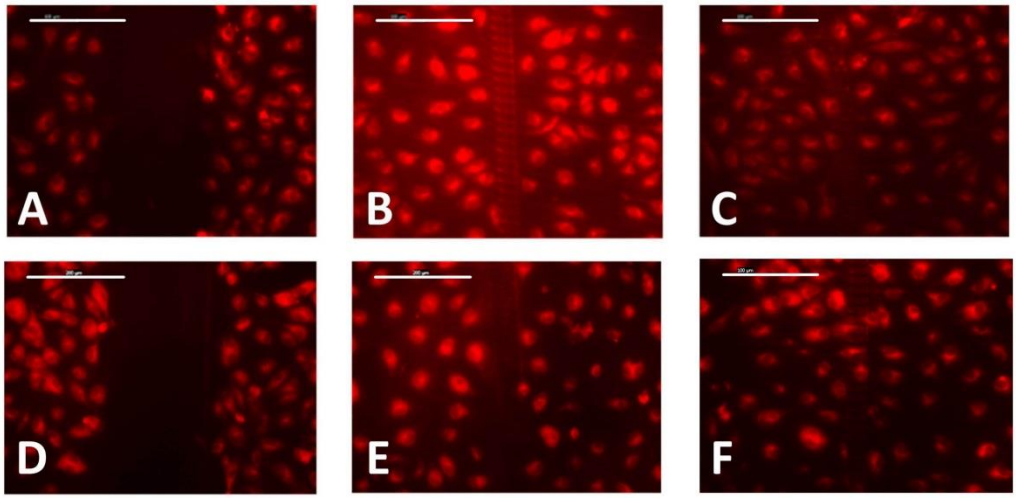

Figure 3.7 Wound-healing assay on photoembossed films with 2.5 μm pitch (top) and 1 μm pitch (bottom) at time points (A) (D) 0 hour, (B) (E) 2 hours, (C) (F) 3 hours. (Scale bars present 200 μm)

A wound-healing assay on films with 6 μm, 10 μm and 20 μm pitches, all with a ridge height of 1 μm were also compared (Figure 3.8). The results show that with a similar strength to scratch the wound on embossed films, the wounds on the samples with a 6 μm pitch appeared significantly narrower compared with the other two sample groups (10 μm and 20 μm pitch) which appeared about the same. After 2 hours, the wounds on the 20 μm pitch samples were clearly narrower than on the 10 μm pitch samples and were similar in size to those on the 6 μm samples which were initially narrower. However, all the wounds had recovered after 4 hours.

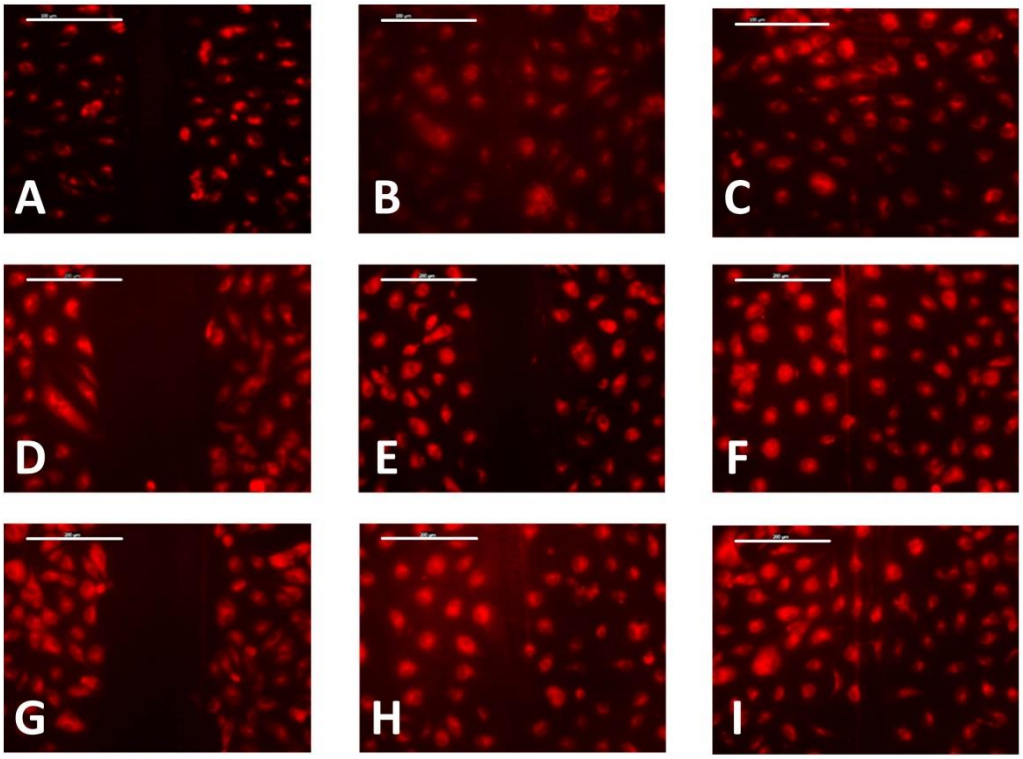

Figure 3.8 6 μm (top), 10 μm (middle) and 20 μm (bottom) pitches films with 1 μm height at 0 hour (A) (D) (G), 2 hours (B) (E) (H) and 4 hours (C) (F) (I). (Scale bars present 200 μm)

Figure 3.9 summarizes the percentage of the recovered area on each kind of sample at every time interval. As there were only minor changes in the first hour, observations at this time interval are not shown. However, from the time points 2 hours to 4 hours, we can still see that the cells migrate in an almost uniform direction.

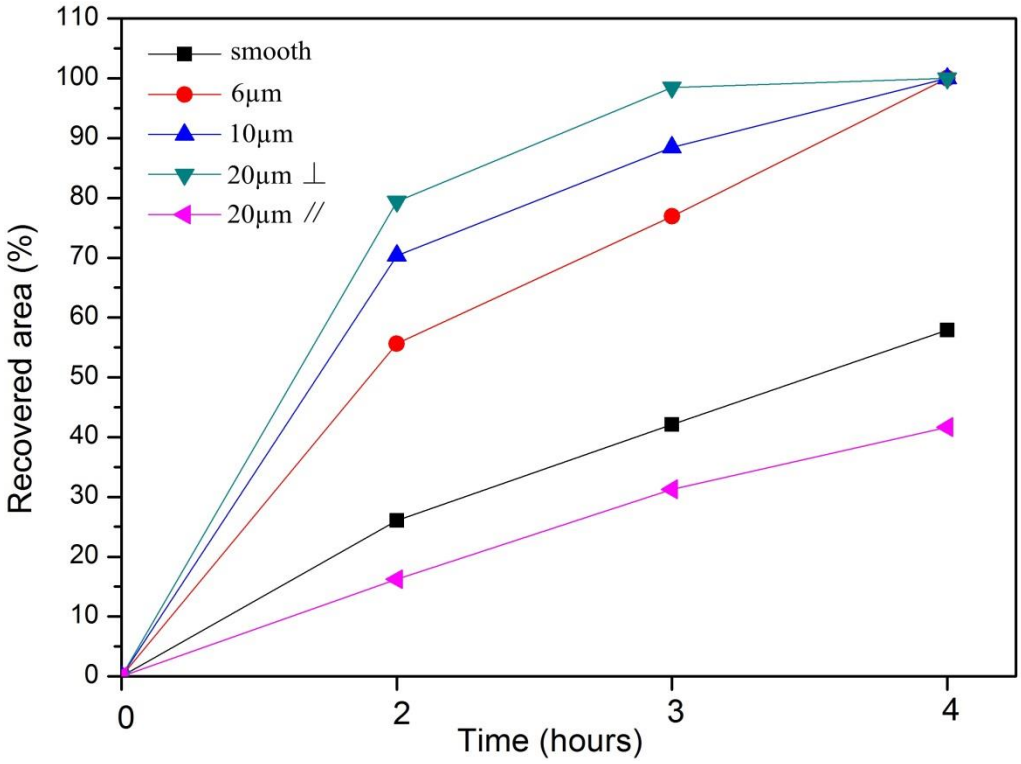

Figure 3.9 The percentage of area coverd by HUVECs on smooth PMMA-TPETA films, embossed films with 6 µm pitch and 10 µm pitch, 20 µm pitch with wound perpendicular and parallel to the direction of the grooves.

3.3 Discussion

PMMA has already shown to exhibit good biocompatibility and is in wide clinic use, such as in rigid intraocular lenses (Apple, 2006), bone cement (Rho et al., 1993), dental filling, dentures (Vallittu, 1996) and cosmetic surgery (Lemperle et al., 1998). Here, we have demonstrated that the addition of the biocompatible monomer TPETA, results in a photopolymer with improved cell attachment and proliferation compared to pure PMMA.

Photoembossing is a relatively new technology in the fabrication of surface textures. Compared to photolithography, which is the most commercially advanced method and is used to pattern a thin film or substrate by microfabrication, photoembossing does not require a wet-etching step which makes it more cost-effective and environment-friendly. In this method, the shape of the relief structure is determined by the pattern of the photomask while our previous work has confirmed that the depth of the relief structure can be adjusted by controlling the UV dosage and temperature during the heating stage (Hughes-Brittain et al., 2014a). It has been shown that there is an optimum UV dosage required to create any particular relief structure (Sánchez et al., 2005). When UV intensities are lower than the optimum, only a small amount of photoinitiator will be active so that only a small amount of monomer will be converted. This results in lower relief structures due to the reduced concentration and chemical gradient in the film. On the other hand, when UV intensities are higher than the optimum, a larger amount of photoinitiator will be active resulting in higher polymerisation rates and the conversion of a larger amount of monomer. This will cause a decrease in mobility of the monomer in the polymer network which again results in lower relief structures. By this process of photoembossing and controlled UV dosages, we successfully fabricated photopolymer films with 1 μm depth relief structures and 6 μm, 10 μm and 20 μm pitches and with 2.5 μm depth and 20 μm pitch.

The changes in surface morphology of the film caused by the photoembossing process lead to changes in wettability. Embossed films are less hydrophilic than smooth films. However, the 6 μm pitch film is more hydrophilic than

either the 10 µm or 20 µm pitch films while the latter two are comparable in wettability. According to van Wachem (van Wachem et al., 1987a), a substrate which is too hydrophilic or too hydrophobic is less preferable for the attachment and proliferation of HUVECs. Similar results have been found for other cell types and materials (Grinnell, 1977, Baier et al., 1968, Coleman et al., 1982, Horbett et al., 1985, Lydon et al., 1985, Hattori et al., 1985). A comparison of the MTS assay results for non-embossed and embossed PMMA-TPETA films indicate that the initial attachment of HUVECs on embossed films is significantly higher than on non-embossed films. Additionally, the proliferation of the cells on embossed films is significantly greater than on smooth films from day 3. This suggests that the decreased wettability due to surface textures through photoembossing in this experiment promotes the adhesion and proliferation of HUVECs.

PMMA-TPETA photopolymer shows improved cell attachment and proliferation compared to pure PMMA which has been confirmed to be biocompatible and is already widely used in medical treatment. Moreover, grooved surfaces significantly promote cell proliferation and, due to the enlarged surface area provided by this topography, enable the accommodation of more cells than smooth surfaces. The surface charges of the films were not measured. However, we have concluded that they are positive charged because they detach easily from the glass cover slips and attach to plastic surfaces which are normally negatively charged due to electrostatic interaction. In this regard, a hydrophilic surface with positive charge has already been reported to promote cell adhesion (Hattori et al., 1985, van Wachem et al., 1987a).

Cells present the most alignment on day 1 and flatten and disperse as time passes. There could be several reasons for this. Firstly, cell orientation depends on cell type. HUVECs cultured in vitro are polygonal cells with a width between 30 μm to 50 μm and tend to return to this shape (Gimbrone et al., 1974) (Figure 3.10). Secondly, as the culture proceeds, contact inhibition between cells becomes stronger and might even become the dominant factor in affecting the cell shape rather than the effect of contact guidance from the surface topography. Additionally, fibronectin (Fn), a protein considered to promote cell adhesion, contained in FBS deposits on the surface of the substrate may also weaken the influence of contact guidance on the cells.

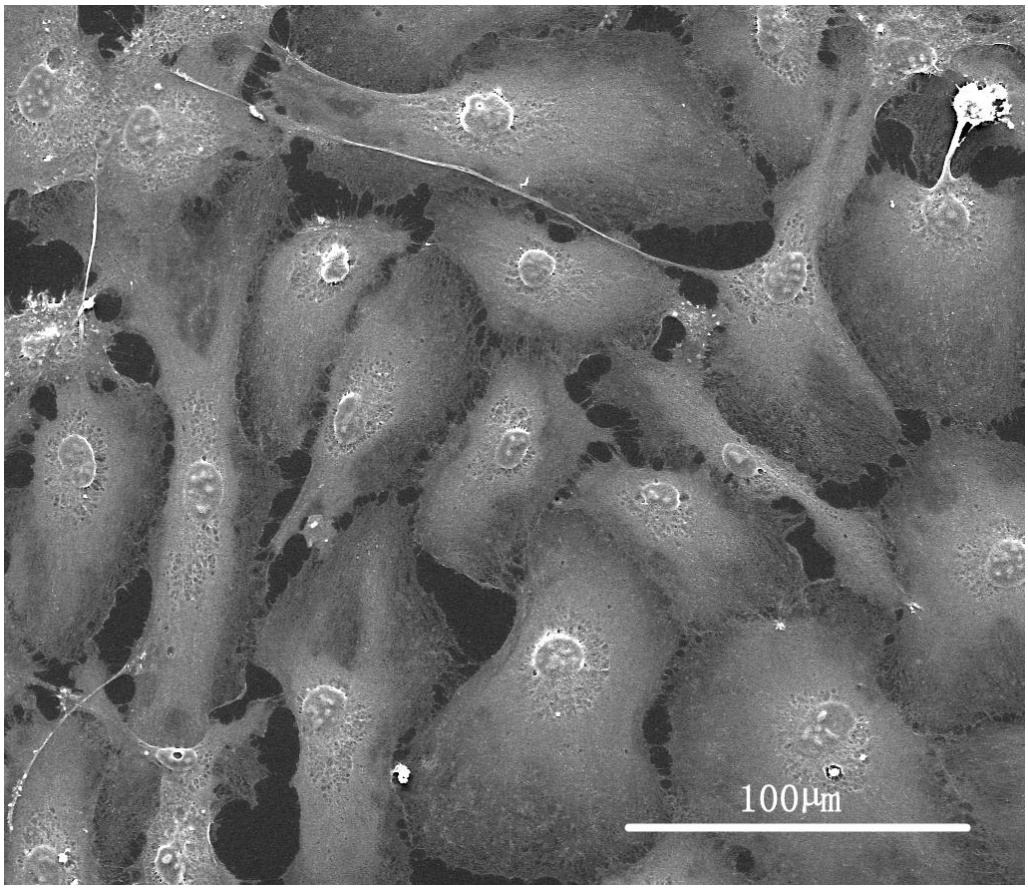

Figure 3.10 SEM picture of HUVECs in vitro

In the conventional wound-healing assay on well plates, the average migration rate is 25 μm/hr (van Der Meer et al., 2010). The results of our wound-healing assay present significantly accelerated recovery speeds with uniform motion, HUVECs with 200 μm wounds are fully recovered after 4 hours on all the embossed films with 6 μm, 10 μm and 20 μm pitches while the wounds on the smooth films are still clearly apparent. Additionally, 20 μm appears to be the most efficient pitch among the three examined while there was no noticeable difference between samples with relief heights of 1 μm and 2.5 μm. On 20 μm embossed films, the wound-healing assay was also conducted with wounds perpendicular to and parallel with the relief structures. The results show that after 3 hours, when the wound which was perpendicular to the textures has fully recovered, the wound parallel to the textures remained relatively unaffected. These results suggest that, with the exception of this last case of a 'parallel wound' all the grooved surface textures and variations of different pitch size we tested accelerate cell migration, with grooves at a 20 μm pitch performing most effectively. Additionally, in accordance with Tamada and Ikada (Tamada and Ikada, 1993) and Shen *et al.* (Shen et al., 2013), films with 10 μm and 20 μm pitches also have water contact angles which are suitable for cell adhesion so that surfaces with a contact angle around 70 ^{o} are not only suitable for cell adhesion but may also accelerate cell migration as the hydrophobicity increases. However, a grooved texture can also inhibit cell migration when the wounds are parallel to the groove direction although, at the same time, preventing the cells from detaching from the substrates.

Additionally, when the pitch of the surface texture is as small as 6 μm, cells are again protected from detaching.

3.4 Conclusions

Photoembossing is a simple, environment-friendly and cost-effective way to fabricate surface topographies. The photopolymer PMMA-TPETA has improved cell attachment and proliferation compared to uncombined PMMA and has great potential in cell and tissue engineering. Surface topography decreases the surface hydrophilicity but promotes cell attachment, proliferation and migration. Cell alignment is affected by the surface relief structure most distinctly in the early stages, and then decreases. Photoembossed surfaces accelerate the migration of HUVECs along the structure, with cells migrating relatively more quickly on embossed films with larger pitches and a contact angle around 70°. Additionally, grooved surface textures with 'parallel wound' and a pitch of 6 μm also inhibit cells from detaching. All the results obtained suggest that photoembossed PMMA-TPETA films can be used to develop a monolayer of HUVECs on the surface of artificial vascular implants in order to prevent the formation of thrombus and fabricate small diameter vascular grafts.

Chapter 4 Interaction between HUVECs and holographic lithography electrospun fibres

PLGA is already used in therapeutic devices which are approved by FDA due to its biocompatibility and biodegradability. The degradation rate of PLGA depends on the ratio between the glycolide and lactic units and can thus be controlled by adjusting the ratio between them. In general, the more glycolide units the copolymer contains, the faster it degrades. However, when the ratio of these two units in the copolymer is 1:1, the fastest degradation period of about two months is reached. A disadvantage of PLGA is that its cellular affinity is not very good. Moreover, the degradation products of PLGA can increase the acidity in the local area which can lead to late-onset non-infectious inflammation. This limits the application of PLGA. In implants, the surface of the biomaterial directly in contact with the cells has the greatest interaction with these cells, so the surface properties of the implant are critical. In order to broaden the utilization of PLGA in bioengineering, improving the cellular affinity is very important.

By adding the biocompatible monomer TPETA to PLGA, a new PLGA-TPETA photopolymer is created that improves the biocompatibility of PLGA through changing the chemical properties, morphology via electrospinning and surface topography via holographic lithography. The added TPETA monomer is not degradable hence causing the resultant photopolymer PLGA-TPETA to be semi-degradable in this system. Based on the evidence of previous research

into cell viability on fibres with different diameters (Kumbar et al., 2008, Christopherson et al., 2009, Badami et al., 2006), in our experiments, we used fibre diameters between 500 nm to 1.5 μm, which is considered to be the best range for cell viability. The primary focus was on cell morphology and adhesion to the photoembossed PLGA-TPETA fibre substrates.

4.1 Materials and methods

4.1.1 Materials

PLGA (Corbion Purac) was used as the polymer binder while the multifunctional monomer and photo initiator were TPETA and Irgacure 369, respectively. The solvent PGMEA was used in film making, and $CHCl_3$ and DMF were used in electrospinning. CellTiter 96® AQueous One Solution was used in the MTS assay as previous described for cell proliferation measurements. 4′,6-diamidino-2-phenylindole (DAPI, Invitrogen) was used to stain the cell nuclei. Cytoskeleton was labelled by Phalloidin–Tetramethylrhodamine B isothiocyanate (phalloidin, Sigma-Aldrich), and vinculin was labelled by a primary and secondary antibody: first by Monoclonal Anti-Vinculin antibody produced in mouse (anti-vinculin, Sigma-Aldrich) and secondly by Alexa Fluor® 594 Donkey Anti-Mouse IgG (H+L) Antibody (anti-mouse, Invitrogen).

4.1.2 PLGA-TPETA films and fibres

Pure PLGA films, non-embossed and embossed PLGA-TPETA films were prepared as previously described in 2.3 for the material biocompatibility observations. A mixture of 1:1 by weight PLGA and TPETA and Irgacure 369 at 5 wt. % of the TPETA was dissolved in a 60 wt. % solution of PGMEA. A 20 μm pitch photomask and 88.4 mJ/cm^2 UV dosage were used in the first UV exposure step. Based on our previous studies (Hughes-Brittain, 2013), the chosen UV dosage and a temperature of 80 ℃ in the heating stage are optimum conditions to photoemboss PLGA-TPETA films.

Because of the uneven surface of electrospun fibre substrates, holographic lithography photoembossing is introduced in preference to the contact mask photoembossing process used for film fabrication. PLGA-TPETA fibres are made through a conventional electrospinning setup (Li et al., 2002, Nair et al., 2004) at ambient temperature and pressure. The solution used in the electrospinning process is slightly different from that used in film fabrication being a 5:4 by weight mixture of PLGA and TPETA dissolved in a solution of $CHCl_3$ and DMF at a ratio of 9:1. Also, the PLGA used in this process has different inherent viscosities of 1.04 dl/g and 1.80dl/g with a different ratio of glycolide to lactic units of 50:50 and 82:18. The proportion of TPETA is reduced in order to produce dry solid fibres on the collector. Irgacure 369 is still at 5 wt. % of TPETA. All components are dissolved in 60 wt. % and 85 wt. % of the $CHCl_3$ and DMF mixture, respectively. The percentage of solvent is chosen based on the morphology of obtained fibres (basically, every single

fibre should be uniform and without any beads). This solution was electrospun using a single nozzle with a 1 mm diameter aperture with a collector at 20 cm distance. The applied voltage was 25 kV with a solution flow rate of 0.3 ml/hr. In all these experiments, 13 mm glass cover slips placed on the collector received the electrospun fibres. The collected samples were removed to a lightproof box until they were processed by holographic lithography. After this, samples were heated at 80 ℃ for 20 min, followed by exposure under a UV light for 1000 sec at full power.

4.1.3 Cell culture

HUVECs were cultured and maintained as previous described in 2.1. All substrates were soaked in 75% ethanol for 30 min, and then washed 3 times with DPBS. Substrates were then transferred to 24-well plates. The cell suspension was pipetted directly onto the substrates at a density of 1.5×10^4 cells/cm^2 and cultured up to 7 days depending on the various experimental requirements.

4.1.4 Analysis of substrates and the influence on HUVECs

The effect of laser dosage on PLGA-TPETA fibres with the pitch of 1.5 μm was studied. This pitch size was chosen based on the fibre diameters according to our previous study (Hughes-Brittain, 2013). Fibres on the glass cover slip are exposed to the UV pattern that generated by interference of two coherent

beams in air at room temperature. The UV dosage is controlled by changing the pulse duration of the laser. The heights of the relief structure on the obtained samples were measured with an AFM.

An MTS cell proliferation assay as previously described was carried out on PLGA-TPETA films. The contact angle was also measured for embossed PLGA-TPETA films with 20 μm pitch for reference purposes.

Cell morphology based on the appearance of actin filaments (F-actin), and cell adhesion based on the presence of vinculin in focal adhesions were both examined under a confocal microscope.

4.1.5 Immunostaining

Specimens were washed 3 times with DPBS and then fixed with 4% PFA for 8 min, followed by washing a further 3 times with DPBS. Cells were permealized by immersing in a 500 μl/well with 0.2% Triton^{TM} X-100 (Sigma-Aldrich) for 5 min, followed by 2 washes with DPBS. They were then immersed in a 500 μl/well of blocking buffer consisting of 0.01g/ml bovine serum albumin (BSA) added to DPBS for 45 min in an incubator at 37 ℃. Because the photopolymer fibres are autofluorescent and appear green under the confocal microscope, F-actin and vinculin are both stained red in seperate samples to distinguish them from the fibres. HUVECs were stained with phalloidin for 45 min to distinguish F-actin and with DAPI for 45 min for nuclear. In the other group of samples, HUVECs were treated with the primary

antibody anti-vinculin for 45 min followed by the secondary antibody anti-mouse and DAPI for 45 min. After all the staining steps were completed, the samples were washed 3 times with DPBS and twice with DI-water.

4.1.6 Data analysis and statistical methods

All quantitative measurements are reported as mean values ± standard deviation. To determine statistical difference when comparing different groups , a student's t-test is used.

4.2 Results

4.2.1 Synthesis and characterization of holographic lithography electrospun fibres

Electrospun PLGA-TPETA fibres with PLGA of two different inherent viscosities are shown in Figure 4.1. In both cases, fibres were randomly oriented and formed a mesh on the surface of the glass cover slip. Fibre morphology can be influenced by the inherent viscosity of polymer, distance between the tip of needle and the collector, injection flow rate and ambient conditions. PLGA with lower inherent viscosity or higher concentration in the solvent will make thicker fibres. Greater distance between nozzle and collector results in thinner fibres but also requires a higher voltage although varying the

voltage at a fixed nozzle distance makes little difference to the diameter of the fibres (Zhang et al., 2008). Using the same solution, a lower speed of injection flow rate results in thinner fibres. Additionally, unsuitable temperature and humidity may cause beads, but this situation can sometimes be modified by changing the solvent. Under the same conditions (distance and injection flow rate), PLGA (82/18) with an inherent viscosity of 1.80dl/g results in fibre diameters ranging from 500 nm to 1.5 µm (Figure 4.1 A) while PLGA (50/50) with an inherent viscosity of 1.04 dl/g results in a larger range of fibre diameters from 2 µm to 5 µm (Figure 4.1 B). The distribution of fibre diameters are shown in Figure 4.1 C and D, respectively.

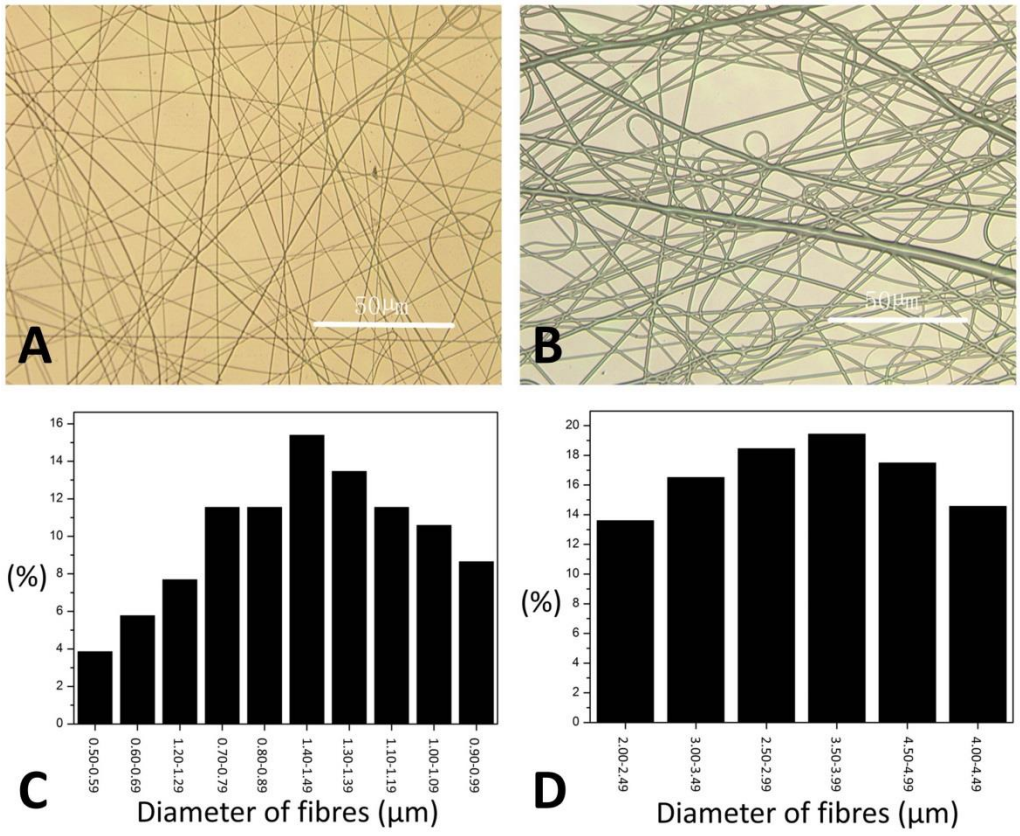

Figure 4.1 Electrospun PLGA-TPETA fibres under optical microscope (A) PLGA with an inherent viscosity of 1.80 dl/g (B) PLGA with an inherent viscosity of 1.04 dl/g (C) the

distribution of fibre diameters obtained from the photopolymer contained the 1.80 dl/g PLGA (D) the distribution of fibre diameters obtained from the photopolymer contained the 1.04 dl/g PLGA

Figure 4.2 shows the height of relief structures measured by AFM caused by different duration of laser pulse. The optimum pulse duration appears to be 350 μs producing a height at 78.82 ± 1.24 nm.

The height of the relief structure produced on the PLGA-TPETA film by photoembossing through the holographic lithography method was also measured for reference and gave the higher result of 93.47 ± 2.31 nm. The thickness (60 μm) of the film may have contributed to this higher value by providing more monomer to participate in the diffusion process. Moreover, this explanation is in accordance with our previous study showing that larger pitches with the same size fibres can also produce higher relief structures (Hughes-Brittain, 2013). After the optimum UV dosage was exceeded, the height of the relief structure dropped, as was the case with the photoembossed films discussed in the last chapter. This can be explained by a higher crosslink density resulting in less available monomer to diffuse.

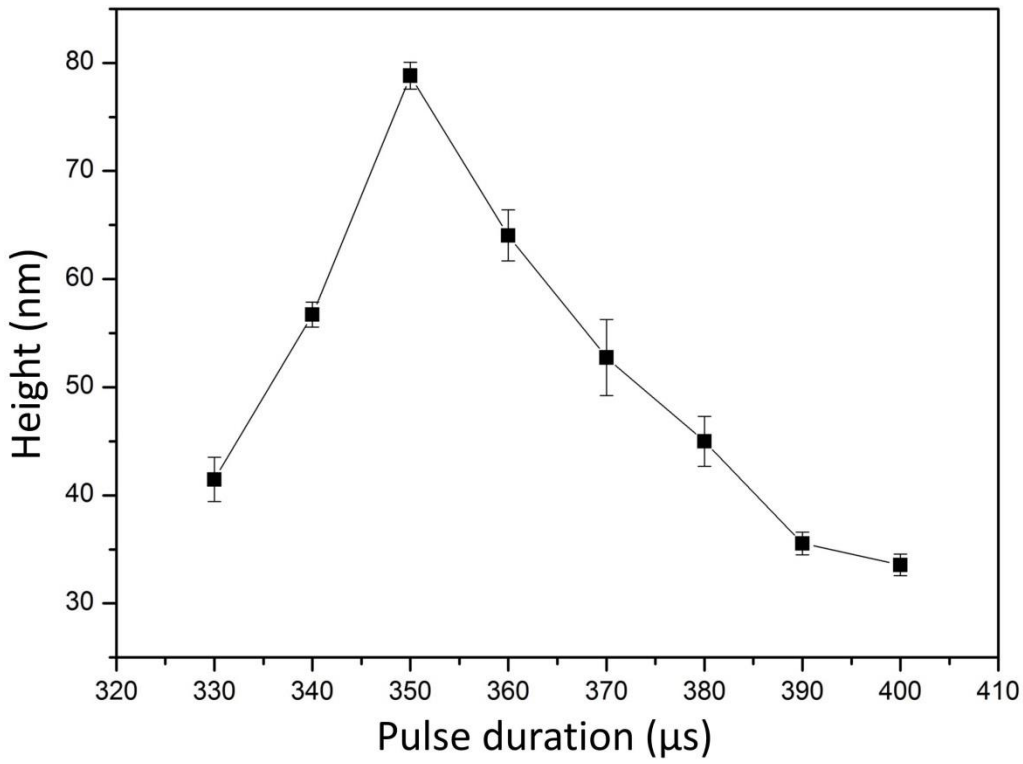

Figure 4.2 Relief height of photoembossed fibres with 1.5 μm pitch at different pulse duration.

The AFM profile of the embossed fibres (Figure 4.3) presents sharper ridges and grooves compared with the embossed films discussed in Chapter 3. This suggests that the monomer is very mobile and well diffused at the given temperature and duration. Luthen (Luthen et al., 2005) pointed out that sharp ridges on titanium substrate influence F-actin formation in osteoblastic cells. However, Degasne (Degasne et al., 1999) reported that a sharp profile on titanium surfaces can damage or injure the cells. Additionally, Den Braber (Den Braber et al., 1995, Den Braber et al., 1996) and Schweikl (Schweikl et al., 2007) suggested that on narrow, shallow and sharp surfaces, cells will bridge over ridges and will also be smaller than those on a smooth surface.

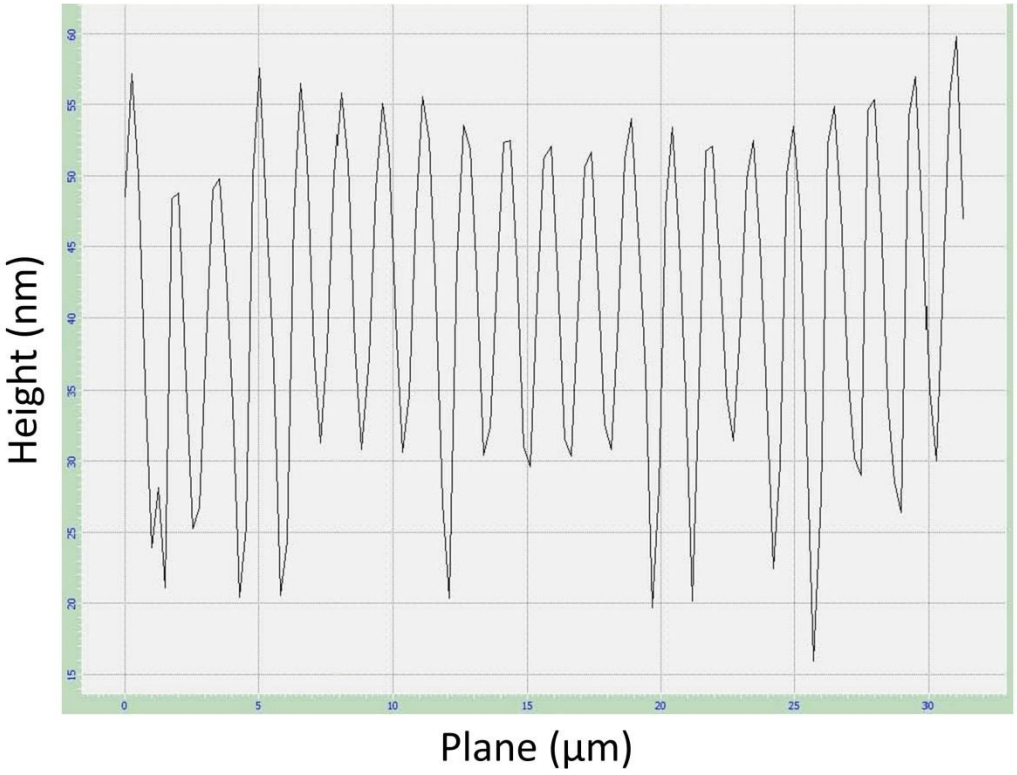

Figure 4.3 AFM profile of the embossed fibres

After photoembossing, the PLGA-TPETA fibres maintained their fibrous structure (Figure 4.4). Fibres are evenly photoembossed in the exposed area. However, depending on the pitch size of the relief structure and the diameter of the fibres, when the interference pattern is parallel to the direction of the fibres, especially those with small diameters, relief structures may not be seen. We define the pitch of the relief structures on the fibres geometrically as follows,

$$P_{interference} = \frac{P_{fibres}}{\sin \alpha}$$

α is the angle between the interference pattern and the direction of fibre.

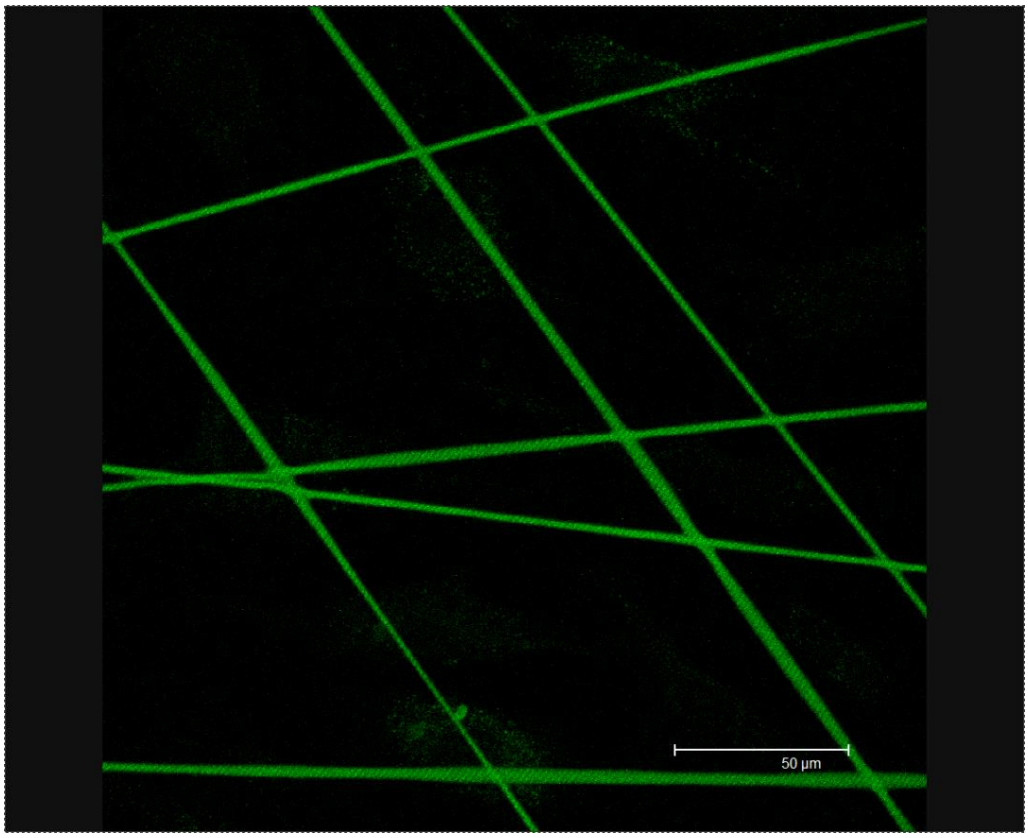

Figure 4.4 Confocal microscopy images of photoembossed PLGA-TPETA fibres

4.2.2 HUVECs proliferation

Pure PLGA films, PLGA-TPETA non-embossed films and PLGA-TPETA embossed films with a 20 µm pitch were used in an MTS assay. Untreated glass cover slips were used as control. Figure 4.5 shows that cell numbers increased on all substrates throughout the experimental period. To be specific, cells seeded on the embossed films exhibit significantly higher proliferation at all of the time points than on both the pure PLGA and non-embossed films. On day 1, cell numbers on the non-embossed films was significantly lower than on

the pure PLGA films. There were approximately equal on days 2 and 3 and, by day 5, cell numbers on the non-embossed films were significantly exceeding those on pure PLGA films. These results suggest that the added TPETA does not initially improved the biocompatibility on cell attachment of pure PLGA, but as the culture proceeds, the PLGA-TPETA films not only become more biocompatible but cell proliferation is also accelerated compared with the pure PLGA films. Nevertheless, the embossed surface showed the greatest improvement in cell attachment of the substrate and accelerated cell proliferation throughout the culture period.

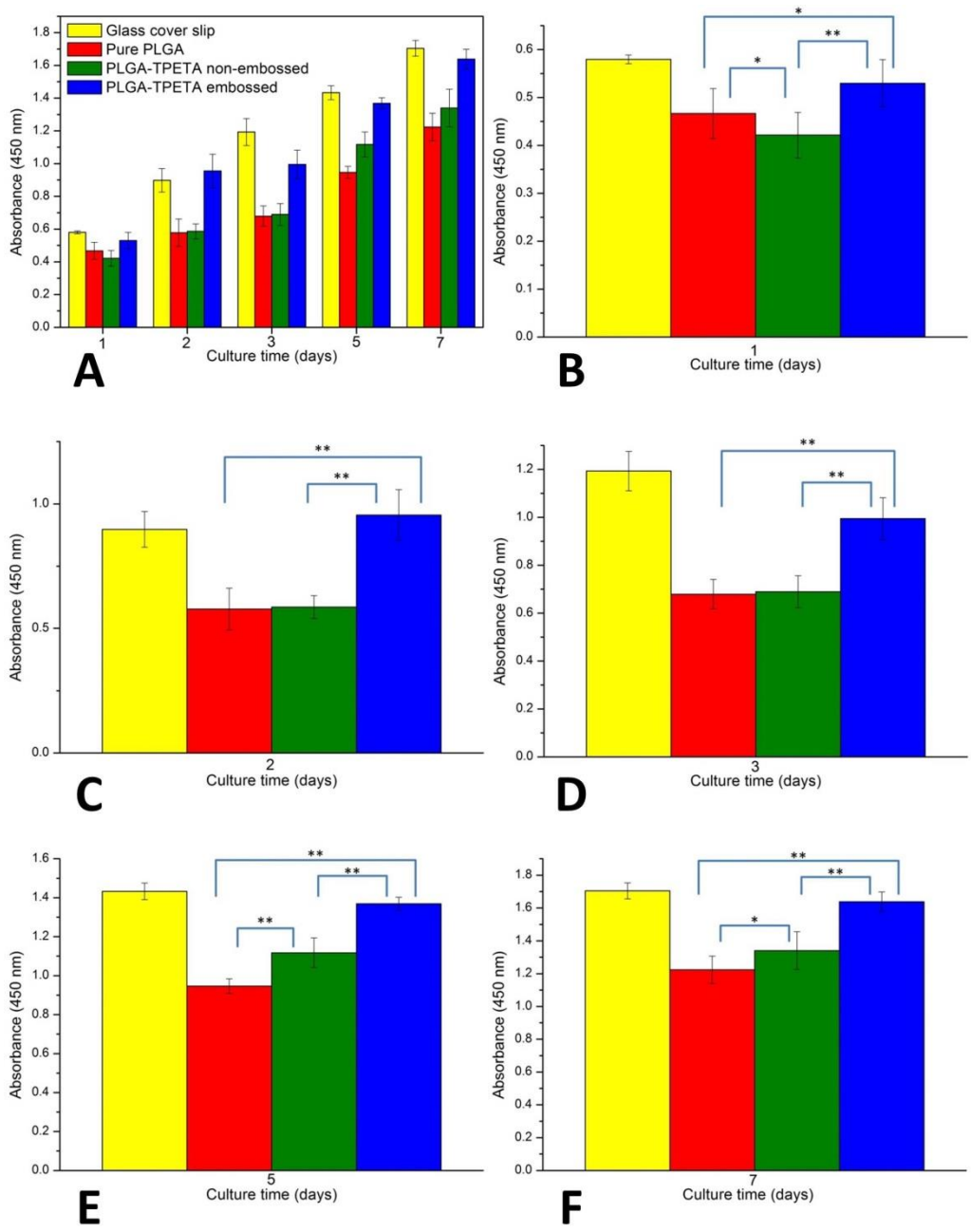

Figure 4.5 Proliferation of HUVECs (* and ** indicates the statistical significance) (A) HUVEC proliferation on glass cover slips, pure PLGA films, non-embossed PLGA-TPETA films and embossed PLGA-TPETA films, (B)HUVEC proliferation on day 1, (C) HUVEC proliferation on day 2, (D) HUVEC proliferation on day 3, (E) HUVEC proliferation on day 5, (F) HUVEC proliferation on day 7.

Surface wettability might be an important factor in these results. It is well known that the biocompatibility of PLGA is limited due to its hydrophobic property. From our contact angle measurements (Table 4.1) we can see that the values on pure PLGA films are 79.31 ± 0.45^{o} and by adding TPETA the value decreases to 61.63 ± 0.86^{o}. However, photoembossing produces a higher contact angle of 68.72 ± 0.56^{o}. The MTS results are in accordance with the PMMA-TPETA films discussed in 3.2.2 that a water contact angle around 70^{o} shows the best cell adhesion.

Table 4.1 Contact angle measurements of PLGA films

Films	Contact angle (degrees)
Pure PLGA	79.31 ± 0.45
Non-embossed PLGA-TPETA	61.63 ± 0.86
Embossed PLGA-TPETA	68.72 ± 0.56

4.2.3 Cell adhesion on PLGA-TPETA fibres

The cytoskeleton of a cell connects with the ECM through focal adhesions. Vinculin is a crucial site in focal adhesion as it is known to reinforce the connection between actin and the ECM (Galbraith et al., 2002). In this study, focal adhesions are visualized by staining the vinculin and examined with a confocal microscope.

The morphology and distribution of vinculin in HUVECs on a glass cover slip are shown in Figure 4.6. Focal adhesions are randomly distributed in the perinuclear region (white arrow) and also close to the edge of the cells (yellow arrow). The former observation suggests the potential for de novo vinculin synthesis (Uttayarat et al., 2005b). Moreover, focal adhesions in elongated cells are more concentrated at the poles (green arrow).

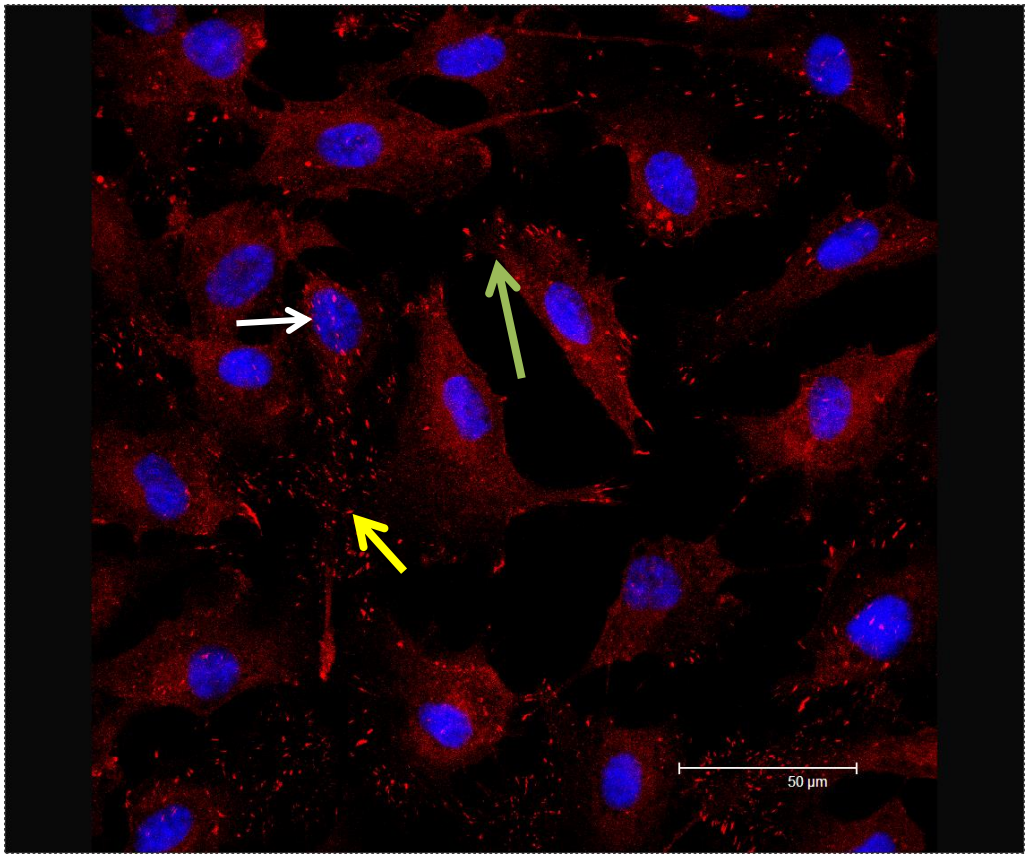

Figure 4.6 Overlay confocal microscopy image of HUVECs stained for the nucleus (blue) and vinculin (red) on glass cover slip. White arrow represents the perinuclear region, yellow arrow represents FAs close to the edge of the cells, green arrow represents FAs in elongated cells are more concentrated at the poles.The HUVECs showed a marked tendency to settle onto fibres

immediately (white arrow) after seeding though not yet adhering to the substrate (Figure 4.7). Subsequently, they begin to grow from the fibre intersections on both non-embossed and embossed fibres (Figure 4.8) and tended to form a monolayer by spreading into the mesh holes.

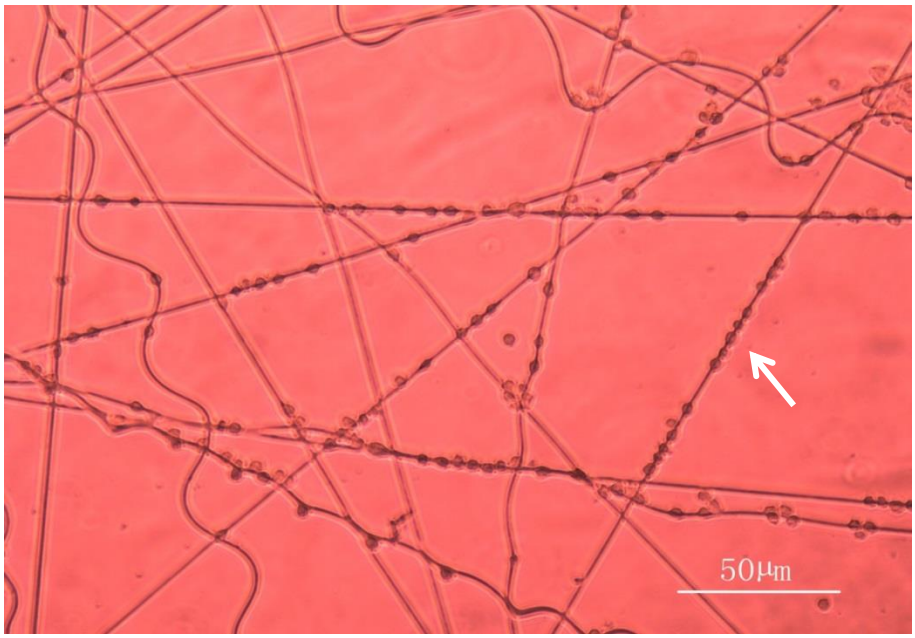

Figure 4.7 Image obtained by optical microscope after HUVECs seeded onto fibres

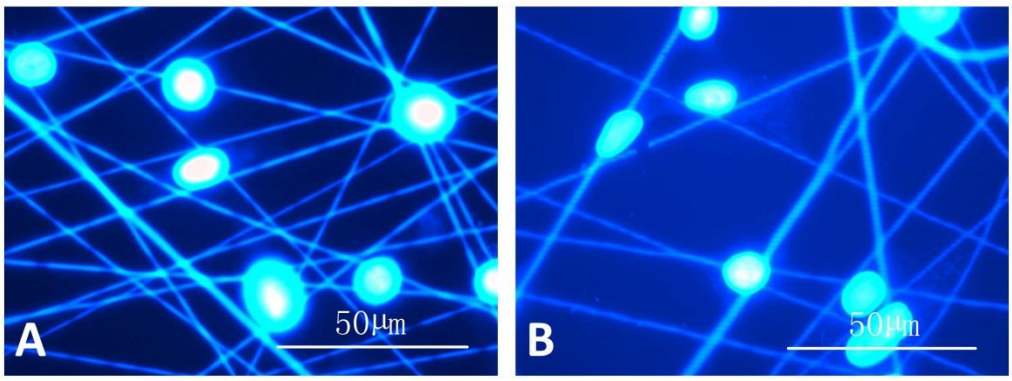

Figure 4.8 Epifluorescence microscope image of HUVECs grow from the intersections on both (A) non-embossed fibres and (B) embossed fibres after cultured for 1 day.

Focal adhesions are found most commonly at the edge of the cells although some are found in the central regions as in those grown on the glass cover slips. However, when focal adhesions are formed on the surface of photoembossed fibres, some of them reflect the pattern of the embossed fibres below (Figure 4.9 A, B, white arrows), others are organized along the side of fibres (Figure 4.9 C, D, white arrows) while the rest are randomly distributed.

Information collected by the confocal microscope allowed us to focus our attention on those sites within the sample where focal adhesions were contiguous with fibres (Figure 4.10). We can see, with respect to these particular sites, focal adhesions appear in the region between the peaks of the ridges (white arrow), the top of the ridges (yellow arrow) and the bottom of the grooves (blue arrow).

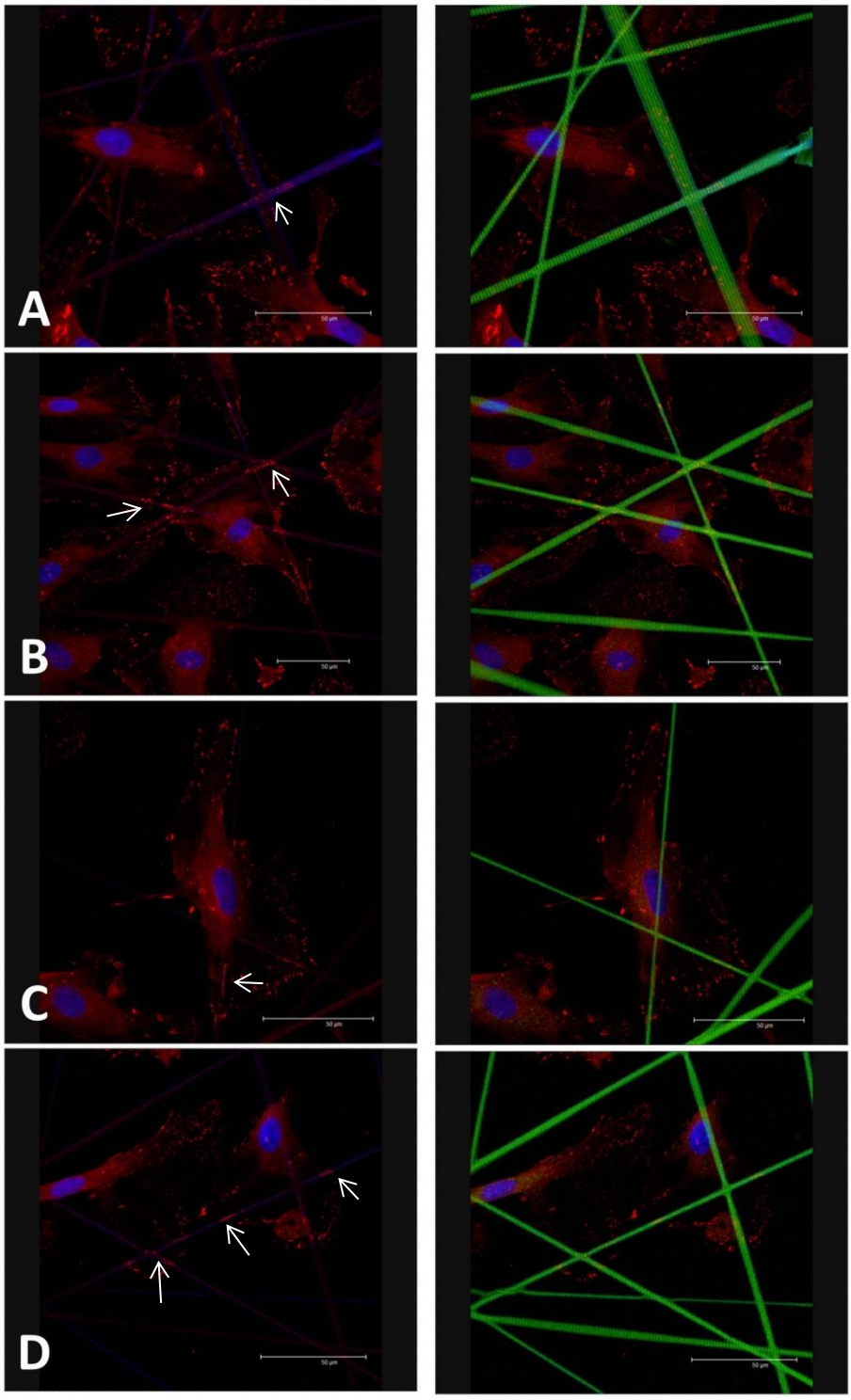

Figure 4.9 Overlay confocal microscopy image of HUVECs stained for the nucleus (blue) and vinculin (red) on photoembossed fibres. Images on the right are the latter merged with image of corresponding fibres (green, autofluorescenced) as reference. Arrows represent highlight areas where (A) (B) FAs on the surface of the fibres or (C) (D) along the fibre sides.

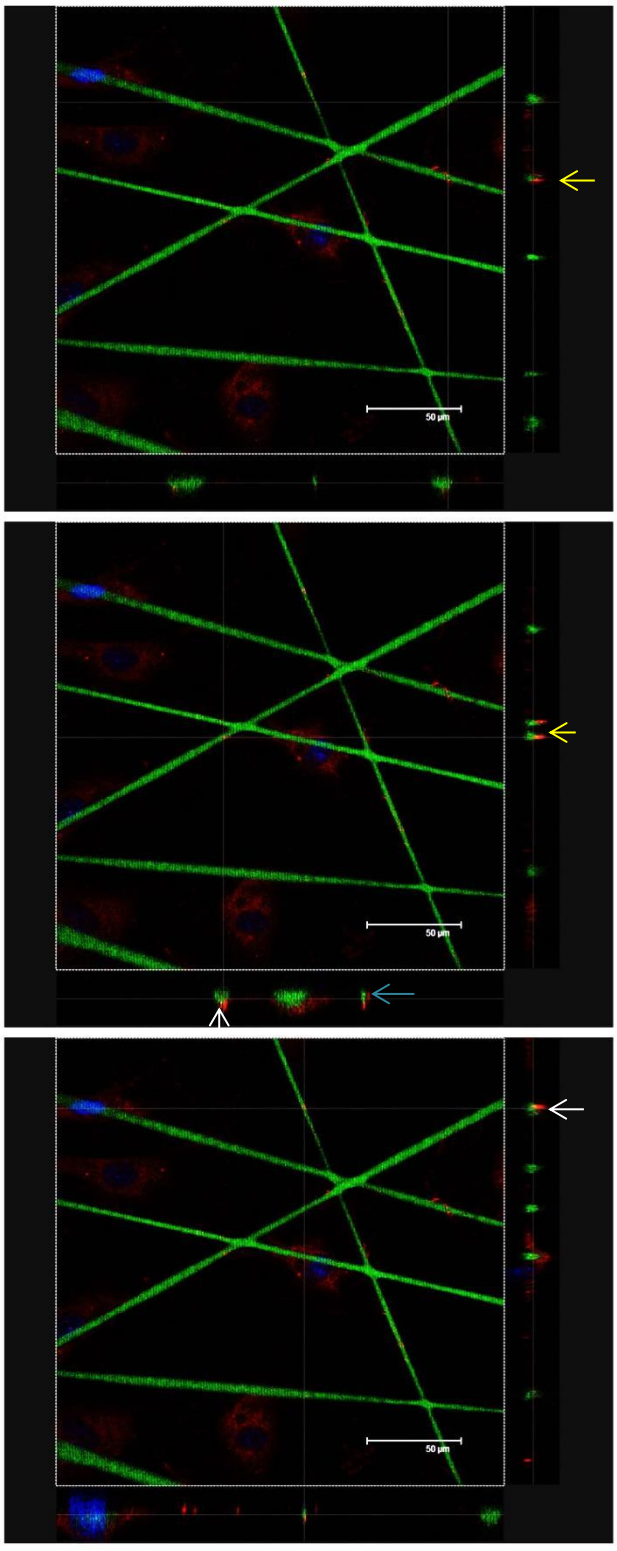

Figure 4.10 Cross section images of focal adhesions where they follow the same pattern as the embossed fibres. White arrows represent FAs appear in the region between the peaks of the ridges, yellow arrows represent FAs on the top of the ridges, blue arrow represent FAs at the bottom of the grooves.

In order to study the influence of the relief structure on the HUVECs, the substrates were coated with 0.25 µg/ml poly(L-lysine)-graft-poly(ethylene glycol)co-polymer (PLL-g-PEG) to prevent protein from adhering to the glass cover slips for 1 hour and then coated with 10 µl/ml fibronectin for 1 hour. After this treatment, HUVECs will only adhere to the fibres in the initial stages of the culture period. On testing, the PLL-g-PEG coating proved effective up to 2 days after which, cells began to adhere to the glass cover slips. Figure 4.11 shows a cell attached to the embossed fibres without adhering to the glass cover slip. In accordance with the previously described observations, focal adhesions appear predominantly at the cell edge, although there are still some present in the central area of the cell. Focal adhesions are either along the side of fibres or follow the same pattern as the fibres, which seem to be organized along the side wall and the botton of the relief structure. And a few of them appear on the ridges.

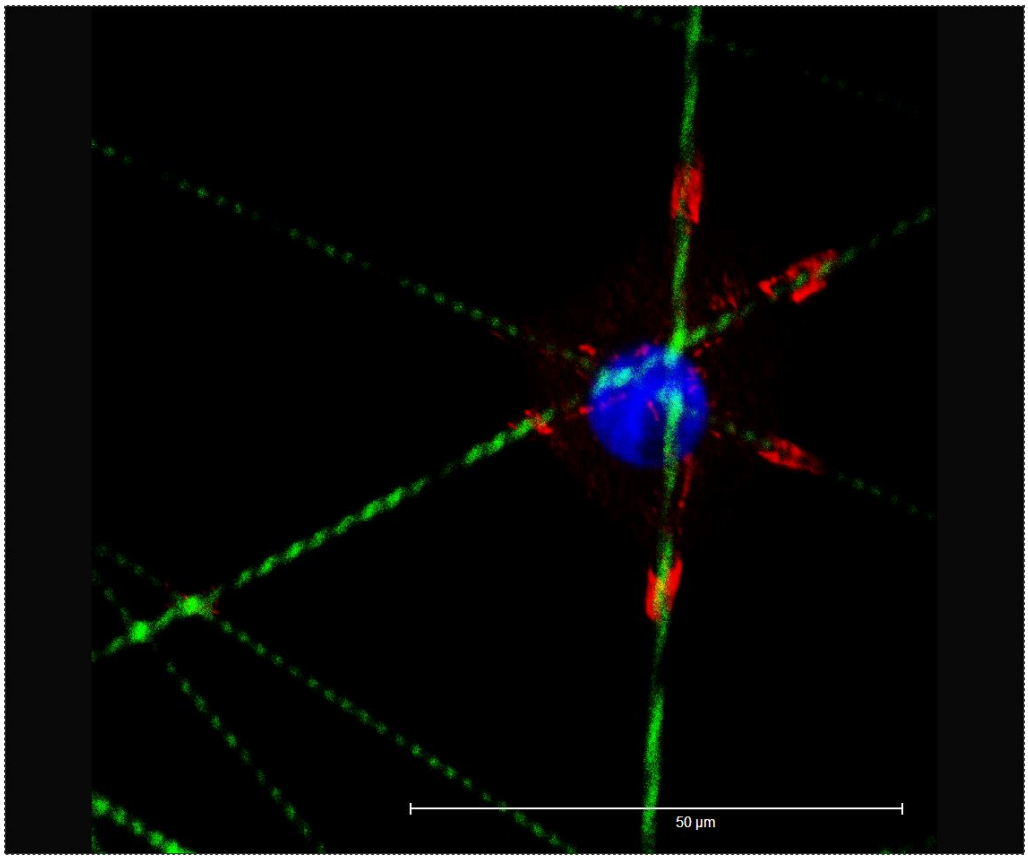

Figure 4.11 Overlay confocal microscopy image of HUVECs stained for the nucleus (blue) and vinculin (red) on PLL-PEG treated substrate.

The area of focal adhesions is measured using Image J software and the percentage of focal adhesions on fibres and glass cover slips wascalculated in the same cells for every count as follows,

$$A_{fibre}\% = \frac{A_{fibre}}{A_{fibre} + A_{glass}} \times 100\%$$

$$A_{glass}\% = 1 - A_{fibre}\%$$

A_{fibre} is the area of focal adhesions on the fibres, A_{glass} is the area of focal adhesions on the glass cover slip.

Images used for Image J analysis are all obtained after 1 day of culture on the substrates not treated with PLL-g-PEG. The percentage of total area covered by focal adhesions on embossed fibre samples was significantly higher than that covered by the same cells on glass cover slips (Figure 4.12). However, this result shows an average trend in the behaviour of focal adhesions and includes individual samples, for instance, where the percentage of focal adhesions on fibres is 43.55% which is lower than the value (56.45%) of those on the glass cover slip in the same cell. Nevertheless, focal adhesions on fibres present a more aggregated arrangement while those on glass cover slips are more dispersed and tend to be situated near the edge of the cell membrane.

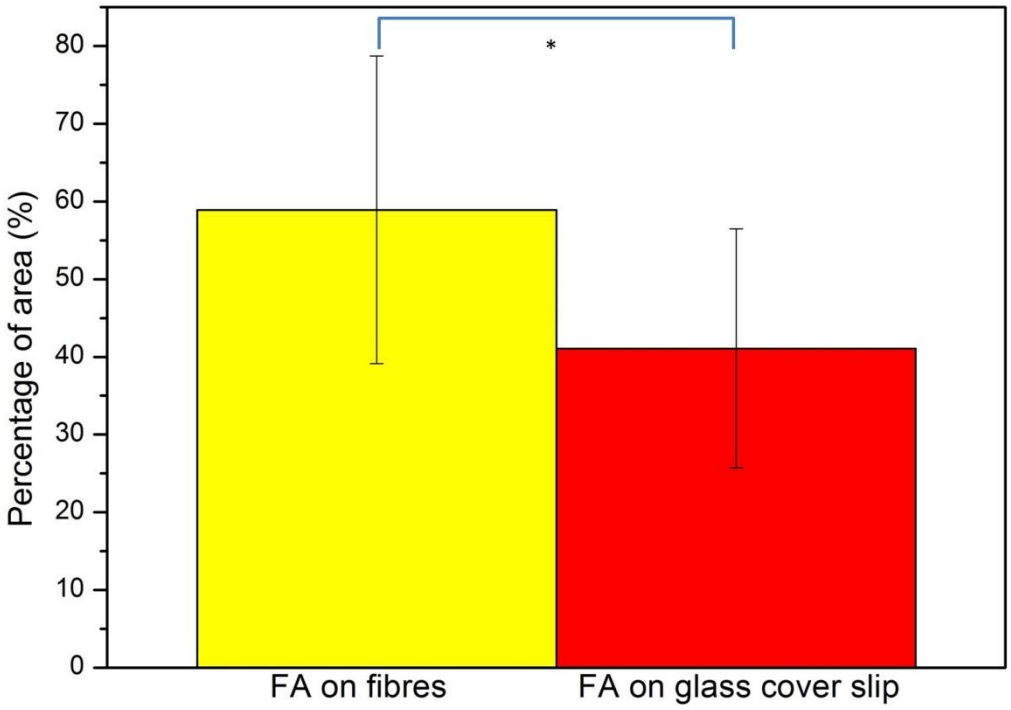

Figure 4.12 The percentage of focal adhesions on fibres and glass cover slips

4.2.4 Cell morphology

The structure and shape of a cell is provided by the cytoskeleton. Microtubules, intermediate filaments and microfilaments are three main kinds of cytoskeletal filaments (Minton, 1992). Microfilaments, also called F-actin, control cytokinesis, provide mechanical properties and allow cells to migrate (Cooper and Hausman, 2009). In particular, the shape and consistency of a cell are determined by the length and attachment architecture of its filaments (Britannica, 2014). In this study, cytoskeleton elements were visualized by staining the F-actin and examined with a confocal microscope.

The morphology and distribution of F-actin in HUVECs on glass cover slips is shown in Figure 4.13. F-actin is present as thin filaments which can be as long as several micrometres distributed throughout the HUVECs forming a contiguous meshwork. The majority of these filaments also exhibit cortical structures and form characteristic ruffles (white arrow).

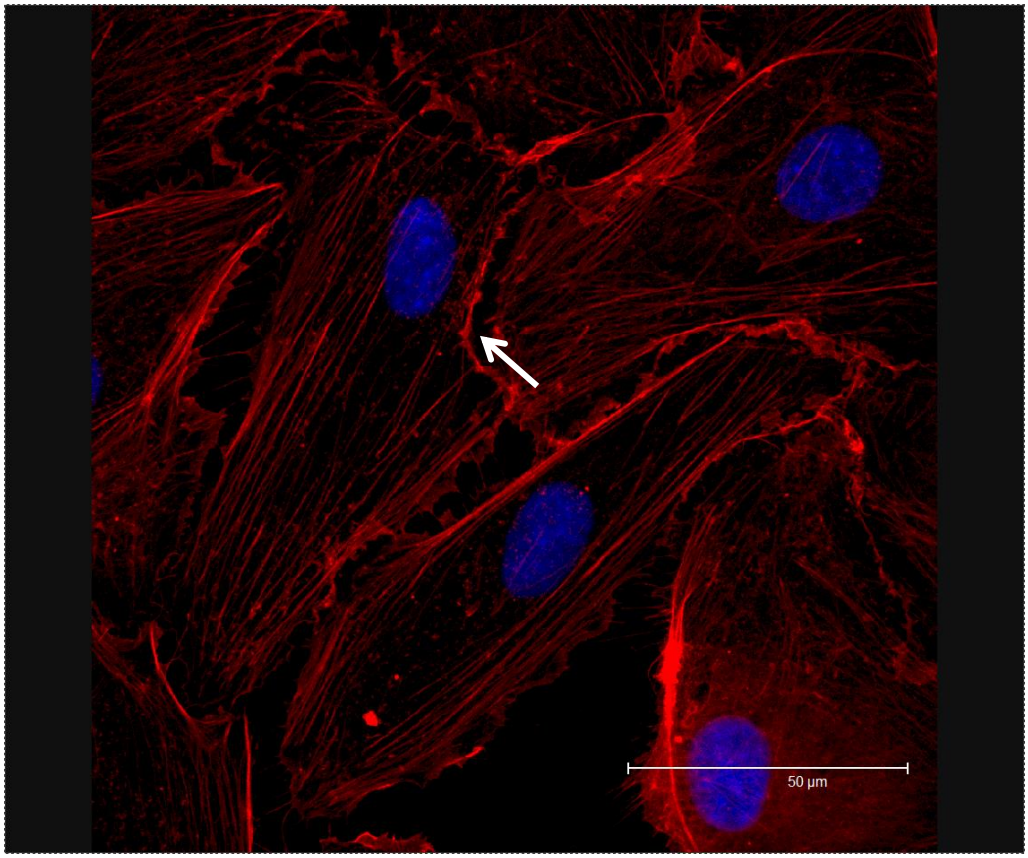

Figure 4.13 Overlay confocal microscopy image of HUVECs stained for the nucleus (blue) and F-actin (red) on glass cover slip. White arrow represent the ruffles area.

Non-embossed fibres of larger diameter seem to have an influence on the orientation of HUVECs. However, F-actin still appear contiguously on them (yellow arrow) while fibres of smaller diameter (white arrow) disrupt the

consistency of the filaments (Figure 4.14 A). When the F-actin is perpendicular to the relief structure (blue arrow), they are significantly affected by the surface texture and present disordered morphology (Figure 4.14 C E). On the other hand, when the F-actin is parallel to the relief structure, no significant influence can be observed and some filaments even become more organized in the concave area of the surface texture (Figure 4.15 A, white arrow on the left). These observations suggest that fibres with larger diameter and the surface textures which are parallel to the orientation of F-actin do not have significant or disruptive influence, whereas smaller fibre diameter and the relief structure that are perpendicular are more positively influential on the morphology of F-actin.

The cross section images (Figure 4.15) suggest that, irrespective of the F-actin being disrupted (Figure 4.15 C) or not (Figure 4.15 B) by the surface texture, the filaments still appear to be on top of the fibres.

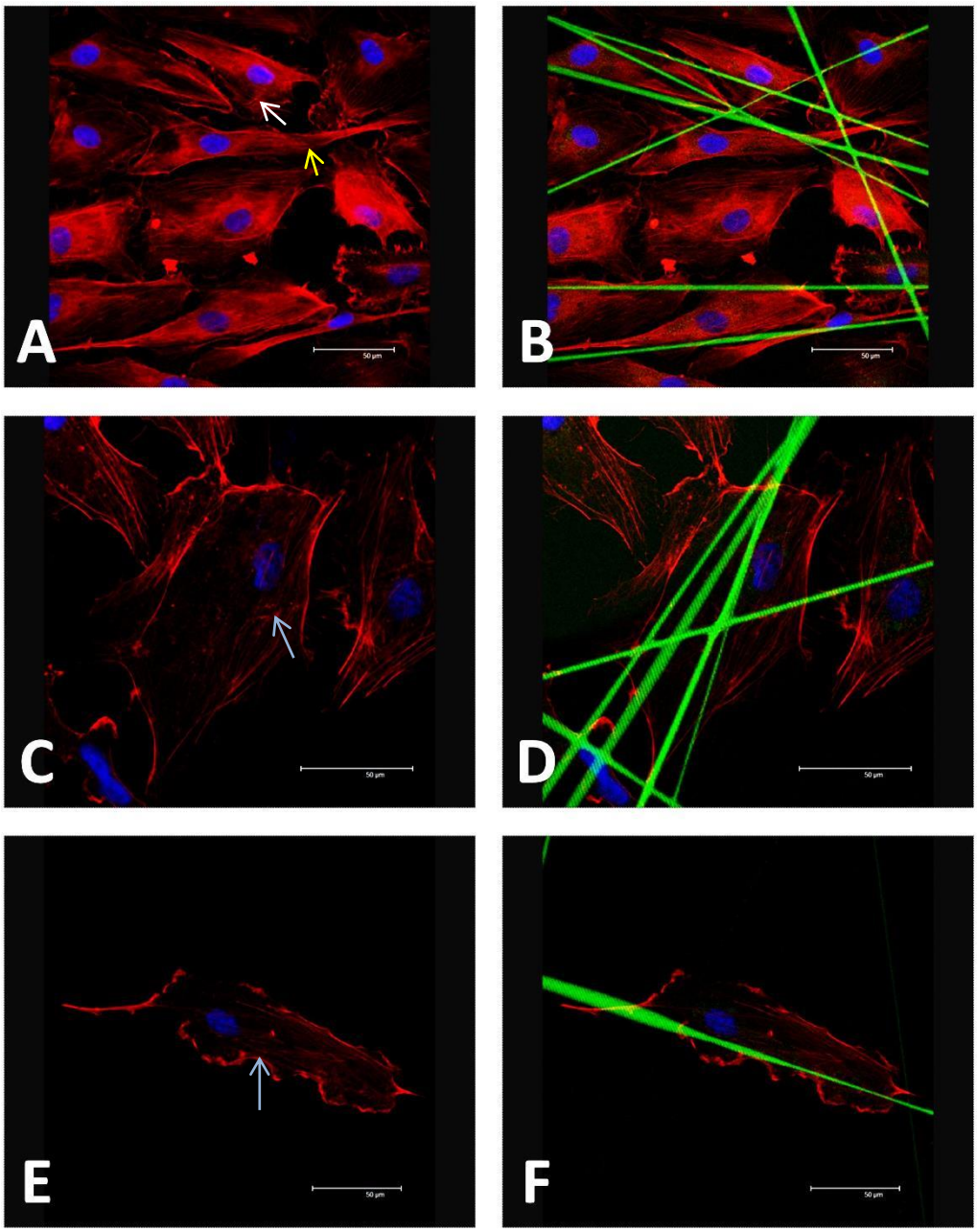

Figure 4.14 Overlay confocal microscopy image of HUVECs stained for the nucleus (blue) and F-actin (red) on photoembossed fibres. Images on the right are those on the left merged with corresponding images of fibres (green, autofluorescenced) as reference. (B) non-embossed fibres (C) and (D) embossed fibres. White arrow represent the disrupted F-actin on smaller diameter fibre, yellow arrow represent the unaffected F-actin on larger diameter fibre, blue arrows represent the F-actin is perpendicular to the relief structure.

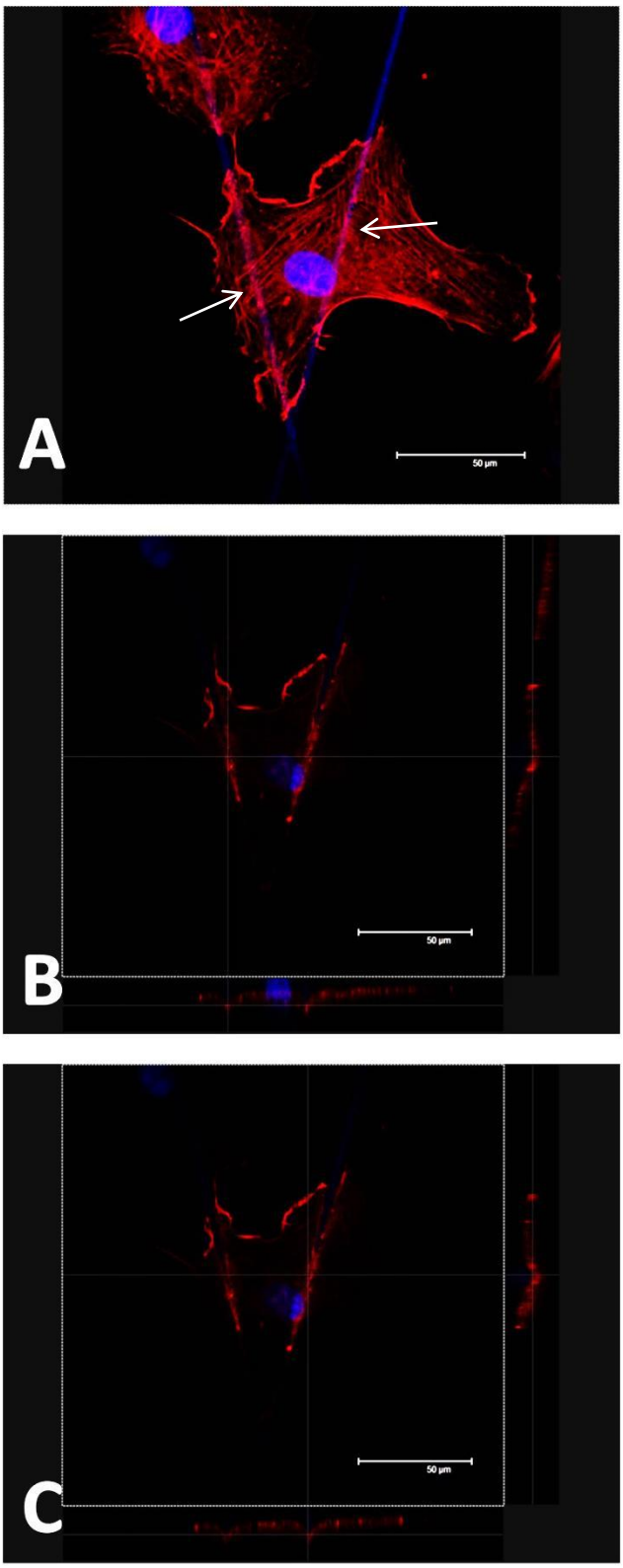

Figure 4.15 Cross section images of F-actin where it is influenced by the relief structure of the embossed fibres. White arrows represent the F-actin on the surface of the fibres.

4.3 Discussion

Due to its adjustable degradability, PLGA is considered to be one of the most potentially valuable biomaterials for bioengineering. However, the acidic environment caused by its degradation products and its surface hydrophobic properties limit the utility of PLGA. Therefore, it is very necessary to improve the cellular affinity and surface wettability of PLGA. The added biocompatible monomer TPETA does indeed lessen its hydrophobic properties, the contact angle being reduced from $79.31 \pm 0.45^{\circ}$ to $61.63 \pm 0.86^{\circ}$, but this does not improve its cellular affinity. The contact angle of photoembossed PLGA-TPETA films with a 20 μm pitch approaches this ideal at $68.72 \pm 0.56^{\circ}$ and, among the three kinds of substrates, the MTS results indicate that HUVECs present best attachment and proliferation on the embossed PLGA-TPETA films. This is in accordance with the literature and our previous results.

The semi-degradable photopolymer PLGA-TPETA was successfully electrospun into fibres with different diameters and photoembossed through holographic lithography without changing their fibrous structure (Figure 4.4). Fibre diameters can be controlled by using PLGA binders with different inherent viscosities: the higher the inherent viscosity of PLGA used, the thinner the fibres obtained (Figure 4.1). Holographic lithography photoembossing does not require the samples to be in contact with a photomask which makes the process extremely suitable for texturing the uneven surface of electrospun fibres. Different heights of the relief structure can be achieved by changing the laser pulse duration which is directly related to the UV dosage. Furthermore,

higher UV dosages are required for smaller pitch surface textures to achieve the optimum height.

HUVECs show a preference for settling onto the fibres immediately after cell seeding, and begin growing from the fibre intersections (Figure 4.8). This is probably because, in this initial stage, the intersections can provide a larger surface area than the isolated fibres and a rougher surface than the glass cover slips.

Focal adhesions play an important role in mediating cell–ECM adhesion, force transmission, cytoskeletal regulation and signalling (Burridge and Chrzanowska-Wodnicka, 1996, Geiger et al., 2001, Bershadsky et al., 2003). The ECM and actin cytoskeleton are linked by focal adhesions at a scale of less than 200nm (Franz and Müller, 2005, Chen and Singer, 1982), the adhesion sites consisting of a complex network of trans-plasmamembrane integrins and cytoplasmic proteins (Zaidel-Bar et al., 2007). At this latter date, the molecular architecture of focal adhesions was still unknown. In addition, it was not clear whether focal adhesions were structurally unorganized, or if the relevant structural organization was in the third dimension (Kanchanawong et al., 2010). It has been reported that in focal adhesions, the integrin-actin does not display a physical overlap which is in accordance with the observed absence of their binding interactions in vitro (Burridge and Chrzanowska-Wodnicka, 1996, Geiger et al., 2001). Furthermore, it is reported that there is a gap of about 40 nm between the integrin cytoplasmic tails and the actin cytoskeleton which is caused by the presence of protein-specific strata. This indicates the importance

of a ‘focal adhesion core’, which is constructed by the presence of protein-specific strata, domain bridging this gap and determining the nanoscale protein organization (Kanchanawong et al., 2010). Integrin-mediated signalling, cytoskeletal adaptors and actin-regulatory proteins are considered to be three functional categories of key focal adhesion proteins. In integrin-mediated signalling, FAK and paxillin are both considered to be signalling/adaptor subcompartment of the focal adhesion core. For cytoskeletal adaptors, vinculin is supposed to reinforce the connection between actin and the ECM (Galbraith et al., 2002) thus making vinculin the crucial site in regulating force transmission. Zyxin and VASP which are considered to be actin-regulatory proteins, are recognised as playing a cooperative role in regulating actin assembly (Yoshigi et al., 2005). Furthermore, α-actin organizes the actin at focal adhesion sites. Kanchanawong (Kanchanawong et al., 2010) demonstrated that talin could act as a vertically oriented scaffold for the stratified focal adhesion core by forming tethers that span the gap between integrin and actin.

Focal adhesions in HUVECs on smooth surfaces are randomly distributed in the perinuclear region and the edge of the cells (Figure 4.6). Particularly when the cell is elongated, focal adhesions will be more concentrated at the poles. When the fibres possess a relief structure on their surface, some focal adhesions exhibit the same pattern as the relief structure, some are organized along the side of fibres, and others seem unaffected (those on the top or the bottom of the relief structures). Moreover, those focal adhesions reflecting the topographic pattern of the fibres also seem to be adhering along the sidewall of

the relief structure rather than on the top of the ridges. It has been shown that a sufficient minimum length of focal contact is required to provide adhesion (Ohara and Buck, 1979). Thus when the surface topography could not provide enough space for focal adhesions to attach, they may not be able to affect the distributions of focal adhesions. Using the same cells, the average area of focal adhesions observed on the fibres was significantly higher than on the glass cover slips, despite individual exceptions to the contrary. However, from all the results we obtained, there is no doubt that focal adhesions on fibres present a more aggregated arrangement, while those on glass cover slips were more randomly dispersed and tended to form near the edge of the cell membrane.

The cytoskeleton provides a cell with structure and shape. To be specific, the shape and consistency of a cell are largely determined by the length and the attachment architecture of F-actin (Britannica, 2014), which forms one of the principal kinds of cytoskeleton filaments (Minton, 1992). HUVECs are seen to orient themselves in the direction of fibres and F-actin does not seen to be influenced by the presence of larger-diameter non-embossed fibres. On the other hand, in general, F-actin seems to be disturbed by smaller diameter fibres and by the surface topographies of textured fibres. However, when the F-actin is parallel with the surface texture, its activity will not be interrupted and may even be more organized in the concave area to reflect the pattern of the substrate. Finally, regardless of whether the F-actin is disturbed or not, it appears on the top of the fibres.

4.4 Conclusions

The added functional biocompatible monomer TPETA was found to increase the hydrophilic properties of PLGA without improving its cellular affinity. Photoembossing however, increased the hydrophobic properties of PLGA-TPETA films but with a contact angle that was still smaller than for PLGA and also obtained good biocompatibility. HUVECs show a preference for settling onto the fibres and grow from the fibre intersections, orientating in the direction of the fibres. Photoembossing through holographic lithography can successfully texture the electrospun nano- and micro-scale PLGA-TPETA fibres, and uniform surface textures can be achieved on the surface of the fibres while keeping their fibrous structure, regardless of the fibre diameters. Focal adhesions may be influenced by both the presence of fibres and their relief structure although F-actin is only affected by fibres with small diameters and the surface topography of textured fibres.

Chapter 5 Fully degradable PLGA-PEGDA-DTT films and fibres

The experimental examination of non-degradable PMMA-TPETA and semi-degradable PLGA-TPETA photopolymers are discussed in Chapter 3 and Chapter 4 and show that, in both cases, the photoembossing treatment improved cell attachment and accelerated cell proliferation of HUVECs. However, fully degradable biomaterials are also needed for use in therapeutic devices such as scaffolds with 3D porous structures, drug delivery vehicles and temporary prostheses (Nair and Laurencin, 2007). The ability of degradable materials to be absorbed by the body, thereby avoiding the need for further surgery to remove the implantation has drawn significant attention from researchers in the bioengineering field.

Instead of TPETA, PEGDA and DTT were added as functional monomers to PLGA to create a fully degradable photopolymer, which was seen to completely degrade during the accelerated degradation experiments. Relief structures could be obtained on the PLGA-PEGDA-DTT substrates through photoembossing on both films and fibres, and the height could be tuned by varying the UV dosages. Biocompatibility of this photopolymer was also investigated in this research as it is one of the most important properties of a biomaterial, especially a degradable biomaterial in which biocompatibility may vary over time.

5.1 Materials and methods

5.1.1 Materials

This chapter will concentrate on the degradation of the photopolymer, so that PLGA (50/50) which supposed to degrade fastest among the PLGA with different ration of glycolide units to lactic units is used as the polymer binder. The cross-linked PEGDA and DTT hydrogel have been extensively studied recently and shown to be hydrolytically degradable, the degradation also being capable of control. We therefore introduce PEGDA and DTT as the functional monomers to create this fully degradable photopolymer. These are dissolved in a mixture of chlorobenzene and DMSO with PLGA and the photo initiator, Irgacure 369. The polymer binder, PLGA is at a ratio of 1:1 by weight with PEGDA, DTT is at 0.8 mol of PEGDA and Irgacure 369 is at 5 wt. % of PEGDA. The chlorobenzene and DMSO are at a 1:1 ratio by weight and twice the total weight of the PLGA and PEGDA. PEGDA with molecular weights of both 258 and 6000 were used in separate experiments.

5.1.2 Preparation of PLGA-PEGDA-DTT films and fibres

In order to successfully obtain the fully degradable photopolymer solution, the chemicals described above have to be added in a certain order. PEGDA should be dissolved in the mixture of chlorobenzene and DMSO first. After the

PEGDA is totally dissolved, the DTT and Irgacure 369 can be added. After the DTT and Irgacure 369 are dissolved, the PLGA can finally be added.

The photopolymer solution was coated onto 13 mm acrylate functionalized glass cover slips with a wire bar coater resulting in films with a thickness of 60±5 μm. Films were allowed to dry in shade on a heater at 40 ℃ for 20 min. The film was textured using a 20 μm pitch photomask and the optimum UV intensity of 704 mJ/cm^2 determined by our previous studies (Hughes-Brittain, 2013). After the first exposure, samples were heated at 120 ℃ for 20 min, followed by a flood UV exposure of 1701 mJ/cm^2.

The photopolymer solution was also used to fabricate electrospun fibres with a voltage of 20 kV, a flow rate of 0.5 ml/hour and a distance between nozzle and collector of 20 cm. These fires were photoembossed by holographic lithography as described in Chapter 4. The fibres were exposed to UV with a pulse duration of 350 μs, followed by heating at 120 ℃ for 20 min and finally subjected to a flood UV exposure.

5.1.3 Cell culture and proliferation

HUVECs were cultured and maintained as previously described in 2.1. Before being seeded, all substrates were soaked in 75% ethanol for 30 min, and then washed 3 times with DPBS. Fibre substrates were used as previously described while film substrates were divided into two groups, one group being used directly as previously described and the other group being aged in DI-water for

3 days before use. Substrates were then transferred into 24-well plates and the cell suspension was pipetted directly onto the substrates at a density of 1.5×10^4 cells/cm^2 and then cultured up to 7 days depending on the various experimental requirements.

A cell proliferation assay with MTS was carried out on the PLGA-PEGDA-DTT films and processes as previously described.

5.1.4 Analysis of substrates

Both PLGA-PEGDA-DTT photopolymer and pure PLGA are separately made into cylindrical shapes in a stainless steel mould with 50 mm holes. The solutions are put into the mould and dried overnight in a convection oven at 80 ℃. The mould containing the polymer is then exposed on each side to UV light for 10 min. The solid polymer cylindrical constructs are then taken out of the mould and again exposed to UV for 20 min. Accelerated hydrolysis of the polymer solids is then carried out in 1 M of NaOH in DI-water at room temperature. The polymer constructs and any probable fragments are removed every 4 to 8 hours, washed with DI-water, dried in a vacuum at room temperature and then weighed.

As cross-linked PEGDA and DTT form a hydrogel which will swell in the culture medium, both dry and swollen PLGA-PEGDA-DTT films were measured with the AFM. The contact angle is also measured on the PLGA-PEGDA-DTT films embossed with a 20 μm pitch. The surface morphology of

degraded PLGA-PEGDA-DTT films is examined with an SEM. Photoembossed fibres are examined with an epifluorescence microscope.

5.1.5 Data analysis and statistical methods

All quantitative measurements are reported as mean values ± standard deviation. To determine statistical differences when comparing the differences between groups, a student's t-test was used.

5.2 Results

5.2.1 Synthesis and characterization of PLGA-PEGDA-DTT films and fibres

PLGA-PEGDA-DTT photopolymer was successfully photoembossed (Figure 5.1 A) by exposure to a UV dosage of 704 mJ/cm^2 with a 20 µm pitch photomask and then heated at 120 ℃. The molecular weight of PEGDA we decided to use was 258 after comparison with the larger (6000) PEGDA molecule. Whereas the smaller PEGDA molecules permitted an even coating of substrate which remained fixed to the acrylate functionalized glass cover slips, the films made with the heavier PEGDA component repeatedly detached from the cover slips once immersed in the medium, tended to get folded during the experiment and even floated to the top of the medium. This may be because

the higher molecular weight PEGDA causes greater swelling. As with PMMA-TPETA and PLGA-TPETA, the height of relief structures produced in the PLGA-PEGDA-DTT photopolymer can be tuned by changing the UV dosages and the temperature used in the heating stage. Details can be found in my colleague's thesis (Hughes-Brittain, 2013). Here we chose the optimum conditions to fabricate the embossed films for the following studies.

As both PEGDA and DTT can be photocross-linked to form a hydrogel network which will swell in the presence of liquid (Hudalla et al., 2008), we speculated that our PLGA-PEGDA-DTT photopolymer would also swell. We has observed phase separation between the cross-linked thiol-acrylate network and the PLGA polymer binder in our previous studies indicating that the thiol-acrylate network had diffused to form the ridges and leaving a higher concentration of PLGA in the grooves with a stiffer surface. Embossed PLGA-PEGDA-DTT films were kept in culture medium up to 7 days and examined with an optical microscope. Dried samples (Figure 5.1 A & C) were created by removing from the medium at the 3- and 7-day time points and drying overnight in a convection oven at 80 ℃. The morphology of relief structures was still in order on day 3 for both dried (Figure 5.1 A) and wet (Figure 5.1 B) samples although the dried sample presented a surface texture with relatively flat ridges (the darker areas) while the wet sample showed swollen ridges (the brighter areas). By the 7^{th} day, neither the dried (Figure 5.1 C) nor the wet (Figure 5.1 D) samples exhibited clear relief structures leaving only traces of the previous textures on the majority of the surface. This swelling phenomenon is in accordance with the AFM measurements of the embossed film taken in

DPBS. Samples were measured after 2 hours kept in DPBS. The AFM results show that even after only 2 hours in DPBS, the relief structure is already swollen and has become extremely rough. In addition, the relief height has increased from an average of around 1.5 μm (average height) to a maximum of 2 μm (Figure 5.2).

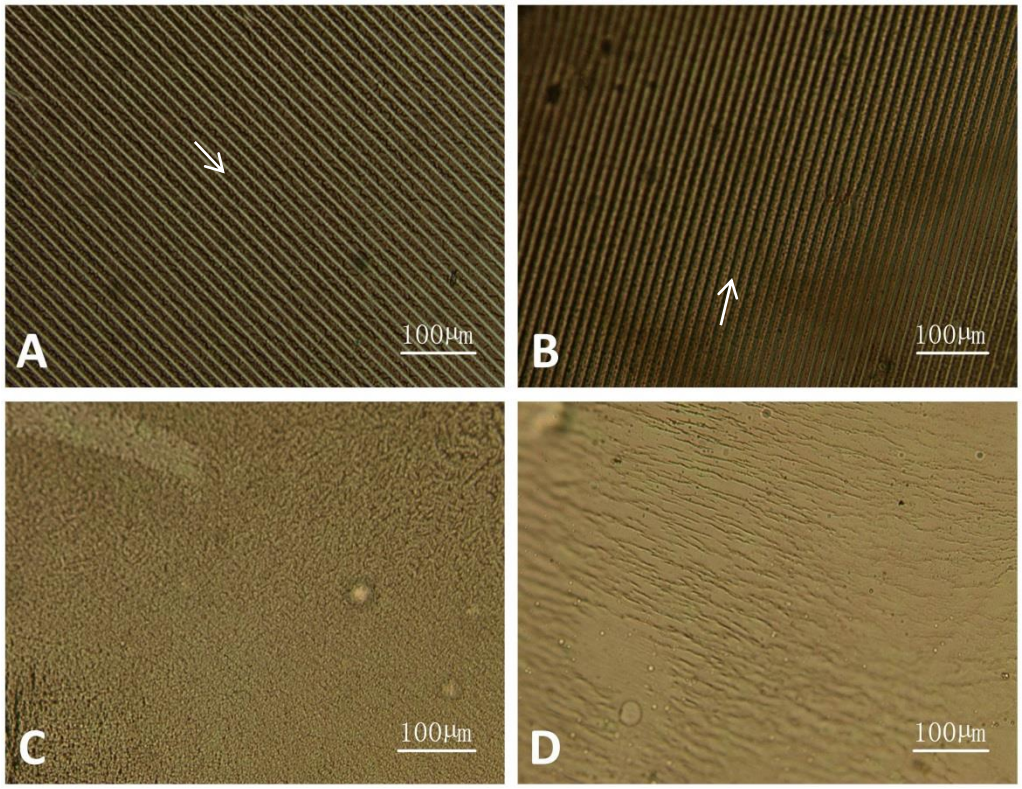

Figure 5.1 Photoembossed PLGA-PEGDA-DTT films after 3 days in culture medium (A) dried (B) wet and after 7 days in the medium (C) dried (D) wet. Arrows indicate the ridge area.

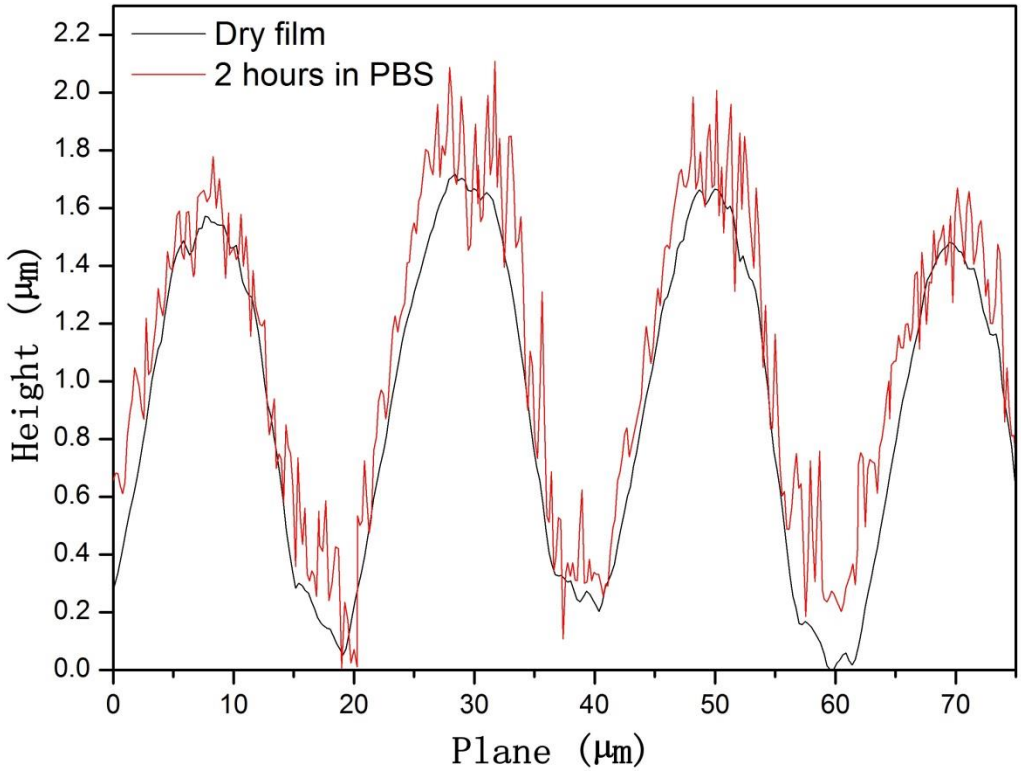

Figure 5.2 AFM graph of PLGA-PEGDA-DTT films dry (black) and 2 hours in PBS (red)

PEGDA with the higher molecular weight of 6000 was used in the electrospinning process as it is known to improve the chances of polymers with higher molecular weight to be spun. The obtained fibres were embossed through holographic lithography. As shown in Figure 5.3, PLGA-PEGDA-DTT photopolymer fibres were successfully electrospun and photoembossed. However, the morphology of these fibres is not as uniform as that of the PLGA-TPETA fibres.

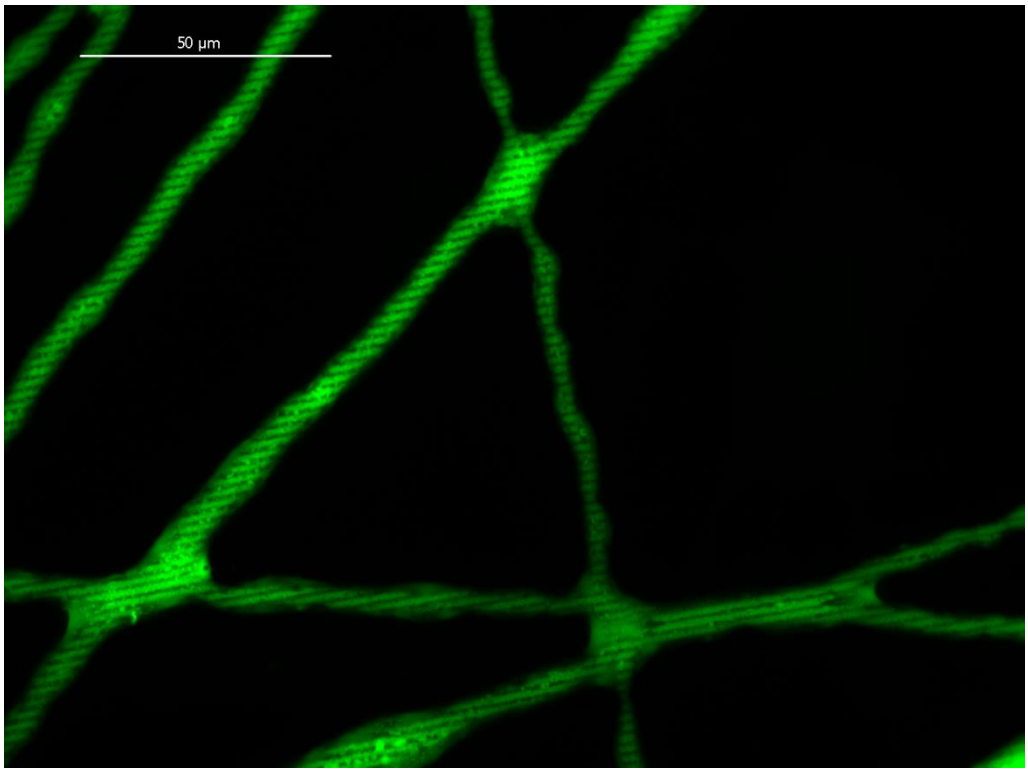

Figure 5.3 Electrospun PLGA-PEGDA-DTT fibres

5.2.2 Degradation

Samples were kept in culture medium in an incubator at 37 ℃ in 95% air/5% CO_2 and dried overnight in a vacuum at room temperature at each time point. The degraded surface of fully degradable PLGA-PEGDA-DTT films and semi-degradable PLGA-TPETA films were examined with an SEM. The most visible changes observed in morphology at each time point are described below.

In accordance with observations by an optical microscope, the embossed texture on PLGA-PEGDA-DTT films was still clear and orderly after 3 days in

the culture medium but with some uneven areas. There were numerous crater-like depressions, sometimes several times the pitch size, various lumps or ‘pimples’ with some smaller pores around and wrinkles along the sides of the ridges (Figure 5.4 A). As the experiment proceeded, the texture gradually become disordered in a variety of ways but in general, became shallower or even approaching a flat morphology. On the other hand, the embossed texture on PLGA-TPETA films appeared more durable and kept its general morphology up to 35 days (Figure 5.4 B D F). The degradation of both kinds of film is very much related to the behaviour of its ‘skin’. This is a thin, relatively smooth layer (white arrow) covering the surface of the films and once it isdisruped , large numbers of PLGA particles will be revealed (Figure 5.6). After 7 days, the PLGA-PEGDA-DTT film had not dramatically changed although showing more flat ridges and shallower grooves. Wrinkles alongside the ridges might have been caused by the drying process. PLGA particles had begun to appear in the grooves (Figure 5.5 A B). After 14 days, the peaks of some of the lower ridges had been dehisced from the centre (white arrow) exposing large numbers of PLGA particles underneath. Furthermore, PLGA particles appear to have become more uniformly dispersed on both ridges and grooves. This is probably because of the flattened profile which means the diffusion process was not intense in that area (Figure 5.5 C). By day 21, the ‘skin’ of the PLGA-TPETA film in the groove area had begun to break revealing PLGA particles (Figure 5.4 D). After 28 days, PLGA particles had also appeared on the surface of high ridges as well as increasing in the grooves, which had previously looked smooth. Moreover, this space between the ridges

had become even smaller due to the swelling of the hydrogel network (Figure 5.5 D). The typical hydrogel morphology with 3D pore structures was observed after 35 days, most of the pores being concentrated on the ridges (Figure 5.4 E). This reflects the phase separation between the cross-linked thiol-acrylate network and the PLGA polymer binder again. In the meantime, some ridges on PLGA-TPETA films had broken up and fewer PLGA particles are left at the bottom of the groove area appearing more numerously at the root of the ridges (Figure 5.4 F).

The ridges seem to coalesce as they become even lower and, after 42 days, the ridges actually appear concave, being higher on either side of the former peak (Figure 5.5 E). Additionally, porous structures have appeared on the surface of these concave ridges and large ‘wells’, presenting a relatively smooth surface look like the surface of the centre of ‘craters’ come out in the first few days. In ‘lumpy’ areas, the underlying hydrogel structure is occasionally visible as are PLGA particles (Figure 5.5 F). By Day 63, PLGA particles are also visible through cracks in the embossed texture which appear to have begun along the grooves (Figure 5.5 G) and after 70 days, PLGA particles have appeared on the surface of ‘lump’ (Figure 5.5 H). By day 77, many holes, which are believed to be associated with the cross-linked thiol-acrylate hydrogel structure of the substrate, have perforated the surface (Figure 5.5 I). In other areas, some area pieces of unattached ‘skin’ and scattered PLGA are the only features visible (Figure 5.5 J).

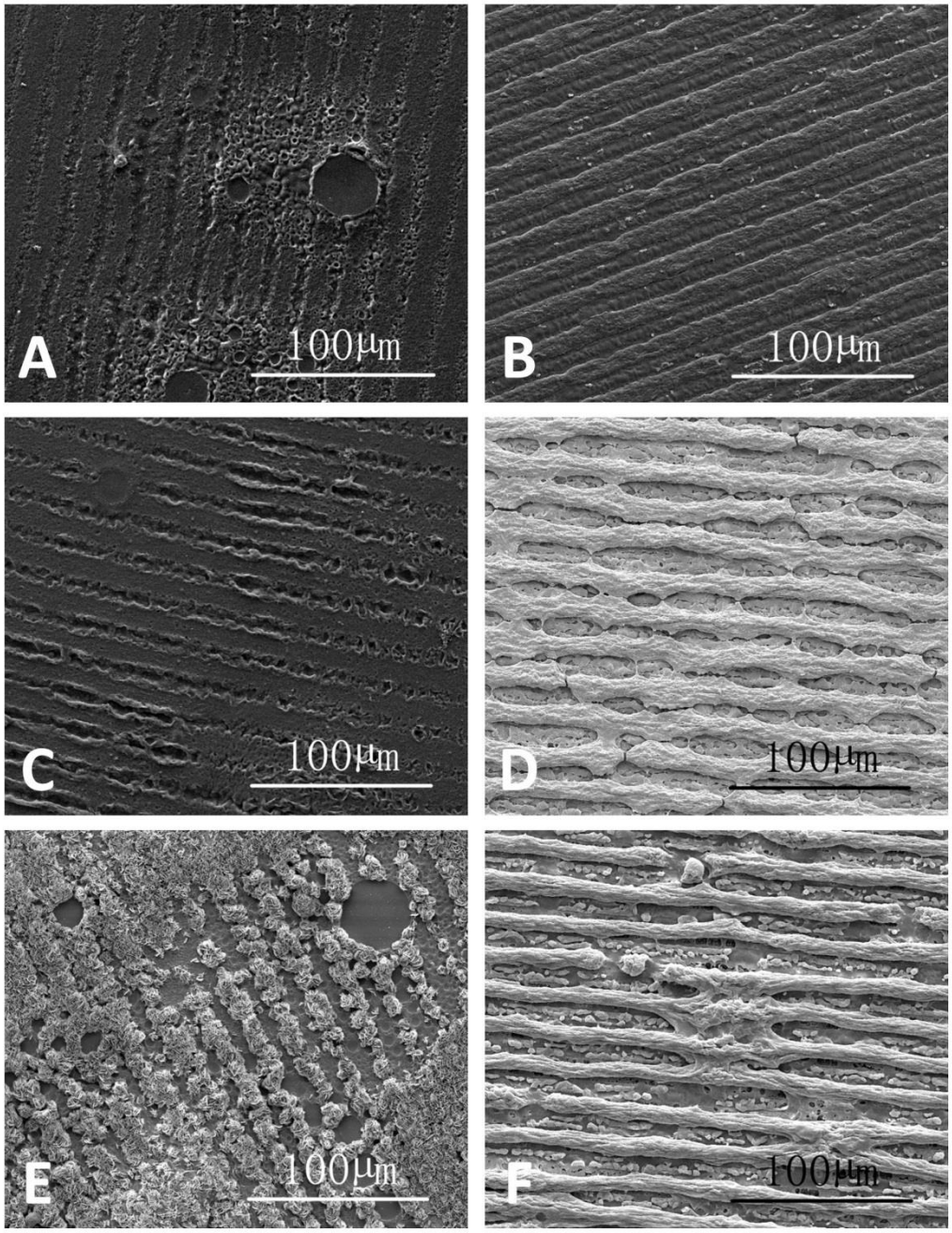

Figure 5.4 SEM image of degraded PLGA-PEGDA-DTT films (left column) and PLGA-TPETA films (right column) on (A) (B) day 3 (C) (D) day 21 (E) (F) day 35.

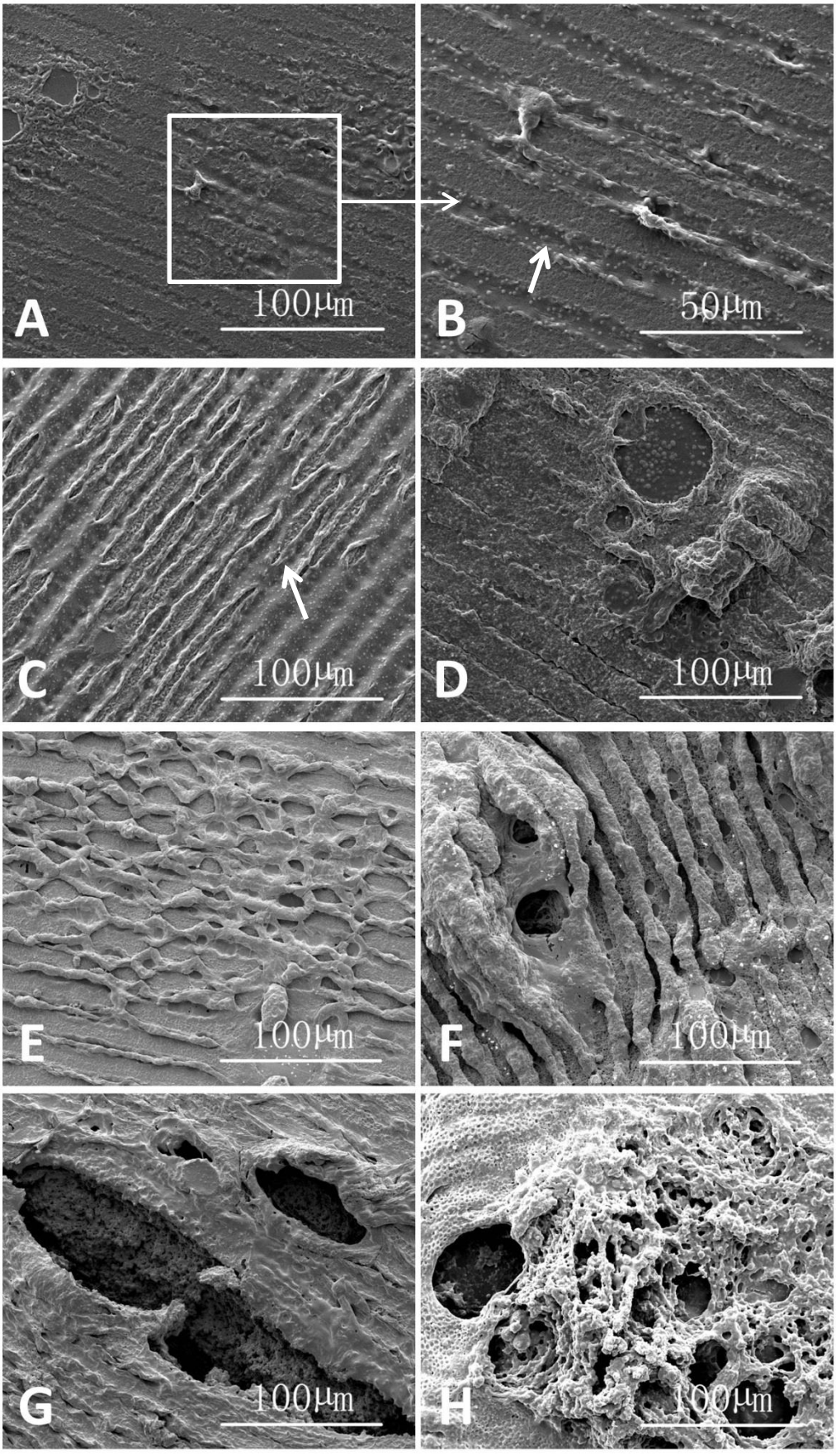
A
100μm
B
50μm
C
100μm
D
100μm
E
100μm
F
100μm
G
100μm
H
100μm

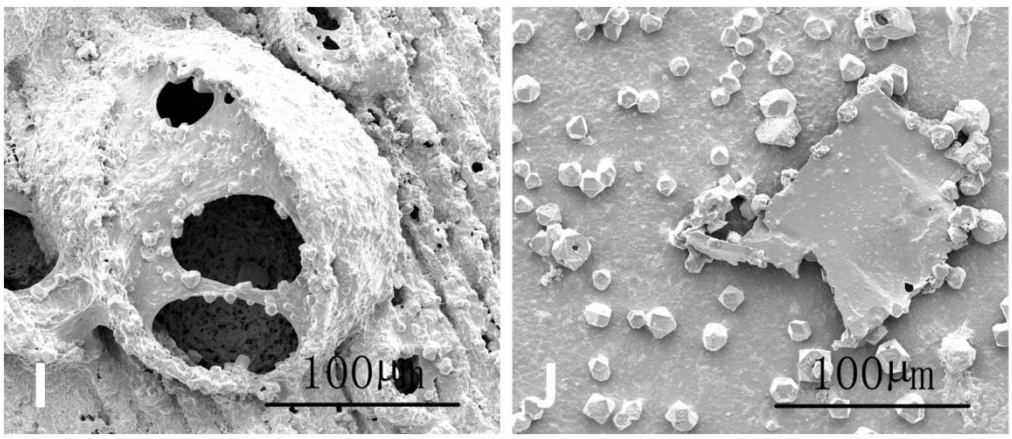

Figure 5.5 SEM images of degraded surface with typical changes of PLGA-PEGDA-DTT films on (A) day7 (C) day 14, arrow indicate the ridge dehisced from the centre (D) day28 (E) day42 (F) day 49 (G) day 63 (H) day 70 (I) (J)day 77, (B) is a higher magnification image of the yellow square area in (A), arrow indicate the PLGA particals.

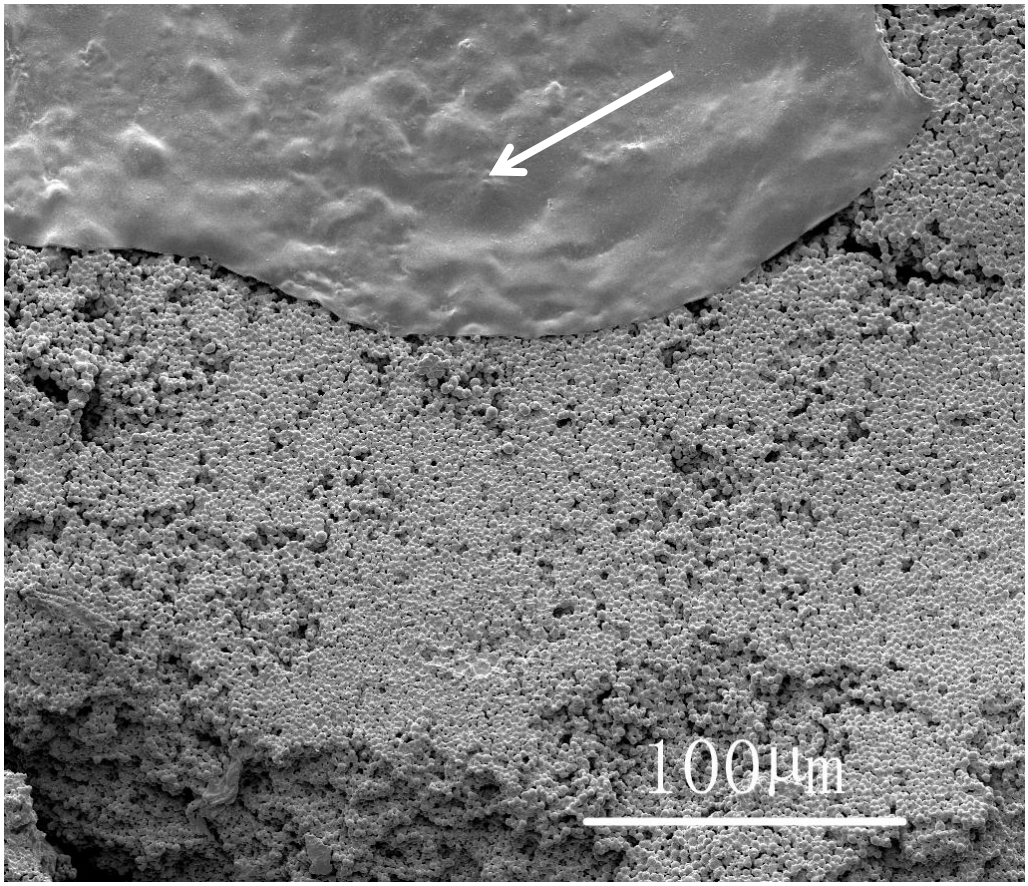

Figure 5.6 PLGA particles under the smooth ‘skin’ on a PLGA-PEGDA-DTT film

Figure 5.7 shows a degraded PLGA-PEGDA-DTT film after 77 days of degradation in the culture medium kept in a 37℃ incubator. In some areas, the trace of the original relief texture can be seen with the naked eye on the underlying glass cover slip. The ratio of the glycolide and lactic units in the PLGA used in this experiment was 1:1, a ratio has been reported which is to cause full degradation in 2 months (Catıker et al., 2000). In the center of the sample where the carbon adhesive tape is underneath, the black areas in this picture should therefore correspond to the original position of the grooves because the diffusion process in the photoembossing procedure resulted in a phase separation between the PLGA polymer binder and the cross-linked thiol-acrylate network which, in turn, caused the PLGA in the ridge area to be protected by a thicker layer of the hydrogel.

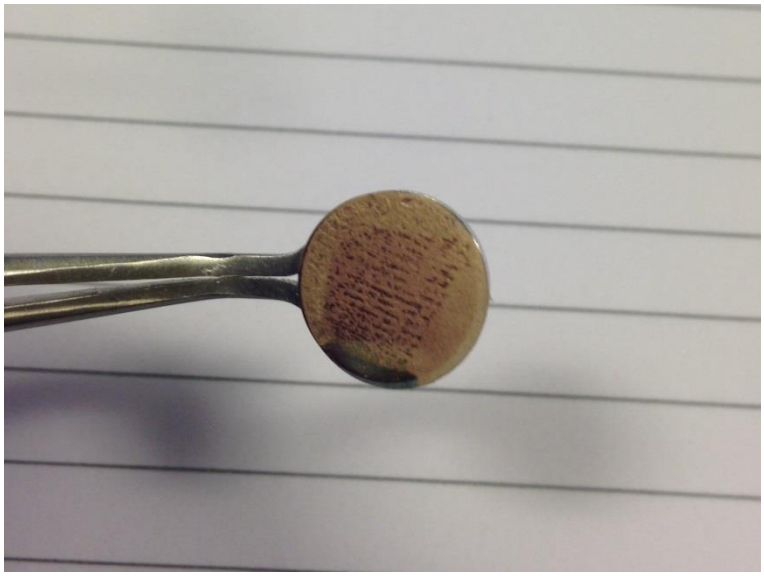

Figure 5.7 Degraded PLGA-PEGDA-DTT film

Accelerated hydrolysis is carried out in 1 M of NaOH in DI-water at room temperature. Polymer bulks and any probable fragments are removed after 4

hours and then every 8 hours, washed with DI-water and then dried in a vacuum at room temperature before weighing. The PLGA-PEGDA-DTT photopolymer demonstrated a much faster degradation than pure PLGA, especially when it comprised the PEGDA with the higher molecular weight, which resulted in full degradation in 8 hours. The pure PLGA degraded at a relatively uniform rate while the degradation of the photopolymer comprising the PEGDA with the lower molecular weight began to slow down after 24 hours when it had lost 80% of its mass. After 56 hours, only 4% of the PLGA-PEGDA(258)-DTT was left while about 68% of the PLGA still remained.

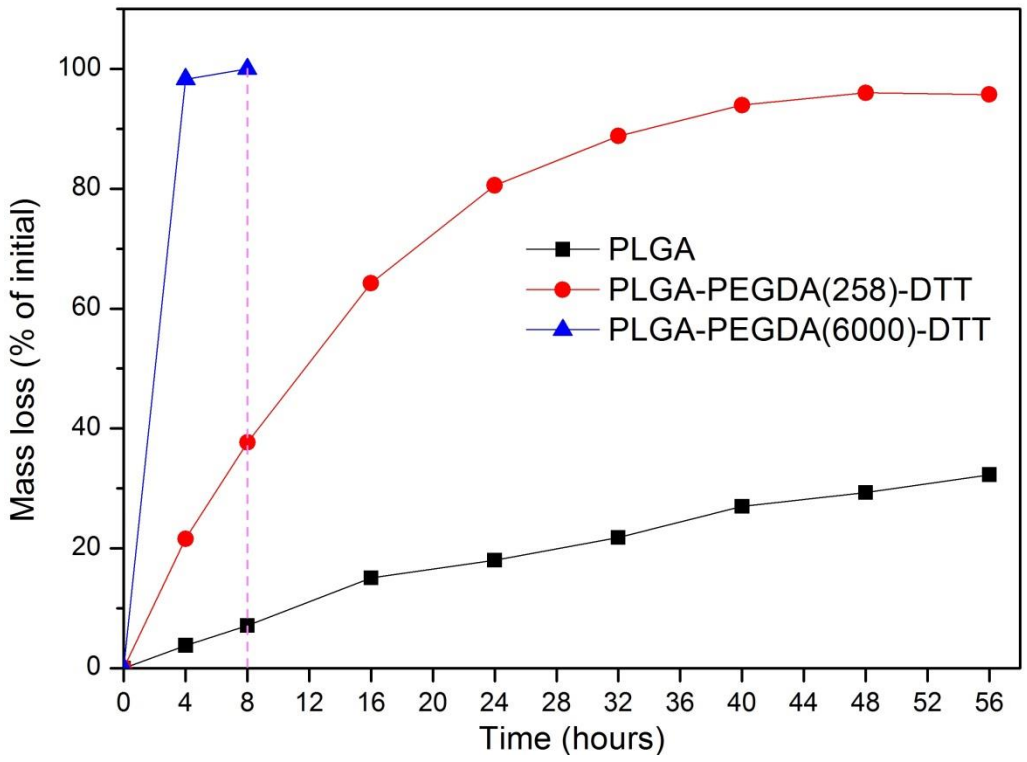

Figure 5.8 Mass loss during accelerated degradation of PLGA, PLGA-PEGDA(258)-DTT and PLGA-PEGDA(6000)-DTT. The numbers in parentheses represent the molecular weight of PEGDA, and the dash line represents complete photopolymer erosion.

5.2.3 HUVEC proliferation

An MTS assay was used to quantify the proliferation of HUVECs as previously described in 2.6. In this case however, before seeding, the cover slips bearing the non-embossed and embossed photopolymer films were each divided into two groups. One group was treated in the normal way by first cleaning and then seeding with HUVECs. The other group of films, (which we called the aged group) were immersed in DPBS for 3 days before proceeding as before. Because no more swelling of the substrates was observed after 3 days. The MTS results (Figure 5.9) show that the proliferation of HUVECs on all the PLGA-PEGDA-DTT films was significant lower than on the pure PLGA film with the exception of those cells on the aged embossed polymer films on the first day. Additionally, HUVECs on the aged group of samples presented significantly higher attachment and proliferation throughout the experimental period compared with the corresponding samples in the normal group. This suggests that the ageing process helped to improve cell attachment on the PLGA-PEGDA-DTT films. However, unlike previous findings for PMMA-TPETA and PLGA-TPETA films, in the majority of cases, there was no significant difference between the non-embossed and embossed photopolymer films in each group, the exceptions being in the normal group on day 2 and day 7.

The water contact angle of PLGA-PEGDA-DTT was measured at 64 ± 4.12^{o} (Figure 5.10). Moreover, with the large error factor of $\pm 4.12^{o}$, the observable

water contact angle is imprecise. This might be caused by the swelling phenomenon during measurement.

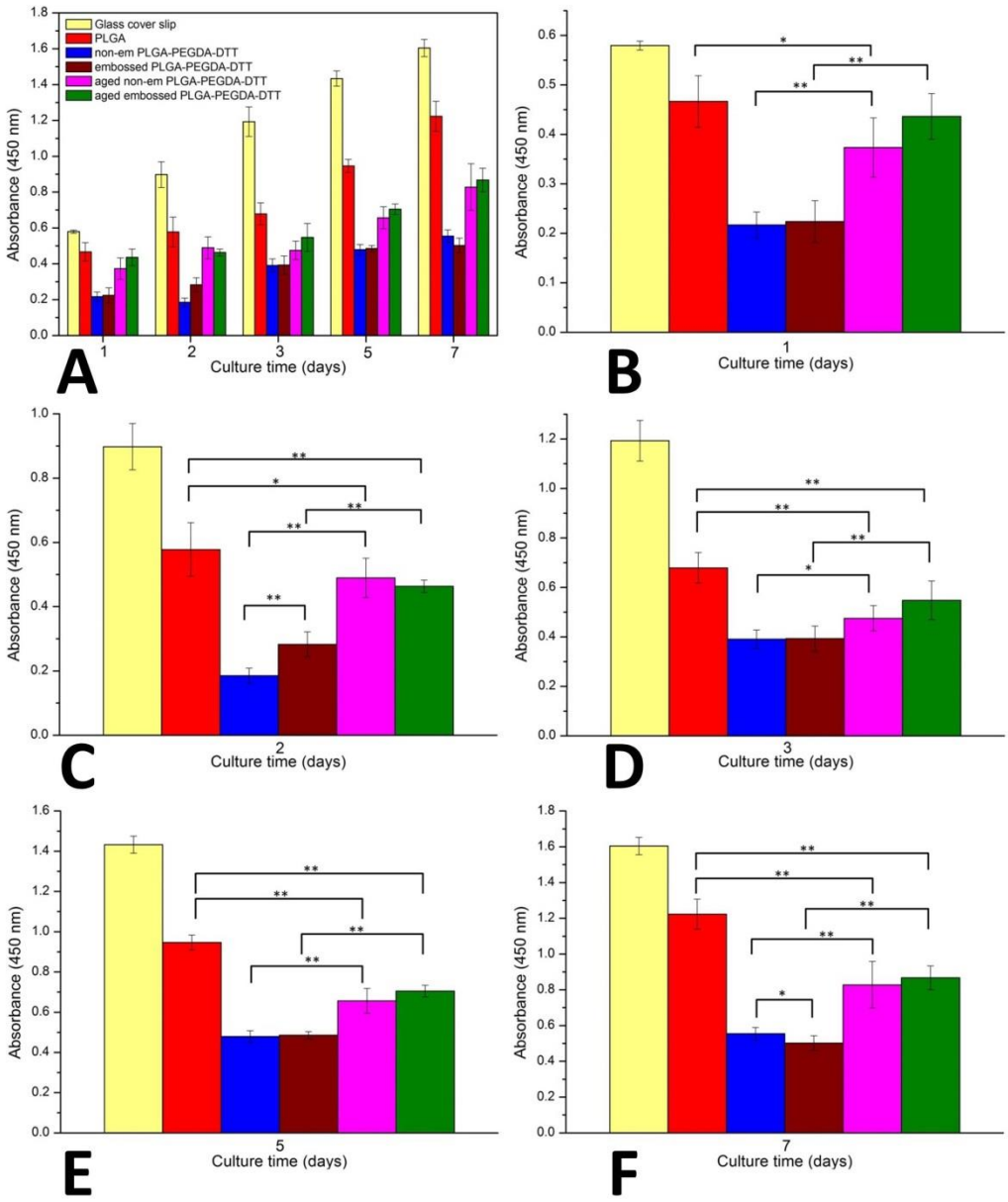

Figure 5.9 Proliferation of HUVECs (* and ** indicates the statistical significance) (A) HUVEC proliferation on glass cover slips, pure PLGA films, non-embossed PLGA-PEGDA-DTT films, embossed PLGA-PEGDA-DTT films, aged non-embossed PLGA-PEGDA-DTT films and aged embossed PLGA-PEGDA-DTT films (B)HUVEC proliferation on day 1, (C) HUVEC proliferation on day 2, (D) HUVEC proliferation on day 3, (E) HUVEC proliferation on day 5, (F) HUVEC proliferation on day 7.

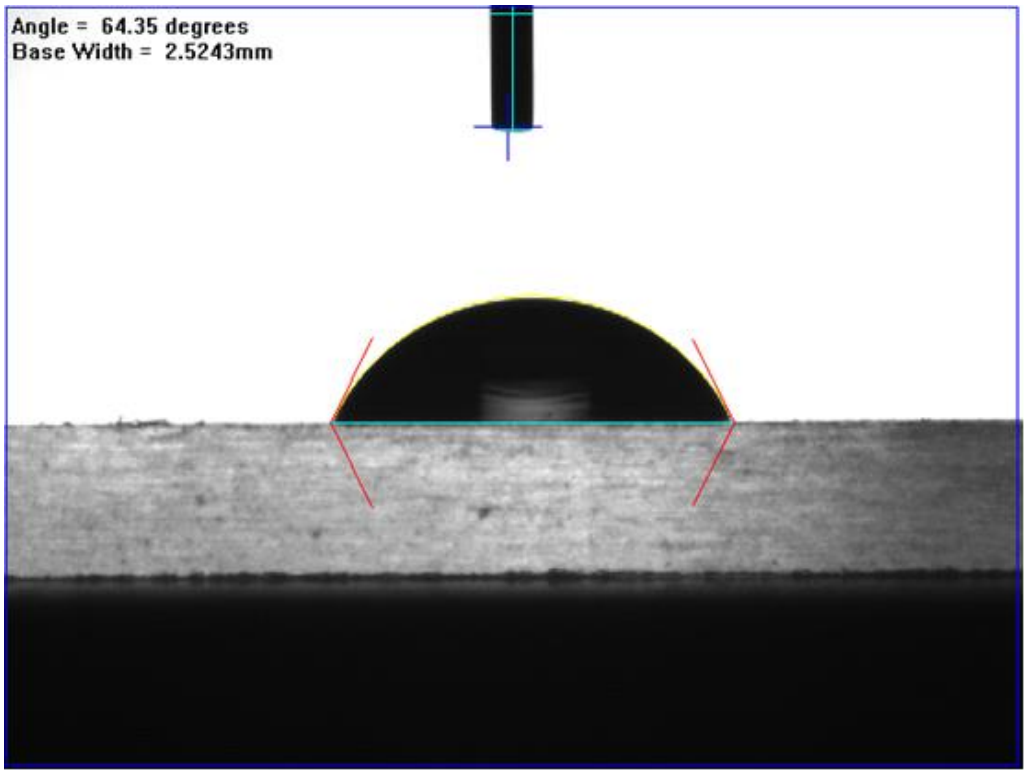

Figure 5.10 Typical contact angle measurements for photoembossed PLGA-PEGDA-DTT film

HUVECs were also seeded on photoembossed PLGA-PEGDA-DTT fibres and examined with an epifluorescence microscope. Substrates were not specially coated with PLL-g-PEG but only washed 3 times with 70% ethanol and 3 times with DPBS before seeding. The epifluorescence microscope images (Figure 5.11) show that, even without coating the substrate with PLL-g-PEG to prevent the cells from attaching to the glass cover slip, the HUVECs still preferred to attach to the fibres even in the regions of low fibre density.

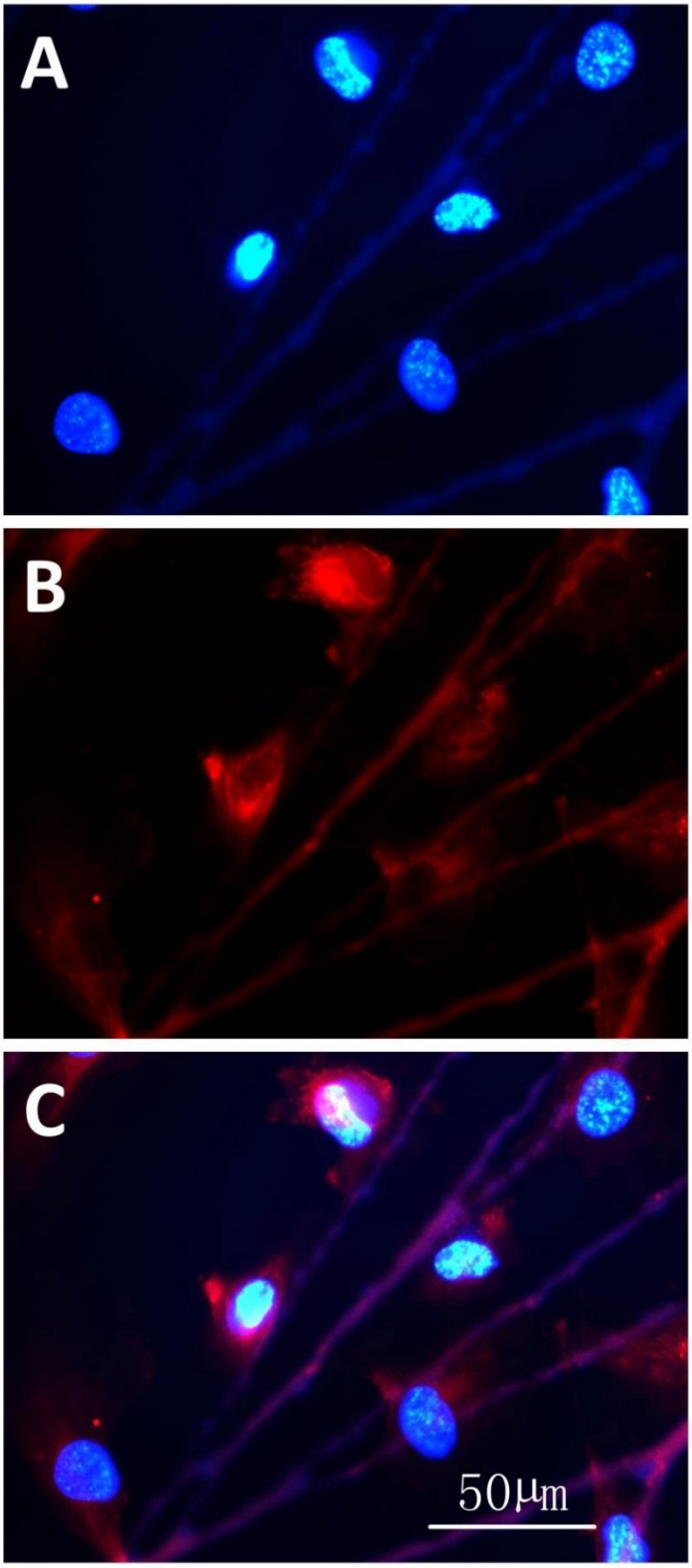

Figure 5.11 Epifluorescence microscope images of HUVECs seeded on PLGA-PEGDA-DTT fibres stained for the (A) nucleus (blue), (B) cytoplasm (red) (The fibres are autofluorescent in both blue and red), (C) is a merged image of (A) and (B)

5.3 Discussion

Due to their ability to swell in water without being dissolved, high water content and elastic properties (Nicodemus and Bryant, 2008), hydrogels are extensively investigated for the purposes of drug delivery (Hoare and Kohane, 2008, Peppas et al., 2000, Peppas et al., 2006, Qiu and Park, 2001), biosensors (Miyata et al., 2002, van Der Linden et al., 2003), protein and polymer purification (Kim and Park, 1998, Galaev and Mattiasson, 2001) and tissue engineering (Lee and Mooney, 2001, Jen et al., 1996, Zisch et al., 2003). Early studies used natural materials, such as collagen, fibrin and alginate (Mikos et al., 1994, Cao et al., 1998, Sims et al., 1998, Perka et al., 2000, Lee and Mooney, 2001), to fabricate hydrogels and had some success in potential utilization. However, it is difficult to control the mechanical properties, gelation process and degradation rates of these natural materials, so artificial biomaterials with the ability to form hydrogels and with controllable properties attracted the attention of researchers. Poly(ethylene glycol) (PEG) is one of the most studied polymers that can form a degradable hydrogel without eliciting the immune response (Zalipsky and Harris, 1997).

PLGA-PEGDA-DTT photopolymer was made by adding PLGA to (-PEG-DTT-)$_n$PEG obtained from the initial reaction between PEGDA and DTT as the polymer binder. When this photopolymer is subjected to the photoembossing process, a hydrogel network is formed as well as the relief structures. PLGA-PEGDA-DTT can be made successfully into films and fibres and

photoembossed through contact mask photoembossing and holographic lithography, respectively.

As a hydrogel, the photoembossed PLGA-PEGDA-DTT films used in our experiments displayed a typical swelling phenomenon in the presence of water. After only 2 hours in DPBS, the film surface had already become extremely rough. Any relief structure could be broadly maintained for up to 3 days but the morphology changed continuously throughout the observation period. Interestingly, the hydrogel in the ridge area gradually aggregated along either side of the original peak making a concave shape with the center of the ridges lower than the sides.

The PLGA-PEGDA-DTT photopolymer exhibits a faster degradation rate than PLGA although both are capable of complete degradation. Additionally, the degradation rate can be tuned in various ways. First of all, the rate can be varied by changing the glycolide/lactic unit ratio used in the photopolymer mixture. As phase separation is observed after photoembossing, the degradation rate of the PLGA component can be very important in controlling the degradation time of the combined photopolymer. Secondly, the molecular weight of the particular PEGDA used can influence the degradation rate for, as we have found, the higher the molecular weight of PEGDA used the faster the photopolymer degrades (Figure 5.8). Additionally, the total amount of DTT in the network also greatly influences the degradation rate. The higher the amount of DTT involved, the faster the hydrogel degrades. Lastly, the rate of degradation is also limited by the solubility of DTT (Hudalla et al., 2008).

During the degradation process, a thin layer or ‘skin’ with a relatively smooth surface can be observed by SEM on the surface of the substrates (Figure 5.6). Where this ‘skin’ breaks, a weak point is created where degradation begins earlier than in other areas. Compared with semi-degradable PLGA-TPETA films, the surface morphology of photoembossed PLGA-PEGDA-DTT films changes more rapidly, losing some of its relief structure after only 7 days while PLGA-TPETA films retain their general morphology throughout the degradation period observed.

Due to the phase separation of photoembossed PLGA-PEGDA-DTT films, PLGA particles first appear in the groove region rather than on the ridges because the diffusion process allows fewer monomers to remain in the former. This view is supported by the fact that when the depth of the ridges is low, indicating insufficient diffusion, PLGA particles will appear uniformly on both ridges and grooves. As degradation proceeds, the top of the ridges tends to split along their axes exhibiting large numbers of PLGA particles underneath. It appears that the material usually begins to degrade from where the stress is concentrated, i.e. where the film is least flat, such as at the top and root of ridges, the craters and ‘lumpy’ areas. One concern, illustrated by Figure 5.5 J, is that the photopolymer film might lose some fragments before they are completely hydrolysed during the degradation process and this is not a desirable complication in therapies.

Unlike the performance of PMMA-TPETA and PLGA-TPETA films described in last two chapters, neither the attachment nor proliferation of HUVECs is

improved by this fully degradable photopolymer compared with pure PLGA films. Neither does photoembossed PLGA-PEGDA-DTT film exhibit cell attachment superior to its non-embossed equivalent. This suggests that the change in surface morphology caused by the characteristic swelling of this material plays a major part in its lack of efficacy. By comparison, the aged substrates tested showed better cell attachment and proliferation suggesting that it might be the rapid surface changes during swelling of the un-aged film that reduces the cellular affinity. Nevertheless, HUVECs show a preference for attaching to PLGA-PEGDA-DTT fibres, even when the substrate is not coated with PLL-g-PEG to stop cells attaching to the glass cover slip or when the fibre density is very low. It is known that electrospinning will increase the hydrophobicity of a material and it is probable that this process increased the water contact angle of the substrate to within the range that is suitable for cell attachment. Moreover, the fibre diameters are much smaller compared with the cells, thus the swelling of the material provides a rougher surface and enhanced the cell attachment.

As cell attachment and proliferation can be improved by simply aging the substrates, this PLGA-PEGDA-DTT photopolymer has a lot of advantages for clinic applications. The degradation rate, surface topography features, wettability and stiffness can be all easily tuned according to specific medical requirements which make this material eligible to be made into customized grafts.

5.4 Conclusions

A fully degradable PLGA-PEGDA-DTT photopolymer was successfully developed and photoembossed. The photoembossed films usually began degradation from stress points where the ‘skin’ is more vulnerable to splitting, leading to considerable loss of original surface texture. The degradation rate of this photopolymer can be tuned in a number of ways. However, this photopolymer films did not improve the attachment or proliferation of HUVECs compared with pure PLGA, although its performance can be improved by ‘aging’. There is still huge potential for the modification of this photopolymer into a desirable biodegradable material.

Chapter 6 Conclusion and future work

6.1 Conclusion

This research has made significant findings, as well as confirming others, relating to the potential utility of certain photopolymer media in bioengineering applications particularly for the regrowth of vascular tissue. The fabrication processes that may be used and some of the factors determining the effectiveness of these media were also investigated.

In the UK alone, approximately 1 in 5 men and 1 in 8 women aged between 50 and 75 have peripheral arterial disease, and around 28,000 people a year undergo a coronary artery bypass graft. There is a critical, clinical need for functional small-diameter conduits. Failures of vascular grafts are normally caused by the lack of a durable and adherent endothelium covering the graft, which leads to thrombus, especially when the diameter of the graft is below 6 mm. A promising approach to overcome this issue is to create a functional, quiescent monolayer of endothelial cells on the surface of implants. The endothelium also acts to regulate the transport of substances across vessel wall. It is beneficial to create a surface that promotes the endothelialisation of the graft. Current synthetic vascular grafts have a number of limitations, including thrombogenicity, increased risk of infection and lack of growth potential. Due to the complex construction of the human body, customizable grafts are in

greater demand than ever. Patient specific requirement is not limited to vascular grafts, but also in other ones, such as in skin and bone replacements. Here, we present three durable (i.e. shelf life) and biocompatible materials with micro-structured surface topography that enhances cell attachment and promote cell proliferation and migration. These materials can be used for a range of medical applications, including vascular grafts. They can be easily fabricated and customized for patient specific needs with a low cost.

Photoembossing is a relatively new, simple, environment-friendly and cost-effective technique to create surface topographies, as there is no etching step or mould needed. Photopolymer films can be successfully photoembossed through contact mask photoembossing and fibres photoembossed through holographic lithography. Furthermore, we are the first to introduce the technique to fabricating reproducible surface textures on electrospun fibres.

We set up three systems: non-degradable PMMA-TPETA, semi-degradable PLGA-TPETA and fully degradable PLGA-PEGDA-DTT, to meet different requirements for potential utilization in bioengineering research and clinical therapy.

Two polymer binders are used in these three systems, PMMA and PLGA, which are both confirmed to be biocompatible and already extensively used in bioengineering research and medical devices.

PMMA-TPETA photopolymer represent an improvement in cell attachment and proliferation over PMMA. Moreover, photoembossed films also show

significantly improved cell attachment and proliferation compared to their non-embossed equivalent. The 20 μm pitch photoembossed surface texture significantly accelerated cell migration in the wound healing assay while the 6 μm pitch surface texture inhibited the cells from detaching.

PLGA-TPETA photopolymer also shows an improvement in cell attachment and proliferation over PLGA, and as with PMMA-TPETA, photoembossed PLGA-TPETA films also exhibit significantly improved cell attachment and proliferation. PLGA-TPETA polymer fibres can be successfully photoembossed through holographic lithography without changing their fibrous structure. Fibre characteristics can be tuned via various methods - we used PLGA with different inherent viscosities to obtain fibres with different diameters. It was demonstrated that HUVECs begin to grow from intersections of fibres and that focal adhesions display a more aggregated organization on surface textured fibres while those on glass cover slips are more randomly dispersed, tending to the edge of the cell membrane. F-actin can be influenced by surface topographies of smaller sizes including smaller diameter fibres and the relief structure.

The performance of the fully degradable photopolymer PLGA-PEGDA-DTT is more complicated, as some of its properties, such as biocompatibility and surface morphology, may vary over time. The photopolymer can be successfully created and processed into photoembossed film or fibre. Swelling of the material is observed, due to the hydrogel network formed by the photocross-linked $(\text{-PEG-DTT-})_n$PEG. Phase separation between the polymer

binder PLGA and the cross-linked thiol-acrylate network is homogenously dispersed with little pressure of large aggregates regions. Accelerated hydrolysis tests confirm that PLGA-PEGDA-DTT can degrade completely and it also shows a significantly faster degradation rate than pure PLGA. The surface morphology of PLGA-PEGDA-DTT films changes rapidly during degradation. Unfortunately, the cell attachment and proliferation of this fully degradable photopolymer film does not represent an improvement over pure PLGA, possibly as a result of the rapid change in surface morphology during swelling but it can be improved by simply pre-aging the material. Nevertheless, HUVECs show a preference to attach to the photopolymer fibres. Additionally, the degradation rate, surface topography features, wettability and stiffness of the obtained substrates can all be easily controlled and has great potential to be used clinically with the availability to be customised to meet different conditions.

The relief structure obtained from photoembossing also changes the surface wettability of the substrates. Photoembossed PMMA-TPETA and PLGA-TPETA benefit from this change, which changes their water contact angle to around 70º. However, photoembossed PLGA-PEGDA-DTT film does not display improved cell attachment compared to smooth film which suggests the change in surface morphology caused by swelling is the primary determining factor.

6.2 Future work

As we have obtained photopolymers PMMA-TPETA and PLGA-TPETA with improved biocompatibility, modifications can be made in these photopolymers according to requirements. Both surface textures and fibre diameters can be made down to nano-scale. Moreover, other chemicals such as cell growth factors can be combined with the photopolymer. Additionally, the surface charge of the substrate can be considered with the aim of optimizing the surface properties for different cell types.

Fibre development will continue to be explored. For example, fibres with uniformly distributed pitches aligned in one direction and exposed perpendicular to the interference pattern can produced anisotropic fibre mats that have been used in studies of tendon and ligament regeneration (Shang et al., 2010).

In order to develop a successful fully degradable system, collaborating with researchers with a strong chemistry background would be very helpful in modifying the properties of PLGA-PEGDA-DTT to make it more useful in bioengineering research and clinical therapy as a gel-like fully degradable material. As this photopolymer can also be surface-textured and the degradation rate can be tuned, it would be ideal for the development of a drug delivery system (Hoare and Kohane, 2008, Peppas et al., 2000, Peppas et al., 2006, Qiu and Park, 2001), biosensor (Miyata et al., 2002, van Der Linden et al., 2003), in protein and polymer purification (Kim and Park, 1998, Galaev

and Mattiasson, 2001) and tissue engineering (Lee and Mooney, 2001, Jen et al., 1996, Zisch et al., 2003). Moreover, the stiffness and elasticity can be studied in the following work as they are two important characters of the PLGA-PEGDA-DTT substrate, and both of them also have influence on cell culture.

Stem cells can also be introduced into the following work. Stem cells are able to differentiate into various lineages, so that a reliable source to direct stem cell fate determination would have great potential for fundamental research and clinical therapy. Surface topography is reported to be able to guide the stem cells for their growth orientation and differentiation, as the feature size and shape can be precisely modified and is more durable than surface chemistry so that it is capable for the desired application. Dalby *et al.* (Dalby et al., 2007) presented that the human mesenchymal stem cells are stimulated to produce bone mineral on nanoscale disordered scaffold with significant differentiation profile compared with those cultured on planar substrate and treated with osteogenic media. Christopherson *et al.* (Christopherson et al., 2009) demonstrated that the 283 nm fibers increase 40% rat hippocampus-derived adult neural stem/progenitor cells in oligodendrocyte differentiation and 749 nm fibres increase 20% in neuronal differentiation. Wingate *et al.* (Wingate et al., 2012) showed that based on the elasticity of the substrates which was determined by the kind of surface features in their experiment, mesenchymal stem cells can differentiation into either endothelial or smooth muscle-like cells, this indicates that the surface topography has great potential to be a tool for vascular tissue regeneration.Moreover, a system sorted by degradation rate,

surface topography features, wettability, stiffness and elasticity of the substrates can be set up as a data base. Different reactions of different cells cultured on different substrates with details mentioned before should be recorded. As the data base gets bigger, the optimum condition for each cell type can be estimated. This can lead to fewer unnecessary attempts, so that could greatly save the time to investigate a new product for clinic use.

References

ADAMS, N., DE GANS, B. J., KOZODAEV, D., SANCHEZ, C., BASTIAANSEN, C. W. M., BROER, D. J. & SCHUBERT, U. S. 2006. High-throughput screening and optimization of photoembossed relief structures. *Journal of Combinatorial Chemistry,* 8**,** 184-191.

AEBISCHER, P., GUÉNARD, V. & VALENTINI, R. F. 1990. The morphology of regenerating peripheral nerves is modulated by the surface microgeometry of polymeric guidance channels. *Brain Research,* 531**,** 211-218.

AHMAD, Z., ZHANG, H., FAROOK, U., EDIRISINGHE, M., STRIDE, E. & COLOMBO, P. 2008. Generation of multilayered structures for biomedical applications using a novel tri-needle coaxial device and electrohydrodynamic flow. *Journal of the Royal Society Interface,* 5**,** 1255-1261.

AIRD, W. C. 2007. Phenotypic heterogeneity of the endothelium I. Structure, function, and mechanisms. *Circulation Research,* 100**,** 158-173.

ALCANTAR, N. A., AYDIL, E. S. & ISRAELACHVILI, J. N. 2000. Polyethylene glycol-coated biocompatible surfaces. *Journal of Biomedical Materials Research,* 51**,** 343-51.

ANENE-NZELU, C. G., CHOUDHURY, D., LI, H., FRAISZUDEEN, A., PEH, K.-Y., TOH, Y.-C., NG, S. H., LEO, H. L. & YU, H. 2013. Scalable cell alignment on optical media substrates. *Biomaterials,* 34**,** 5078-5087.

APPLE, D. J. 2006. *Sir Harold Ridley and his fight for sight : he changed the world so that we may better see it,* Thorofare, NJ, Slack.

ARIMA, Y. & IWATA, H. 2007. Effect of wettability and surface functional groups on protein adsorption and cell adhesion

using well-defined mixed self-assembled monolayers. *Biomaterials,* 28**,** 3074-3082.

ARORA, P., WANG, Y., BRESNICK, A., DAWSON, J., JANMEY, P. & MCCULLOCH, C. 2013. Collagen remodeling by phagocytosis is determined by collagen substrate topology and calcium-dependent interactions of gelsolin with nonmuscle myosin IIA in cell adhesions. *Molecular Biology of the Cell,* 24**,** 734-747.

ATALA, A., BAUER, S. B., SOKER, S., YOO, J. J. & RETIK, A. B. 2006. Tissue-engineered autologous bladders for patients needing cystoplasty. *Lancet,* 367**,** 1241-1246.

BADAMI, A. S., KREKE, M. R., THOMPSON, M. S., RIFFLE, J. S. & GOLDSTEIN, A. S. 2006. Effect of fiber diameter on spreading, proliferation, and differentiation of osteoblastic cells on electrospun poly(lactic acid) substrates. *Biomaterials,* 27**,** 596-606.

BAIER, R. E., SHAFRIN, E. G. & ZISMAN, W. A. 1968. Adhesion: mechanisms that assist or impede it. *Science,* 162**,** 1360-8.

BALA, I., HARIHARAN, S. & KUMAR, M. N. V. R. 2004. PLGA nanoparticles in drug delivery: The state of the art. *Critical Reviews in Therapeutic Drug Carrier Systems,* 21**,** 387-422.

BARBUCCI, R. 2002. *Integrated biomaterials science,* Springer.

BARBUCCI, R., PASQUI, D., WIRSEN, A., AFFROSSMAN, S., CURTIS, A. & TETTA, C. 2003. Micro and nano-structured surfaces. *Journal of Materials Science: Materials in Medicine,* 14**,** 721-725.

BERRY, C. C., CAMPBELL, G., SPADICCINO, A., ROBERTSON, M. & CURTIS, A. S. 2004. The influence of microscale topography on fibroblast attachment and motility. *Biomaterials,* 25**,** 5781-5788.

BERSHADSKY, A. D., BALABAN, N. Q. & GEIGER, B. 2003. Adhesion-dependent cell mechanosensitivity. *Annual Review of Cell and Developmental Biology,* 19**,** 677-695.

BHARDWAJ, R. & BLANCHARD, J. 1998. In vitro characterization and in vivo release profile of a poly(D,L-lactide-co-glycolide)-based implant delivery system for the alpha-MSH analog, melanotan-I. *International Journal of Pharmaceutics,* 170**,** 109-117.

BIELA, S. A., SU, Y., SPATZ, J. P. & KEMKEMER, R. 2009. Different sensitivity of human endothelial cells, smooth muscle cells and fibroblasts to topography in the nano-micro range. *Acta Biomaterialia,* 5**,** 2460-6.

BOWMAN, L. 2004. *Study on dogs yields hope in human paralysis treatment* [Online]. Available: http://www.seattlepi.com/lifestyle/health/article/Study-on-dogs-yields-hope-in-human-paralysis-1161183.php.

BRANDHONNEUR, N., CHEVANNE, F., VIÉ, V., FRISCH, B., PRIMAULT, R., LE POTIER, M.-F. & LE CORRE, P. 2009. Specific and non-specific phagocytosis of ligand-grafted PLGA microspheres by macrophages. *European Journal of Pharmaceutical Sciences,* 36**,** 474-485.

BRITANNICA, E. 2014. *Actin filaments* [Online]. Available: http://www.britannica.com/EBchecked/topic/101396/cell/37427/Actin-filaments.

BRITLAND, S., CLARK, P., CONNOLLY, P. & MOORES, G. 1992. Micropatterned Substratum Adhesiveness - a Model for Morphogenetic Cues Controlling Cell Behavior. *Experimental Cell Research,* 198**,** 124-129.

BRITLAND, S., MORGAN, H., WOJIAK-STODART, B., RIEHLE, M., CURTIS, A. & WILKINSON, C. 1996a. Synergistic and hierarchical adhesive and topographic guidance of BHK cells. *Experimental Cell Research,* 228**,** 313-325.

BRITLAND, S., PERRIDGE, C., DENYER, M., MORGAN, H., CURTIS, A. & WILKINSON, C. 1996b. Morphogenetic guidance cues can interact synergistically and hierarchically in steering nerve cell growth. *Experimental Biology Online,* 1**,** 1-15.

BRUNETTE, D., KENNER, G. & GOULD, T. 1983. Grooved titanium surfaces orient growth and migration of cells from human gingival explants. *Journal of Dental Research,* 62**,** 1045-1048.

BURRIDGE, K. & CHRZANOWSKA-WODNICKA, M. 1996. Focal adhesions, contractility, and signaling. *Annual Review of Cell and Developmental Biology,* 12**,** 463-519.

BUSCHOW, K. H. J., CAHN, R. W., FLEMINGS, M. C., ILSCHNER, B., KRAMER, E. J. & MAHAJAN, S. 2001. Encyclopedia of Materials - Science and Technology, Volumes 1-11. Elsevier.

BYRNE, M. E., HENTHORN, D., HUANG, Y. & PEPPAS, N. A. 2002. Micropatterning biomimetic materials for bioadhesion and drug delivery. *Biomimetic materials and design Dillow AK, Lowman AM,* 443-470.

CAO, Y. L., RODRIGUEZ, A., VACANTI, M., IBARRA, C., AREVALO, C. & VACANTI, C. A. 1998. Comparative study of the use of poly(glycolic acid), calcium alginate and pluronics in the engineering of autologous porcine cartilage. *Journal of Biomaterials Science-Polymer Edition,* 9**,** 475-487.

CARDWELL, R. D., DAHLGREN, L. A. & GOLDSTEIN, A. S. 2012. Electrospun fibre diameter, not alignment, affects mesenchymal stem cell differentiation into the tendon/ligament lineage. *Journal of Tissue Engineering and Regenerative Medicine*.

CARPENTER, S., GARZA, A. & PALMAZ, J. C. 2012. Method for making topographical features on a surface of a medical device. Google Patents.

CATıKER, E., GÜMÜŞDERELIOĞLU, M. & GÜNER, A. 2000. Degradation of PLA, PLGA homo-and copolymers in the presence of serum albumin: a spectroscopic investigation. *Polymer International,* 49**,** 728-734.

CHEN, W.-T. & SINGER, S. 1982. Immunoelectron microscopic studies of the sites of cell-substratum and cell-cell contacts in cultured fibroblasts. *J. Cell Biol,* 95**,** 205-222.

CHESMEL, K., CLARK, C., BRIGHTON, C. & BLACK, J. 1995. Cellular responses to chemical and morphologic aspects of biomaterial surfaces. II. The biosynthetic and migratory response of bone cell populations. *Journal of Biomedical Materials Research,* 29**,** 1101-1110.

CHOQUET, D., FELSENFELD, D. P. & SHEETZ, M. P. 1997. Extracellular matrix rigidity causes strengthening of integrin–cytoskeleton linkages. *Cell,* 88**,** 39-48.

CHRISTOPHERSON, G. T., SONG, H. & MAO, H. Q. 2009. The influence of fiber diameter of electrospun substrates on neural stem cell differentiation and proliferation. *Biomaterials,* 30**,** 556-564.

CHUA, K.-N., CHAI, C., LEE, P.-C., TANG, Y.-N., RAMAKRISHNA, S., LEONG, K. W. & MAO, H.-Q. 2006. Surface-aminated electrospun nanofibers enhance adhesion and expansion of human umbilical cord blood hematopoietic stem/progenitor cells. *Biomaterials,* 27**,** 6043-6051.

CHUNG, T. W., LIU, D. Z., WANG, S. Y. & WANG, S. S. 2003. Enhancement of the growth of human endothelial cells by surface roughness at nanometer scale. *Biomaterials,* 24**,** 4655-4661.

CHUNG, T. W., TSA, Y. L., HSIEH, J. H. & TSAI, W. J. 2006. Different ratios of lactide and glycolide in PLGA affect the surface property and protein delivery characteristics of the PLGA microspheres with hydrophobic additives. *Journal of Microencapsulation,* 23**,** 15-27.

CINES, D. B., POLLAK, E. S., BUCK, C. A., LOSCALZO, J., ZIMMERMAN, G. A., MCEVER, R. P., POBER, J. S., WICK, T. M., KONKLE, B. A., SCHWARTZ, B. S., BARNATHAN, E. S., MCCRAE, K. R., HUG, B. A., SCHMIDT, A. M. & STERN, D. M. 1998. Endothelial cells in physiology and in the pathophysiology of vascular disorders. *Blood,* 91**,** 3527-3561.

CLARK, P., CONNOLLY, P., CURTIS, A., DOW, J. & WILKINSON, C. 1987. Topographical control of cell behaviour. I. Simple step cues. *Development,* 99**,** 439-448.

CLARK, P., CONNOLLY, P., CURTIS, A., DOW, J. & WILKINSON, C. 1990. Topographical control of cell behaviour: II. Multiple grooved substrata. *Development,* 108**,** 635-644.

CLARK, P., CONNOLLY, P., CURTIS, A., DOW, J. & WILKINSON, C. 1991. Cell guidance by ultrafine topography in vitro. *Journal of Cell Science,* 99**,** 73-77.

CLARK, P., CONNOLLY, P. & MOORES, G. R. 1992. Cell guidance by micropatterned adhesiveness in vitro. *Journal of Cell Science,* 103 (Pt 1)**,** 287-92.

COLEMAN, D. L., GREGONIS, D. E. & ANDRADE, J. D. 1982. Blood-materials interactions: the minimum interfacial free energy and the optimum polar/apolar ratio hypotheses. *Journal of Biomedical Materials Research,* 16**,** 381-98.

COOLEY, J. F. 1902. *U.S. Patent 692,631*. US patent application.

COOPER, G. M. A. & HAUSMAN, R. E. A. 2009. *The cell : a molecular approach*.

CRAIG, S. W. & JOHNSON, R. P. 1996. Assembly of focal adhesions: progress, paradigms, and portents. *Current Opinion in Cell Biology,* 8**,** 74-85.

CRAIGHEAD, H., JAMES, C. & TURNER, A. 2001. Chemical and topographical patterning for directed cell attachment.

Current Opinion in Solid State and Materials Science, 5**,** 177-184.

CURTIS, A., QUINN, R. & MCGRATH, M. 1996. Activation of neuron adhesion and neurite extension by tethered neurotrophins and adhesion molecules. *Experimental Biology Online,* 1**,** 1-13.

CURTIS, A. & VARDE, M. 1964. Control of cell behavior: topological factors. *Journal of the National Cancer Institute,* 33**,** 15-26.

CURTIS, A. & WILKINSON, C. 1997. Topographical control of cells. *Biomaterials,* 18**,** 1573-1583.

CURTIS, A., WILKINSON, C. & WOJCIAK-STOTHARD, B. 1995. Accelerating cell movement. *Cell. Eng,* 1**,** 35-38.

CURTIS, A. S. & SEEHAR, G. M. 1978. The control of cell division by tension or diffusion. *Nature,* 274**,** 52-3.

CURTIS, A. S. & WILKINSON, C. D. 1998. Reactions of cells to topography. *Journal of Biomaterials Science, Polymer Edition,* 9**,** 1313-1329.

DALBY, M. J., GADEGAARD, N., TARE, R., ANDAR, A., RIEHLE, M. O., HERZYK, P., WILKINSON, C. D. & OREFFO, R. O. 2007. The control of human mesenchymal cell differentiation using nanoscale symmetry and disorder. *Nature materials,* 6**,** 997-1003.

DAVIS, F. F. 2002. Commentary - The origin of pegnology. *Advanced Drug Delivery Reviews,* 54**,** 457-458.

DE VRIEZE, S. & DE CLERCK, K. 80 years of electrospinning. 2009. 60.

DE VRIEZE, S., WESTBROEK, P., VAN CAMP, T. & VAN LANGENHOVE, L. 2007. Electrospinning of chitosan nanofibrous structures: feasibility study. *Journal of materials science,* 42**,** 8029-8034.

DEGASNE, I., BASLE, M. F., DEMAIS, V., HURE, G., LESOURD, M., GROLLEAU, B., MERCIER, L. & CHAPPARD, D. 1999. Effects of roughness, fibronectin and vitronectin on attachment, spreading, and proliferation of human osteoblast-like cells (Saos-2) on titanium surfaces. *Calcified Tissue International,* 64**,** 499-507.

DEJANA, E. 2004. Endothelial cell–cell junctions: happy together. *Nature Reviews Molecular Cell Biology,* 5**,** 261-270.

DEJANA, E., TOURNIER-LASSERVE, E. & WEINSTEIN, B. M. 2009. The control of vascular integrity by endothelial cell junctions: molecular basis and pathological implications. *Developmental Cell,* 16**,** 209-221.

DEN BRABER, E., DE RUIJTER, J., GINSEL, L., VON RECUM, A. & JANSEN, J. 1996. Quantitative analysis of fibroblast morphology on microgrooved surfaces with various groove and ridge dimensions. *Biomaterials,* 17**,** 2037-2044.

DEN BRABER, E., DE RUIJTER, J., GINSEL, L., VON RECUM, A. & JANSEN, J. 1998. Orientation of ECM protein deposition, fibroblast cytoskeleton, and attachment complex components on silicone microgrooved surfaces. *Journal of Biomedical Materials Research,* 40**,** 291-300.

DEN BRABER, E., DE RUIJTER, J., SMITS, H., GINSEL, L., VON RECUM, A. & JANSEN, J. 1995. Effect of parallel surface microgrooves and surface energy on cell growth. *Journal of Biomedical Materials Research,* 29**,** 511-518.

DESAI, T. A. 2000. Micro- and nanoscale structures for tissue engineering constructs. *Medical Engineering & Physics,* 22**,** 595-606.

DICKINSON, L. E., RAND, D. R., TSAO, J., EBERLE, W. & GERECHT, S. 2012. Endothelial cell responses to micropillar substrates of varying dimensions and stiffness. *Journal of biomedical materials research. Part A,* 100**,** 1457-66.

DING, S., LI, J., LUO, C., LI, L., YANG, G. & ZHOU, S. 2013. Synergistic effect of released dexamethasone and surface nanoroughness on mesenchymal stem cell differentiation. *Biomaterials Science,* 1**,** 1091-1100.

DOMB, A. J., KOST, J. & WISEMAN, D. M. 1997. *Handbook of biodegradable polymers,* Amsterdam ; United Kingdom, Harwood Academic.

DONALD, A. M. 2003. The use of environmental scanning electron microscopy for imaging wet and insulating materials. *Nature Materials,* 2**,** 511-516.

DONG, Y., LIAO, S., NGIAM, M., CHAN, C. K. & RAMAKRISHNA, S. 2009. Degradation behaviors of electrospun resorbable polyester nanofibers. *Tissue Engineering Part B: Reviews,* 15**,** 333-351.

DOSHI, J. & RENEKER, D. H. 1995. Electrospinning process and applications of electrospun fibers. *Journal of Electrostatics,* 35**,** 151-160.

DOW, J. A., CLARK, P., CONNOLLY, P., CURTIS, A. S. & WILKINSON, C. D. 1987a. Novel methods for the guidance and monitoring of single cells and simple networks in culture. *Journal of Cell Science. Supplement,* 8**,** 55-79.

DOW, J. A. T., CLARK, P., CONNOLLY, P., CURTIS, A. S. G. & WILKINSON, C. D. W. 1987b. Novel Methods for the Guidance and Monitoring of Single Cells and Simple Networks in Culture. *Journal of Cell Science***,** 55-79.

DRELICH, J., LASKOWSKI, J. S. & MITTAL, K. L. 2000. Apparent and Microscopic Contact Angles. VSP - An imprint of BRILL.

DUNN, G. A. & BROWN, A. F. 1986. Alignment of fibroblasts on grooved surfaces described by a simple geometric transformation. *Journal of Cell Science,* 83**,** 313-40.

DUSASTRE, V. 2009. Boom time for biomaterials. *Nature materials,* 8**,** 439-439.

EDWARDS, W. S. & TAPP, J. S. 1955. Chemically treated nylon tubes as arterial grafts. *Surgery,* 38**,** 61.

ENAYATI, M., CHANG, M.-W., BRAGMAN, F., EDIRISINGHE, M. & STRIDE, E. 2011. Electrohydrodynamic preparation of particles, capsules and bubbles for biomedical engineering applications. *Colloids and Surfaces A: Physicochemical and Engineering Aspects,* 382**,** 154-164.

FORMHALS, A. 1934. *Process and apparatus for preparing artificial threads*.

FRANCO, D., MILDE, F., KLINGAUF, M., ORSENIGO, F., DEJANA, E., POULIKAKOS, D., CECCHINI, M., KOUMOUTSAKOS, P., FERRARI, A. & KURTCUOGLU, V. 2012. Accelerated endothelial wound healing on microstructured substrates under flow. *Biomaterials*.

FRANZ, C. M. & MÜLLER, D. J. 2005. Analyzing focal adhesion structure by atomic force microscopy. *Journal of Cell Science,* 118**,** 5315-5323.

FREED, L. E., LANGER, R., MARTIN, I., PELLIS, N. R. & VUNJAK-NOVAKOVIC, G. 1997. Tissue engineering of cartilage in space. *Proceedings of the National Academy of Sciences,* 94**,** 13885-13890.

FRENOT, A., HENRIKSSON, M. W. & WALKENSTRÖM, P. 2007. Electrospinning of cellulose based nanofibers. *Journal of Applied Polymer Science,* 103**,** 1473-1482.

FREY, M. T., TSAI, I. Y., RUSSELL, T. P., HANKS, S. K. & WANG, Y.-L. 2006. Cellular responses to substrate topography: role of myosin II and focal adhesion kinase. *Biophysical Journal,* 90**,** 3774-3782.

FURCHGOTT, R. F. & ZAWADZKI, J. V. 1980. The obligatory role of endothelial cells in the relaxation of arterial smooth muscle by acetylcholine. *Nature,* 288**,** 373-376.

GAIL, M. H. & BOONE, C. W. 1972. Cell-substrate adhesivity. A determinant of cell motility. *Experimental Cell Research,* 70**,** 33-40.

GALAEV, I. & MATTIASSON, B. 2001. *Smart polymers for bioseparation and bioprocessing*, CRC Press.

GALBRAITH, C. G., YAMADA, K. M. & SHEETZ, M. P. 2002. The relationship between force and focal complex development. *The Journal of cell biology,* 159**,** 695-705.

GANGJEE, T., COLAIZZO, R. & VONRECUM, A. F. 1985. Species-Related Differences in Percutaneous Wound-Healing. *Annals of Biomedical Engineering,* 13**,** 451-467.

GEIGER, B., BERSHADSKY, A., PANKOV, R. & YAMADA, K. M. 2001. Transmembrane crosstalk between the extracellular matrix and the cytoskeleton. *Nature Reviews Molecular Cell Biology,* 2**,** 793-805.

GIESSIBL, F. J. 2003. Advances in atomic force microscopy. *Reviews of Modern Physics,* 75**,** 949-983.

GILBERT, W. M. D. & LOCHMAN, W. 1628. *Tractatus, sive Physiologia nova de Magnete, magneticisque corporibus et magno magnete tellure sex libris comprehensus a Guilielmo Gilberto ... Omnia nunc diligenter recognita & emendatius quam ante in lucem edita, aucta, & figuris illustrata opera et studio Wolfgangi Lochmans*, pp. 232. Typis Go\0308tzianis sumptibus authoris: Sedini.

GILDING, D. K. & REED, A. M. 1979. Biodegradable Polymers for Use in Surgery - Polyglycolic-Poly(Actic Acid) Homopolymers and Copolymers .1. *Polymer,* 20**,** 1459-1464.

GIMBRONE, M. A., JR., COTRAN, R. S. & FOLKMAN, J. 1974. Human vascular endothelial cells in culture. Growth and DNA synthesis. *The Journal of cell biology,* 60**,** 673-84.

GREEN, A. M., JANSEN, J. A., VANDERWAERDEN, J. P. C. M. & VONRECUM, A. F. 1994. Fibroblast Response to Microtextured Silicone Surfaces - Texture Orientation into or out of the Surface. *Journal of Biomedical Materials Research,* 28**,** 647-653.

GRINNELL, F. 1977. Cellular adhesiveness and extracellular substrata. *International Review of Cytology,* 53**,** 65-144.

GU, M. 1996. *Principles of three-dimensional imaging in confocal microscopes,* Singapore ; River Edge, NJ, World Scientific.

GUVENDIREN, M. & BURDICK, J. A. 2013. Stem cell response to spatially and temporally displayed and reversible surface topography. *Advanced healthcare materials,* 2**,** 155-164.

HARRISON, R. G. 1912. The cultivation of tissues in extraneous media as a method of morpho-genetic study. *The Anatomical Record,* 6**,** 181-193.

HARRISON, R. H., ST-PIERRE, J.-P. & STEVENS, M. M. 2014. Tissue engineering and regenerative medicine: a Year in Review. *Tissue Engineering Part B: Reviews,* 20**,** 1-16.

HATTORI, S., ANDRADE, J. D., HIBBS, J. B., GREGONIS, D. E. & KING, R. N. 1985. Fibroblast Cell-Proliferation on Charged Hydroxyethyl Methacrylate Copolymers. *Journal of Colloid and Interface Science,* 104**,** 72-78.

HE, W., MA, Z., TEO, W. E., DONG, Y. X., ROBLESS, P. A., LIM, T. C. & RAMAKRISHNA, S. 2009. Tubular nanofiber scaffolds for tissue engineered small©\diameter vascular grafts. *Journal of Biomedical Materials Research Part A,* 90**,** 205-216.

HOARE, T. R. & KOHANE, D. S. 2008. Hydrogels in drug delivery: Progress and challenges. *Polymer,* 49**,** 1993-2007.

HOHMAN, M. M., SHIN, M., RUTLEDGE, G. & BRENNER, M. P. 2001. Electrospinning and electrically forced jets. I. Stability theory. *Physics of Fluids,* 13**,** 2201.

HOLLAND, S. J., TIGHE, B. J. & GOULD, P. L. 1986. Polymers for biodegradable medical devices. 1. The potential of polyesters as controlled macromolecular release systems. *Journal of Controlled Release,* 4**,** 155-180.

HONG, H. & BRUNETTE, D. 1987. Effect of cell shape on proteinase secretion by epithelial cells. *Journal of Cell Science,* 87**,** 259-267.

HORBETT, T. A., SCHWAY, M. B. & RATNER, B. D. 1985. Hydrophilic-Hydrophobic Copolymers as Cell Substrates - Effect on 3t3 Cell-Growth Rates. *Journal of Colloid and Interface Science,* 104**,** 28-39.

HUANG, Z. M., ZHANG, Y. Z., KOTAKI, M. & RAMAKRISHNA, S. 2003. A review on polymer nanofibers by electrospinning and their applications in nanocomposites. *Composites Science and Technology,* 63**,** 2223-2253.

HUDALLA, G. A., ENG, T. S. & MURPHY, W. L. 2008. An approach to modulate degradation and mesenchymal stem cell behavior in poly(ethylene glycol) networks. *Biomacromolecules,* 9**,** 842-849.

HUGHES-BRITTAIN, N. F. 2013. *Photoembossing for biomedical application.* Doctor of Philosophy, Queen Mary, University of London.

HUGHES-BRITTAIN, N. F., PICOT, O. T., QIU, L., SANCHEZ, C., PEIJS, T. & BASTIAANSEN, K. Photoembossing for Surface Texturing of Films and Fibres for Biomedical Applications. MRS Proceedings, 2012. Cambridge Univ Press.

HUGHES-BRITTAIN, N. F., QIU, L., WANG, W., PEIJS, T. & BASTIAANSEN, C. W. 2014a. Photoembossing of surface relief structures in polymer films for biomedical applications.

Journal of biomedical materials research. Part B, Applied biomaterials, 102**,** 214-20.

HUGHES-BRITTAIN, N. F., QIU, L., WANG, W., PEIJS, T. & BASTIAANSEN, C. W. M. 2014b. Photoembossing of surface relief structures in polymer films for biomedical applications. *Journal of Biomedical Materials Research Part B-Applied Biomaterials,* 102**,** 214-220.

INAI, R., KOTAKI, M. & RAMAKRISHNA, S. 2005. Structure and properties of electrospun PLLA single nanofibres. *Nanotechnology,* 16**,** 208.

INGBER, D. E. 1993. Cellular tensegrity: defining new rules of biological design that govern the cytoskeleton. *Journal of Cell Science,* 104**,** 613-613.

JEN, A. C., WAKE, M. C. & MIKOS, A. G. 1996. Review: Hydrogels for cell immobilization. *Biotechnology and Bioengineering,* 50**,** 357-364.

JENKINS, D. H. R., FORSTER, I. W., MCKIBBIN, B. & RALIS, Z. A. 1977. Induction of Tendon and Ligament Formation by Carbon Implants. *Journal of Bone and Joint Surgery-British Volume,* 59**,** 53-57.

JIANG, X., TAKAYAMA, S., QIAN, X., OSTUNI, E., WU, H., BOWDEN, N., LEDUC, P., INGBER, D. E. & WHITESIDES, G. M. 2002. Controlling mammalian cell spreading and cytoskeletal arrangement with conveniently fabricated continuous wavy features on poly (dimethylsiloxane). *Langmuir,* 18**,** 3273-3280.

JOSHI, M., BHATTACHARYYA, A. & ALI, S. W. 2008. Characterization techniques for nanotechnology applications in textiles. *Indian Journal of Fiber and Textile Research,* 33**,** 304-317.

KANCHANAWONG, P., SHTENGEL, G., PASAPERA, A. M., RAMKO, E. B., DAVIDSON, M. W., HESS, H. F. &

WATERMAN, C. M. 2010. Nanoscale architecture of integrin-based cell adhesions. *Nature,* 468**,** 580-584.

KARURI, N. W., NEALEY, P. F., MURPHY, C. J. & ALBRECHT, R. M. 2008. Structural organization of the cytoskeleton in SV40 human corneal epithelial cells cultured on nano- and microscale grooves. *Scanning,* 30**,** 405-13.

KIM, D. H. & MARTIN, D. C. 2006. Sustained release of dexamethasone from hydrophilic matrices using PLGA nanoparticles for neural drug delivery. *Biomaterials,* 27**,** 3031-3037.

KIM, J. J. & PARK, K. 1998. Smart hydrogels for bioseparation. *Bioseparation,* 7**,** 177-184.

KOMATSU, R., UEDA, M., NARUKO, T., KOJIMA, A. & BECKER, A. E. 1998. Neointimal tissue response at sites of coronary stenting in humans macroscopic, histological, and immunohistochemical analyses. *Circulation,* 98**,** 224-233.

KOOTEN, T. G. V. & RECUM, A. F. V. 1999. Cell adhesion to textured silicone surfaces: the influence of time of adhesion and texture on focal contact and fibronectin fibril formation. *Tissue Engineering,* 5**,** 223-240.

KORMAN, N. J., SUDILOVSKY, O. & GIBBONS, D. F. 1984. The Effect of Humoral Components on the Cellular-Response to Textured and Nontextured Ptfe. *Journal of Biomedical Materials Research,* 18**,** 225-241.

KOUFAKI, N., RANELLA, A., AIFANTIS, K. E., BARBEROGLOU, M., PSYCHARAKIS, S., FOTAKIS, C. & STRATAKIS, E. 2011. Controlling cell adhesion via replication of laser micro/nano-textured surfaces on polymers. *Biofabrication,* 3**,** 045004.

KRISTL, J., PLAJNŠEK, K. T., KREFT, M. E., JANKOVIĆ, B. & KOCBEK, P. 2013. Intracellular trafficking of solid lipid nanoparticles and their distribution between cells through

tunneling nanotubes. *European Journal of Pharmaceutical Sciences,* 50**,** 139-148.

KRONENTHAL, R. L. 1975. *Biodegradable polymers in medicine and surgery*, Springer.

KUMBAR, S. G., NUKAVARAPU, S. P., JAMES, R., NAIR, L. S. & LAURENCIN, C. T. 2008. Electrospun Poly(lactic acid-co-glycolic acid) Scaffolds for Skin Tissue Engineering. *Biomaterials,* 29**,** 4100-4107.

KUPP, T., HOCHMAN, P., HALE, J. & BLACK, J. 1982. Effect of motion on polymer implant capsule formation in muscle. *Biomaterials. New York: Wiley*.

KWOK, D. Y., GIETZELT, T., GRUNDKE, K., JACOBASCH, H. J. & NEUMANN, A. W. 1997. Contact Angle Measurements and Contact Angle Interpretation. 1. Contact Angle Measurements by Axisymmetric Drop Shape Analysis and a Goniometer Sessile Drop Technique. *Langmuir,* 13**,** 2880-2894.

L'HEUREUX, N., MCALLISTER, T. N. & DE LA FUENTE, L. M. 2007. Tissue-engineered blood vessel for adult arterial revascularization. *New England Journal of Medicine,* 357**,** 1451-1453.

LACO, F., GRANT, M. H. & BLACK, R. A. 2013. Collagen–nanofiber hydrogel composites promote contact guidance of human lymphatic microvascular endothelial cells and directed capillary tube formation. *Journal of Biomedical Materials Research Part A,* 101**,** 1787-1799.

LE, D. M., KULANGARA, K., ADLER, A. F., LEONG, K. W. & ASHBY, V. S. 2011. Dynamic Topographical Control of Mesenchymal Stem Cells by Culture on Responsive Poly (ϵ-caprolactone) Surfaces. *Advanced Materials,* 23**,** 3278-3283.

LEE, J. H., KHANG, G., LEE, J. W. & LEE, H. B. 1998. Interaction of Different Types of Cells on Polymer Surfaces

with Wettability Gradient. *Journal of Colloid and Interface Science,* 205**,** 323-330.

LEE, J. H., PARK, S. J., GU, B. K., KIM, M. S. & KIM, C.-H. 2014. Selectively Micro-Patterned Fibronectin for Regulating Fate of Human Mesenchymal Stem Cell. *Journal of nanoscience and nanotechnology,* 14**,** 7402-7409.

LEE, K. Y. & MOONEY, D. J. 2001. Hydrogels for tissue engineering. *Chemical Reviews,* 101**,** 1869-1880.

LEE, S. Y., OH, J. H., KIM, J. C., KIM, Y. H., KIM, S. H. & CHOI, J. W. 2003. In vivo conjunctival reconstruction using modified PLGA grafts for decreased scar formation and contraction. *Biomaterials,* 24**,** 5049-5059.

LEMPERLE, G., GAUTHIER-HAZAN, N. & LEMPERLE, M. 1998. PMMA-Microspheres (Artecoll) for long-lasting correction of wrinkles: refinements and statistical results. *Aesthetic Plastic Surgery,* 22**,** 356-65.

LI, D. & XIA, Y. 2004. Electrospinning of nanofibers: Reinventing the wheel? *Advanced Materials,* 16**,** 1151-1170.

LI, J. & SHI, R. 2007. Fabrication of patterned multi-walled poly-l-lactic acid conduits for nerve regeneration. *Journal of Neuroscience Methods,* 165**,** 257-264.

LI, S., BHATIA, S., HU, Y. L., SHIU, Y. T., LI, Y. S., USAMI, S. & CHIEN, S. 2001. Effects of morphological patterning on endothelial cell migration. *Biorheology,* 38**,** 101-8.

LI, S. & VERT, M. 2002. Biodegradation of aliphatic polyesters. *Degradable polymers.* Springer.

LI, S. M. 1999. Hydrolytic degradation characteristics of aliphatic polyesters derived from lactic and glycolic acids. *Journal of Biomedical Materials Research,* 48**,** 342-353.

LI, W. J., LAURENCIN, C. T., CATERSON, E. J., TUAN, R. S. & KO, F. K. 2002. Electrospun nanofibrous structure: a novel

scaffold for tissue engineering. *J Biomed Mater Res,* 60**,** 613-21.

LICHTMAN, J. W. & CONCHELLO, J.-A. 2005. Fluorescence microscopy. *Nature Methods,* 2**,** 910-919.

LIM, J. Y. & DONAHUE, H. J. 2007. Cell sensing and response to micro-and nanostructured surfaces produced by chemical and topographic patterning. *Tissue Engineering,* 13**,** 1879-1891.

LIM, T. Y., POH, C. K. & WANG, W. 2009. Poly (lactic-co-glycolic acid) as a controlled release delivery device. *Journal of Materials Science-Materials in Medicine,* 20**,** 1669-1675.

LIN, H. B., SUN, W., MOSHER, D. F., GARC ÍA-ECHEVERR ÍA, C., SCHAUFELBERGER, K., LELKES, P. I. & COOPER, S. L. 1994. Synthesis, surface, and cell-adhesion properties of polyurethanes containing covalently grafted RGD-peptides. *Journal of Biomedical Materials Research,* 28**,** 329-342.

LLOYD, A. W. 2002. Interfacial bioengineering to enhance surface biocompatibility. *Medical Device Technology,* 13**,** 18-21.

LOEB, L. & FLEISHER, M. S. 1917. On the Factors which determine the Movements of Tissues in Culture Media. *The Journal of medical research,* 37**,** 75-99.

LÖFGREN, A., ALBERTSSON, A.-C., DUBOIS, P. & JÉRÔME, R. 1995. Recent advances in ring-opening polymerization of lactones and related compounds. *Journal of Macromolecular Science, Part C: Polymer Reviews,* 35**,** 379-418.

LU, X. & LENG, Y. 2003. Quantitative analysis of osteoblast behavior on microgrooved hydroxyapatite and titanium substrata. *Journal of biomedical materials research. Part A,* 66**,** 677-87.

LU, X. & LENG, Y. 2009. Comparison of the osteoblast and myoblast behavior on hydroxyapatite microgrooves. *Journal of biomedical materials research. Part B, Applied biomaterials,* 90**,** 438-45.

LUDWIG, T., OSSIG, R., GRAESSEL, S., WILHELMI, M., OBERLEITHNER, H. & SCHNEIDER, S. W. 2002. The electrical resistance breakdown assay determines the role of proteinases in tumor cell invasion. *American Journal of Physiology-Renal Physiology,* 283**,** F319-F327.

LUTHEN, F., LANGE, R., BECKER, P., RYCHLY, J., BECK, U. & NEBE, J. G. B. 2005. The influence of surface roughness of titanium on beta 1-and beta 3-integrin adhesion and the organization of fibronectin in human osteoblastic cells. *Biomaterials,* 26**,** 2423-2440.

LYDON, M. & CLAY, C. 1985. Substratum topography and cell traction on sulphuric acid treated bacteriological-grade plastic. *Cell Biology International Reports,* 9**,** 911-921.

LYDON, M. J., MINETT, T. W. & TIGHE, B. J. 1985. Cellular Interactions with Synthetic-Polymer Surfaces in Culture. *Biomaterials,* 6**,** 396-402.

MACCHIARINI, P., JUNGEBLUTH, P., GO, T., ASNAGHI, M. A., REES, L. E., COGAN, T. A., DODSON, A., MARTORELL, J., BELLINI, S., PARNIGOTTO, P. P., DICKINSON, S. C., HOLLANDER, A. P., MANTERO, S., CONCONI, M. T. & BIRCHALL, M. A. 2008. Clinical transplantation of a tissue-engineered airway. *Lancet,* 372**,** 2023-2030.

MACRAE, S. M., MATSUDA, M. & YEE, R. 1985. The effect of long-term hard contact lens wear on the corneal endothelium. *The CLAO journal : official publication of the Contact Lens Association of Ophthalmologists, Inc,* 11**,** 322-6.

MACROMERS, P. Degradable Poly (ethylene glycol) Hydrogels for 2D and 3D Cell Culture. *Polymers for Advanced Architectures***,** 67.

MELCHER, J. & TAYLOR, G. 1969. Electrohydrodynamics: a review of the role of interfacial shear stresses. *Annual Review of Fluid Mechanics,* 1**,** 111-146.

MENG, Q. & HOU, Y. 2011. Experimental study on hydro-viscous drive speed-regulating start. *Industrial Lubrication and Tribology,* 63**,** 239-244.

MEYLE, J., GULTIG, K., BRICH, M., HAMMERLE, H. & NISCH, W. 1994. Contact Guidance of Fibroblasts on Biomaterial Surfaces. *Journal of Materials Science-Materials in Medicine,* 5**,** 463-466.

MEYLE, J., GULTIG, K. & NISCH, W. 1995. Variation in Contact Guidance by Human-Cells on a Microstructured Surface. *Journal of Biomedical Materials Research,* 29**,** 81-88.

MEYLE, J., WOLBURG, H. & VON RECUM, A. F. 1993. Surface micromorphology and cellular interactions. *Journal of Biomaterials Applications,* 7**,** 362-74.

MICROSCOPY, A. F. 2005. Atomic Force Microscopy.

MIKOS, A. G., PAPADAKI, M. G., KOUVROUKOGLOU, S., ISHAUG, S. L. & THOMSON, R. C. 1994. Islet Transplantation to Create a Bioartificial Pancreas - Mini Review. *Biotechnology and Bioengineering,* 43**,** 673-677.

MILLER, M. S., FILIATRAULT, H. L., DAVIDSON, G. J., LUO, M. & CARMICHAEL, T. B. 2009. Selectively metallized polymeric substrates by microcontact printing an aluminum (III) porphyrin complex. *Journal of the American Chemical Society,* 132**,** 765-772.

MILLER, R. A., BRADY, J. M. & CUTRIGHT, D. E. 1977. Degradation Rates of Oral Resorbable Implants (Polylactates and Polyglycolates) - Rate Modification with Changes in Pla-Pga Copolymer Ratios. *Journal of Biomedical Materials Research,* 11**,** 711-719.

MINAL, P. & JOHN, P. F. 2008. *Biodegradable materials for tissue engineering* [Online]. Available: http://www.accessscience.com/content/biodegradable-materials-for-tissue-engineering/YB080510.

MINSKY, M. 1961. Microscopy apparatus. Google Patents.

MINTON, A. P. 1992. Confinement as a Determinant of Macromolecular Structure and Reactivity. *Biophysical Journal,* 63**,** 1090-1100.

MIQIN, Z. 2007. *Alginate-based nanofibers and related scaffolds*. US patent application.

MIYATA, T., URAGAMI, T. & NAKAMAE, K. 2002. Biomolecule-sensitive hydrogels. *Advanced Drug Delivery Reviews,* 54**,** 79-98.

MORTON, W. J. 1902. *US Patent 705,691*. US patent application.

MUKHATYAR, V. J., SALMERÓN-SÁNCHEZ, M., RUDRA, S., MUKHOPADAYA, S., BARKER, T. H., GARC ÍA, A. J. & BELLAMKONDA, R. V. 2011. Role of fibronectin in topographical guidance of neurite extension on electrospun fibers. *Biomaterials,* 32**,** 3958-3968.

NAGATA, I., KAWANA, A. & NAKATSUJI, N. 1993. Perpendicular contact guidance of CNS neuroblasts on artificial microstructures. *Development,* 117**,** 401-8.

NAIR, L. S., BHATTACHARYYA, S. & LAURENCIN, C. T. 2004. Development of novel tissue engineering scaffolds via electrospinning. *Expert opinion on biological therapy,* 4**,** 659-68.

NAIR, L. S. & LAURENCIN, C. T. 2007. Biodegradable polymers as biomaterials. *Progress in Polymer Science,* 32**,** 762-798.

NAKAMURA, T., HITOMI, S., WATANABE, S., SHIMIZU, Y., JAMSHIDI, K., HYON, S. H. & IKADA, Y. 1989. Bioabsorption of Polylactides with Different Molecular-Properties. *Journal of Biomedical Materials Research,* 23**,** 1115-1130.

NANDAKUMAR, A., BIRGANI, Z. T., SANTOS, D., MENTINK, A., AUFFERMANN, N., VAN DER WERF, K., BENNINK,

M., MORONI, L., VAN BLITTERSWIJK, C. & HABIBOVIC, P. 2013. Surface modification of electrospun fibre meshes by oxygen plasma for bone regeneration. *Biofabrication,* 5**,** 015006.

NICODEMUS, G. D. & BRYANT, S. J. 2008. Cell encapsulation in biodegradable hydrogels for tissue engineering applications. *Tissue Engineering Part B-Reviews,* 14**,** 149-165.

NORMAN, J. J. & DESAI, T. A. 2006. Methods for fabrication of nanoscale topography for tissue engineering scaffolds. *Annals of Biomedical Engineering,* 34**,** 89-101.

NORTON, C. L. 1936. *U.S. Patent 2,048,651*. US patent application.

NUZZO, V. A. 1996. Structure of cliff vegetation on exposed cliffs and the effect of rock climbing. *Canadian Journal of Botany,* 74**,** 607-617.

OAKLEY, C. & BRUNETTE, D. M. 1993. The sequence of alignment of microtubules, focal contacts and actin filaments in fibroblasts spreading on smooth and grooved titanium substrata. *Journal of Cell Science,* 106 (Pt 1)**,** 343-54.

OBERPENNING, F., MENG, J., YOO, J. J. & ATALA, A. 1999. De novo reconstitution of a functional mammalian urinary bladder by tissue engineering. *Nature Biotechnology,* 17**,** 149-155.

OHARA, P. T. & BUCK, R. C. 1979. Contact guidance in vitro: a light, transmission, and scanning electron microscopic study. *Experimental Cell Research,* 121**,** 235-249.

OLSON, A. D. 1993. Contraction of collagen gels by intestinal epithelial cells depends on microfilament function. *Digestive Diseases and Sciences,* 38**,** 388-95.

PARETA, R., BRINDLEY, A., EDIRISINGHE, M. J., JAYASINGHE, S. N. & LUKLINSKA, Z. B. 2005.

Electrohydrodynamic atomization of protein (bovine serum albumin). *Journal of materials science. Materials in medicine,* 16**,** 919-25.

PARKER, S. & KINNERSLEY, R. 2004. A computational and wind tunnel study of particle dry deposition in complex topography. *Atmospheric Environment,* 38**,** 3867-3878.

PAWLEY, J. B. 2006. *Handbook of biological confocal microscopy,* New York, NY, Springer.

PEPPAS, N. A., BURES, P., LEOBANDUNG, W. & ICHIKAWA, H. 2000. Hydrogels in pharmaceutical formulations. *European Journal of Pharmaceutics and Biopharmaceutics,* 50**,** 27-46.

PEPPAS, N. A., HILT, J. Z., KHADEMHOSSEINI, A. & LANGER, R. 2006. Hydrogels in biology and medicine: From molecular principles to bionanotechnology. *Advanced Materials,* 18**,** 1345-1360.

PERKA, C., SPITZER, R. S., LINDENHAYN, K., SITTINGER, M. & SCHULTZ, O. 2000. Matrix-mixed culture: New methodology for chondrocyte culture and preparation of cartilage transplants. *Journal of Biomedical Materials Research,* 49**,** 305-311.

PICHA, G. J. & DRAKE, R. 1990. The effect of pillard surface microstructure and implant microenvironment on the soft tissue response. *16th Annual Meeting Transactions, Society for Biomaterials, Charleston, SC.*

PLACE, E. S., EVANS, N. D. & STEVENS, M. M. 2009. Complexity in biomaterials for tissue engineering. *Nature materials,* 8**,** 457-470.

POLLOCK, H. 1993. Breast Capsular Contracture - a Retrospective Study of Textured Versus Smooth Silicone Implants. *Plastic and Reconstructive Surgery,* 91**,** 404-407.

PORTAL, E. *Endothelial Cells: Function, Lesson & Quiz* [Online]. Available: http://education-portal.com/academy/lesson/endothelial-cells-function-lesson-quiz.html#lesson.

POWELL, E. & GIBBONS, D. 1982. Effect of implant compliance and surface texture on fibrous capsule morphology and myofibroblast population. *Biol. Eng. Soc***,** 31-37.

PRITCHARD, D. J., MORGAN, H. & COOPER, J. M. 1995. Micron-Scale Patterning of Biological Molecules. *Angewandte Chemie International Edition in English*, 34**,** 91-93.

QIU, Y. & PARK, K. 2001. Environment-sensitive hydrogels for drug delivery. *Advanced Drug Delivery Reviews*, 53**,** 321-339.

QUAKE, S. R. & SCHERER, A. 2000. From micro-to nanofabrication with soft materials. *Science*, 290**,** 1536-1540.

RAJNICEK, A., BRITLAND, S. & MCCAIG, C. 1997. Contact guidance of CNS neurites on grooved quartz: influence of groove dimensions, neuronal age and cell type. *Journal of Cell Science*, 110 (Pt 23)**,** 2905-13.

RAJNICEK, A. & MCCAIG, C. 1997. Guidance of CNS growth cones by substratum grooves and ridges: effects of inhibitors of the cytoskeleton, calcium channels and signal transduction pathways. *Journal of Cell Science*, 110 (Pt 23)**,** 2915-24.

RATNER, B. D. & BRYANT, S. J. 2004. Biomaterials: Where we have been and where we are going. *Annual Review of Biomedical Engineering*, 6**,** 41-75.

RATNER, B. D., HOFFMAN, A. S., SCHOEN, F. J. & LEMONS, J. 2004. Biomaterials science: a multidisciplinary endeavor. *Biomaterials Science: An Introduction to Materials in Medicine***,** 1-9.

RECUM, A. F., SHANNON, C. E., CANNON, C. E., LONG, K. J., KOOTEN, T. G. & MEYLE, J. 1996. Surface roughness,

porosity, and texture as modifiers of cellular adhesion. *Tissue Engineering,* 2**,** 241-53.

RENEKER, D. H. & CHUN, I. 1996. Nanometre diameter fibres of polymer, produced by electrospinning. *Nanotechnology,* 7**,** 216.

REZNIK, S., YARIN, A., THERON, A. & ZUSSMAN, E. 2004. Transient and steady shapes of droplets attached to a surface in a strong electric field. *Journal of Fluid Mechanics,* 516**,** 349-377.

RHO, J. Y., ASHMAN, R. B. & TURNER, C. H. 1993. Young's modulus of trabecular and cortical bone material: ultrasonic and microtensile measurements. *Journal of Biomechanics,* 26**,** 111-9.

RIEHLE, M., FERRIS, D., HAMILTON, D. & CURTIS, A. 1998. Cell behaviour in tubes. *Experimental Biology Online,* 3**,** 1-15.

ROSA, A. L., BELOTI, M. M. & VAN NOORT, R. 2003. Osteoblastic differentiation of cultured rat bone marrow cells on hydroxyapatite with different surface topography. *Dental Materials,* 19**,** 768-772.

ROSALES-LEAL, J., RODRÍGUEZ-VALVERDE, M., MAZZAGLIA, G., RAMON-TORREGROSA, P., DIAZ-RODRIGUEZ, L., GARCIA-MARTINEZ, O., VALLECILLO-CAPILLA, M., RUIZ, C. & CABRERIZO-VILCHEZ, M. 2010. Effect of roughness, wettability and morphology of engineered titanium surfaces on osteoblast-like cell adhesion. *Colloids and Surfaces A: Physicochemical and Engineering Aspects,* 365**,** 222-229.

ROVENSKY, Y. A., SLAVNAJA, I. L. & VASILIEV, J. M. 1971. Behaviour of Fibroblast-Like Cells on Grooved Surfaces. *Experimental Cell Research,* 65**,** 193-&.

ROVENSKY YU, A. & SAMOILOV, V. I. 1994. Morphogenetic response of cultured normal and transformed fibroblasts, and

epitheliocytes, to a cylindrical substratum surface. Possible role for the actin filament bundle pattern. *Journal of Cell Science,* 107 (Pt 5)**,** 1255-63.

SÁNCHEZ, C., DE GANS, B. J., KOZODAEV, D., ALEXEEV, A., ESCUTI, M. J., VAN HEESCH, C., BEL, T., SCHUBERT, U. S., BASTIAANSEN, C. W. M. & BROER, D. J. 2005. Photoembossing of Periodic Relief Structures Using Polymerization-Induced Diffusion: A Combinatorial Study. *Advanced Materials,* 17**,** 2567-2571.

SANFORD, K. K., EARLE, W. R. & LIKELY, G. D. 1948. The growth in vitro of single isolated tissue cells. *Journal of the National Cancer Institute,* 9**,** 229-46.

SARDER, P. & NEHORAI, A. 2006. Deconvolution methods for 3-D fluorescence microscopy images. *Signal Processing Magazine, IEEE,* 23**,** 32-45.

SCHMIDT, J. A. & VON RECUM, A. F. 1992. Macrophage response to microtextured silicone. *Biomaterials,* 13**,** 1059-69.

SCHMIDT, J. A. & VON RECUM, A. F. 1993. On the Use of Primary Reference Grade Polydimethylsiloxane. *Journal of Applied Biomaterials,* 4**,** 73-75.

SCHWACH, G., COUDANE, J., ENGEL, R. & VERT, M. 1996. Zn lactate as initiator of DL-lactide ring opening polymerization and comparison with Sn octoate. *Polymer Bulletin,* 37**,** 771-776.

SCHWEIKL, H., MÜLLER, R., ENGLERT, C., HILLER, K.-A., KUJAT, R., NERLICH, M. & SCHMALZ, G. 2007. Proliferation of osteoblasts and fibroblasts on model surfaces of varying roughness and surface chemistry. *Journal of Materials Science: Materials in Medicine,* 18**,** 1895-1905.

SEEMANN, R., BRINKMANN, M., KRAMER, E. J., LANGE, F. F. & LIPOWSKY, R. 2005. Wetting morphologies at microstructured surfaces. *Proceedings of the National*

Academy of Sciences of the United States of America, 102**,** 1848-1852.

SEIFALIAN, A. M., TIWARI, A., HAMILTON, G. & SALACINSKI, H. J. 2002. Improving the clinical patency of prosthetic vascular and coronary bypass grafts: the role of seeding and tissue engineering. *Artificial Organs,* 26**,** 307-320.

SHANG, S. H., YANG, F., CHENG, X. R., WALBOOMERS, X. F. & JANSEN, J. A. 2010. The Effect of Electrospun Fibre Alignment on the Behaviour of Rat Periodontal Ligament Cells. *European Cells & Materials,* 19**,** 180-192.

SHEN, Y., MA, Y., GAO, M., LAI, Y., WANG, G., YU, Q., CUI, F. Z. & LIU, X. 2013. Integrins-FAK-Rho GTPases pathway in endothelial cells sense and response to surface wettability of plasma nanocoatings. *Acs Applied Materials & Interfaces,* 5**,** 5112-21.

SHIREMAN, P. K. & PEARCE, W. H. 1996. Endothelial cell function: Biologic and physiologic functions in health and disease. *American Journal of Roentgenology,* 166**,** 7-13.

SIMS, C. D., BUTLER, P. E. M., CAO, Y. L., CASANOVA, R., RANDOLPH, M. A., BLACK, A., VACANTI, C. A. & YAREMCHUK, M. J. 1998. Tissue engineered neocartilage using plasma derived polymer substrates and chondrocytes. *Plastic and Reconstructive Surgery,* 101**,** 1580-1585.

SINGHVI, R., STEPHANOPOULOS, G. & WANG, D. I. 1994. Effects of substratum morphology on cell physiology. *Biotechnology and Bioengineering,* 43**,** 764-771.

SMAHEL, J., HURWITZ, P. J. & HURWITZ, N. 1993. Soft-Tissue Response to Textured Silicone Implants in an Animal-Experiment. *Plastic and Reconstructive Surgery,* 92**,** 474-479.

SMITH, W. F. & HASHEMI, J. 2010. *Foundations of materials science and engineering,* Boston, Mass., McGraw-Hill.

SMOLINSKE, S. C. 1992. *CRC Handbook of Food, Drug, and Cosmetic Excipients*, CRC press.

SUPP, D. M. & BOYCE, S. T. 2005. Engineered skin substitutes: practices and potentials. *Clinics in Dermatology,* 23**,** 403-412.

TAMADA, Y. & IKADA, Y. 1993. Effect of Preadsorbed Proteins on Cell-Adhesion to Polymer Surfaces. *Journal of Colloid and Interface Science,* 155**,** 334-339.

TAYLOR, G. 1964. Disintegration of water drops in an electric field. *Proceedings of the Royal Society of London. Series A. Mathematical and Physical Sciences,* 280**,** 383.

TAYLOR, G. 1966. The force exerted by an electric field on a long cylindrical conductor. *Proceedings of the Royal Society of London. Series A. Mathematical and Physical Sciences,* 291**,** 145.

TAYLOR, G. 1969. Electrically driven jets. *Proceedings of the Royal Society of London. A. Mathematical and Physical Sciences,* 313**,** 453.

TEIXEIRA, A. I., ABRAMS, G. A., BERTICS, P. J., MURPHY, C. J. & NEALEY, P. F. 2003. Epithelial contact guidance on well-defined micro-and nanostructured substrates. *Journal of Cell Science,* 116**,** 1881.

TEO, W. E., GOPAL, R., RAMASESHAN, R., FUJIHARA, K. & RAMAKRISHNA, S. 2007. A dynamic liquid support system for continuous electrospun yarn fabrication. *Polymer,* 48**,** 3400-3405.

TERNAUX, J.-P., WILSON, R., DOW, J., CURTIS, A., CLARK, P., PORTALIER, P. & MOORES, J. 1992. Dendritic processing: using microstructures to solve a hitherto intractable neurobiological problem. *Medical and Biological Engineering and Computing,* 30**,** CE37-CE41.

THESLEFF, T., LEHTIMÄKI, K., NISKAKANGAS, T., MANNERSTRÖM, B., MIETTINEN, S., SUURONEN, R.

& ÖHMAN, J. 2011. Cranioplasty with adipose-derived stem cells and biomaterial: a novel method for cranial reconstruction. *Neurosurgery,* 68**,** 1535-1540.

TOADER, O., CHAN, T. Y. & JOHN, S. 2004. Photonic band gap architectures for holographic lithography. *Physical Review Letters,* 92**,** 043905.

TSENG, A. A., CHEN, K., CHEN, C. D. & MA, K. J. 2003. Electron beam lithography in nanoscale fabrication: recent development. *Electronics Packaging Manufacturing, IEEE Transactions on,* 26**,** 141-149.

TSENG, A. A., NOTARGIACOMO, A. & CHEN, T. 2005. Nanofabrication by scanning probe microscope lithography: A review. *Journal of Vacuum Science & Technology B,* 23**,** 877-894.

TZONEVA, R., FAUCHEUX, N. & GROTH, T. 2007. Wettability of substrata controls cell-substrate and cell-cell adhesions. *Biochimica Et Biophysica Acta-General Subjects,* 1770**,** 1538-1547.

UTTAYARAT, P., TOWORFE, G. K., DIETRICH, F., LELKES, P. I. & COMPOSTO, R. J. 2005a. Topographic guidance of endothelial cells on silicone surfaces with micro- to nanogrooves: orientation of actin filaments and focal adhesions. *Journal of biomedical materials research. Part A,* 75**,** 668-80.

UTTAYARAT, P., TOWORFE, G. K., DIETRICH, F., LELKES, P. I. & COMPOSTO, R. J. 2005b. Topographic guidance of endothelial cells on silicone surfaces with micro-to nanogrooves: Orientation of actin filaments and focal adhesions. *Journal of Biomedical Materials Research Part A,* 75**,** 668-680.

VALLITTU, P. K. 1996. A review of fiber-reinforced denture base resins. *Journal of prosthodontics : official journal of the American College of Prosthodontists,* 5**,** 270-6.

VAN DER LINDEN, H. J., HERBER, S., OLTHUIS, W. & BERGVELD, P. 2003. Stimulus-sensitive hydrogels and their applications in chemical (micro)analysis. *Analyst,* 128**,** 325-331.

VAN DER MEER, A. D., VERMEUL, K., POOT, A. A., FEIJEN, J. & VERMES, I. 2010. A microfluidic wound-healing assay for quantifying endothelial cell migration. *American Journal of Physiology-Heart and Circulatory Physiology,* 298**,** H719-H725.

VAN WACHEM, P. B., HOGT, A. H., BEUGELING, T., FEIJEN, J., BANTJES, A., DETMERS, J. P. & VANAKEN, W. G. 1987a. Adhesion of Cultured Human-Endothelial Cells onto Methacrylate Polymers with Varying Surface Wettability and Charge. *Biomaterials,* 8**,** 323-328.

VAN WACHEM, P. B., VAN LUYN, M. J., OLDE DAMINK, L. H., DIJKSTRA, P. J., FEIJEN, J. & NIEUWENHUIS, P. 1994. Biocompatibility and tissue regenerating capacity of crosslinked dermal sheep collagen. *Journal of Biomedical Materials Research,* 28**,** 353-63.

VAN WACHEM, P. B., VRERIKS, C. M., BEUGELING, T., FEIJEN, J., BANTJES, A., DETMERS, J. P. & VANAKEN, W. G. 1987b. The Influence of Protein Adsorption on Interactions of Cultured Human-Endothelial Cells with Polymers. *Journal of Biomedical Materials Research,* 21**,** 701-718.

VERT, M. 2004. Lactic and glycolic acid-based bioresorbable polymeric materials in ACL reconstruction. *Controversies in Knee Surgery***,** 97.

VERT, M., LI, S. M., SPENLEHAUER, G. & GUERIN, P. 1992. Bioresorbability and Biocompatibility of Aliphatic Polyesters. *Journal of Materials Science-Materials in Medicine,* 3**,** 432-446.

VIOLA, J., LAL, B. & GRAD, O. 2003. The emergence of tissue engineering as a research field. *United States National Science Foundation*.

VONRECUM, A. F. 1990. New Aspects of Biocompatibility - Motion at the Interface. *Clinical Implant Materials,* 9**,** 297-302.

WANG, H.-J., CAO, Y., CAO, C., SUN, Y.-Y., YU, X.-H., ZHU, L.-F. & YANG, L. 2011. Parinaric acid methyl ester polymer films with hill-structured features: fabrication and different sensitivities to normal and tumor cells. *Acs Applied Materials & Interfaces,* 3**,** 2755-2763.

WANG, N., BUTLER, J. P. & INGBER, D. E. 1993. Mechanotransduction across the cell surface and through the cytoskeleton. *Science,* 260**,** 21.

WANG, X., TUOMI, J., MÄKITIE, A. A., PALOHEIMO, K.-S., PARTANEN, J. & YLIPERTTULA, M. 2013. The integrations of biomaterials and rapid prototyping techniques for intelligent manufacturing of complex organs.

WANG, X., ZHANG, K., ZHU, M., YU, H., ZHOU, Z., CHEN, Y. & HSIAO, B. S. 2008. Continuous polymer nanofiber yarns prepared by self-bundling electrospinning method. *Polymer,* 49**,** 2755-2761.

WATT, F. M. & HUCK, W. T. S. 2013. Role of the extracellular matrix in regulating stem cell fate. *Nature Reviews Molecular Cell Biology,* 14**,** 467-473.

WEBB, D. J. & BROWN, C. M. 2013. Epi-fluorescence microscopy. *Methods in Molecular Biology,* 931**,** 29-59.

WEISS, P. 1929. Erzwingung elementarer Strukturverschiedenheiten am in vitro wachsenden Gewebe. *Wilhelm Roux'Archiv für Entwicklungsmechanik der Organismen,* 116**,** 438-554.

WEISS, P. 1934. In vitro experiments on the factors determining the course of the outgrowing nerve fiber. *Journal of Experimental Zoology,* 68**,** 393-448.

WEISS, P. 1945. Experiments on cell and axon orientation in vitro: the role of colloidal exudates in tissue organization. *Journal of Experimental Zoology,* 100**,** 353-386.

WILLIAMS, D. F. 1987. *Definitions in biomaterials : proceedings of a consensus conference of the European Society for Biomaterials, Chester, England, March 3-5, 1986,* Amsterdam ; Oxford, Elsevier.

WILLIAMS, D. W., KURIYAMA, T., SILVA, S., MALIC, S. & LEWIS, M. A. 2011. Candida biofilms and oral candidosis: treatment and prevention. *Periodontology 2000,* 55**,** 250-265.

WILLIAMSON, M. R., BLACK, R. & KIELTY, C. 2006. PCL-PU composite vascular scaffold production for vascular tissue engineering: Attachment, proliferation and bioactivity of human vascular endothelial cells. *Biomaterials,* 27**,** 3608-3616.

WINGATE, K., BONANI, W., TAN, Y., BRYANT, S. J. & TAN, W. 2012. Compressive elasticity of three-dimensional nanofiber matrix directs mesenchymal stem cell differentiation to vascular cells with endothelial or smooth muscle cell markers. *Acta Biomaterialia,* 8**,** 1440-9.

WÓJCIAK-STOTHARD, B., CURTIS, A., MONAGHAN, W., MACDONALD, K. & WILKINSON, C. 1996. Guidance and activation of murine macrophages by nanometric scale topography. *Experimental Cell Research,* 223**,** 426-435.

WOJCIAK-STOTHARD, B., DENYER, M., MISHRA, M. & BROWN, R. A. 1997. Adhesion, orientation, and movement of cells cultured on ultrathin fibronectin fibers. *In Vitro Cellular and Developmental Biology. Animal,* 33**,** 110-7.

WOJCIAK, B., CROSSAN, J., CURTIS, A. S. G. & WILKINSON, C. D. W. 1995. Grooved Substrata Facilitate in-Vitro Healing

of Completely Divided Flexor Tendons. *Journal of Materials Science-Materials in Medicine,* 6**,** 266-271.

WOODWARD, R. P. FTÅ200 Measurement Capabilities.

XIE, J., NG, W. J., LEE, L. Y. & WANG, C. H. 2008. Encapsulation of protein drugs in biodegradable microparticles by co-axial electrospray. *Journal of Colloid and Interface Science,* 317**,** 469-76.

XU, C., INAI, R., KOTAKI, M. & RAMAKRISHNA, S. 2004. Aligned biodegradable nanofibrous structure: a potential scaffold for blood vessel engineering. *Biomaterials,* 25**,** 877-886.

YANG, F., MURUGAN, R., WANG, S. & RAMAKRISHNA, S. 2005. Electrospinning of nano/micro scale poly (L-lactic acid) aligned fibers and their potential in neural tissue engineering. *Biomaterials,* 26**,** 2603-2610.

YANG, S., LEONG, K.-F., DU, Z. & CHUA, C.-K. 2002. The design of scaffolds for use in tissue engineering. Part II. Rapid prototyping techniques. *Tissue Engineering,* 8**,** 1-11.

YAO, J., KUANG LIM, L., XIE, J., HUA, J. & WANG, C.-H. 2008. Characterization of electrospraying process for polymeric particle fabrication. *Journal of Aerosol Science,* 39**,** 987-1002.

YOSHIGI, M., HOFFMAN, L. M., JENSEN, C. C., YOST, H. J. & BECKERLE, M. C. 2005. Mechanical force mobilizes zyxin from focal adhesions to actin filaments and regulates cytoskeletal reinforcement. *The Journal of cell biology,* 171**,** 209-215.

ZAIDEL-BAR, R., ITZKOVITZ, S., MA'AYAN, A., IYENGAR, R. & GEIGER, B. 2007. Functional atlas of the integrin adhesome. *Nature Cell Biology,* 9**,** 858-867.

ZALIPSKY, S. & HARRIS, J. M. 1997. Introduction to chemistry and biological applications of poly (ethylene glycol). *Poly (ethylene glycol),* 680**,** 1-13.

ZELENY, J. 1914. The Electrical Discharge from Liquid Points, and a Hydrostatic Method of Measuring the Electric Intensity at Their Surfaces. *Physical Review,* 3**,** 69.

ZHANG, R., BURES, M., HÖFFLER, H.-K., ZINNE, N., LÄNGER, F., BISDAS, T., HAVERICH, A. & KRÜGER, M. 2012. TissuePatch™ as a novel synthetic sealant for repair of superficial lung defect: in vitro tests results. *Annals of surgical innovation and research,* 6**,** 12.

ZHANG, X., BAUGHMAN, C. B. & KAPLAN, D. L. 2008. In vitro evaluation of electrospun silk fibroin scaffolds for vascular cell growth. *Biomaterials,* 29**,** 2217-2227.

ZHANG, X. C., MACDONALD, D. A., GOOSEN, M. F. A. & MCAULEY, K. B. 1994. Mechanism of Lactide Polymerization in the Presence of Stannous Octoate - the Effect of Hydroxy and Carboxylic-Acid Substances. *Journal of Polymer Science Part a-Polymer Chemistry,* 32**,** 2965-2970.

ZHANG, Y., WANG, X., FENG, Y., LI, J., LIM, C. & RAMAKRISHNA, S. 2006. Coaxial electrospinning of (fluorescein isothiocyanate-conjugated bovine serum albumin)-encapsulated poly (Å-caprolactone) nanofibers for sustained release. *Biomacromolecules,* 7**,** 1049-1057.

ZHAO, X.-M., XIA, Y. & WHITESIDES, G. M. 1997. Soft lithographic methods for nano-fabrication. *Journal of Materials Chemistry,* 7**,** 1069-1074.

ZIABICKI, A. 1976. *Fundamentals of fibre formation : the science of fibre spinning and drawing,* London, Wiley.

ZISCH, A. H., LUTOLF, M. P. & HUBBELL, J. A. 2003. Biopolymeric delivery matrices for angiogenic growth factors. *Cardiovascular Pathology,* 12**,** 295-310.

ZOLNIK, B. S. & BURGESS, D. J. 2007. Effect of acidic pH on PLGA microsphere degradation and release. *Journal of Controlled Release,* 122**,** 338-344.